Metal Nanoparticles on TiO_2 Based Supports as an Electrocatalysts for Oxygen Reduction Reaction

BUKKA SANTHOSH
Japan Advanced Institute of Science and Technology

Doctoral Dissertation

Metal Nanoparticles on TiO_2 Based Supports as an Electrocatalysts for Oxygen Reduction Reaction

BUKKA SANTHOSH

Supervisor: Prof. Noriyoshi Matsumi

School of Materials Science
Japan Advanced Institute of Science and Technology

December 2018

Abstract

Fuel cells and Li air batteries are foreseen to be the future sustainable energy sources to mitigate the problem of global warming. Since the byproducts of these two sources are not harm ful, research community is focussing to undertake a paradigm shift from petroleum based energy sources to fuel based systems. But to come into market there are many issues that need to be solved. Generally an electrocatalyst will be employed to catalyze the two main reactions that occur towards the anode side and cathode side. Pt based metal catalyst supported on carbon will be employed as electrocatalyst for enhancing the reactions. But the major problem lies towards the cathode side where oxygen reduction reaction occurs (ORR). This reaction is highly sluggish with slow kinetics. So in order to improve this reaction, catalyst loading will be increased because of which the cost is booming and almost 50% of fuel cell cost is from Pt based catalyst. Apart from this problem of high cost, another major problem is the stability of the catalyst. During the continuous cycling of fuel cells, carbon on which Pt nanoparticles were supported gets corroded as a result Pt nanoparticles will aggregate and efficiency of the catalyst comes down. So chapter 1 focusses on the current scenerio of research is focussing on two main important problems of research i.e, to design electrocatalyst in such a manner that the amount of Pt utilization is minimized and to replace the carbon as support material either as partially or completely.

So far many Pt free metal based electrocatalysts and metal free electrocatalysts were designed and used. But none of them could replace Pt based electrocatalysts. So the focus is specifically oriented towards the minimization of Pt content. This can be achieved by designing core shell nanoparticles. In this core shell nanoparticles, inner material, acting as core, is made of any other metal other than Pt and outer material acting as shell, is made of Pt. There are wide variety of metals that can be utilized as core materials such as Ni, Co, Fe, Pd and Au. But of all the metals Au is most preferred as it has an extra advantages when compare to other metals such as high resistance to corrosion. Hence Au is most preferred core material. In order to synthesize core shell nanoparticles, wide variety of methods were designed. These include physical methods, wet chemical methods and electrodeposition techniques. Literature provides volumes and volumes of different core shell nanoparticles that were synthesized by using any of the forementioned methods. But all those methods involves huge experimental setup, tedious process, expensive chemicals, high temperature and above all, time and energy consuming aspects are making the process cumbersome. Hence there is a need to shift the focus in designing core shell nanoparticles

in the easiest method. Since the carbon undergoes corrosion during long term cycling of fuel cell, it is even more desirable to replace this carbon as support materials. Many semiconducting materials can act as support in place of carbon for holding the nanoparticles. But of all, TiO_2 with tube morphology is superior because it is low cost, environmentally friendly and possessing high resistance to corrosion.

Hence keeping in view of above required demands, chapter 2 focusses on a new method of depositing the core shell nanoparticles of Pt and Au over titania nanotubes. The synthesis was achieved through electrodeposition by applying potential of -2.0 V for 60 sec. The novelty of this method lies in the fact that the synthesis was achieved without long reaction time, high temparature and without any reducing agent. The as synthesized core shell nanoparticles were tested for electrochemical activity towards ORR and were found to be active.

Chapter 3 focusses on the cost reduction and enhancing durability of the catalyst. Hence to attain this, a composite made of titania nanotubes and functionalized acetylene black was used as support material for Pt decoration. In this Pt nanoparticles were decorated over this composite through photoreduction method by utilizing the spill over of electrons from titania. The successful formation of composite and decoration of Pt nanoparticles was characterized by various morphological techniques and found that Pt content was 3.5 wt%. As prepared material showed excellent ORR activity and found to have high electrochemical active surface area (ECSA) than commercially available Pt Vulcan XC-72.

Key words: Oxygen Reduction Reaction, Titania Nanotubes, Metal Nanoparticles, Electrochemical Deposition, Photochemical Reduction.

Preface

The present dissertation is submitted for the doctor of Materials Science at Japan Advanced Institute of Science and Technology. The dissertation is consolidation of results of the work on the topic "Metal nanoparticles on TiO_2 based supports as an electrocatalysts for oxygen reduction reaction" under the supervision of *Prof. Noriyoshi Matsumi* at the School of Materials Sciences, Japan Advanced Institute of Science and Technology during October 2015- September 2018.

Most of the current problems such as global warming and air pollution are arising from continuous exploration and depletion of fossil fuels. This has captured the attention of scientific community to shift to alternate and sustainable energy sources. One of the promising technologies that can serve as alternative to fossil fuels is fuel cell technology. A fuel cell provides clean and efficient energy directly by converting chemical energy into electrical energy. Recently there has been a special interest in development of polymer electrolyte membrane (PEM) fuel cells. This PEMFCs employs hydrogen as fuel. To spread the application of PEMFCs, there is a great need to develop a catalyst towards the cathode to accelerate highly sluggish oxygen reduction reaction (ORR) at the cathode. Pt/C, the state of the art catalyst has some problems such as high cost, corrosion and durability. Hence there is a need to design a catalyst that can solve these problems.

The work presented in this thesis covers the synthesis of nanoparticles over titania nanotubes and their utilization as electrocatalyst materials for oxygen reduction reaction as an alternative to Pt/C. To the best of my knowledge, the work is original and no part of the thesis has been plagarised.

Bukka Santhosh

School of Materials Science

Japan Advanced Institute of Science and Technology

December 2018

Acknowledgment

Firstly, the author expresses his sincere gratitude to the supervisor Prof. Noriyoshi Matsumi, School of Materials Science, Japan Advanced Institute of Science and Technology, for his kind guidance, valuable suggestions and heartfelt encouragements throught this work. I am thankful to him for his patience, motivation and immense knowledge. His guidance helped me in all the time of research and writing the thesis.

I would like to thank the members of my review committee Prof. Tamao Ishida (Tokyo Metropolitan University), Prof. Yuzuru Takamura (JAIST), Prof. Yuko Yamamoto (JAIST), Prof. Kazuaki Matsumura (JAIST) who have spent their valuable time to read my manuscript, for their insightful comments and remarks to enhance the quality of this dissertation from various perspectives.

The author is thankful to Prof. Sai Sathish Ramamurthy, Assistant professor, Department of Chemistry, Sri Sathya Sai Institute of Higher Learning, India for giving the opportunity to join his team as an intern and carryout experiments at India during 3 weeks of minor research. Furthermore the author wishes to express his special thanks to Prof. Sai Sathish Ramamurthy's lab members for their warm support and valuable suggestions during the author's stay in India.

The author also takes an opportunity to thank assistant professor Raman Vedarajan and Rajashekar Badam for their valuable guidance and encouragement at a professional and personal level. I am also greatful to other laboratory members, for their valuable inputs, cooperation and stimulating discussions, for the all the time we were working tighter before deadlines and for all the fun we had throught out my time at JAIST.

The author express his heartfelt gratitude to his parents and dear ones, for their relentless encouragement and support at difficult times. Finally, the author express his humble gratitude to the almighty for all the good things.

Bukka Santhosh

School of Materials Science

Japan Advanced Institute of Science and Technology

December 2018

List of figures

List of Tables

Table of Contents

Chapter 2

Ultrafast Electrochemical Deposition of Core Shell Metal Nanoparticles on TiO_2 Nanotubes for Electrocatalytic Applications

Chapter 3

TiO_2 Nanotubes/Functionalized Acetylene Black Composite Decorated with Pt Nanoparticles as Efficient Electrocatalyst for ORR

Chapter 4

General conclusions

Chapter 1

1.1. General Introduction

Environmental pollution is the major global concern especially due to harmful gases such as NOx and SOx[1]. These are evolving due to combustion of fossil fuels and are responsible for acid rains. At the same time, carbon dioxide emission has led to global warming. The disadvantage of these fossil fuels is they are non renewable and continuous usage of these resources will result in depletion. In addition to these fossil fuels, CO that is evolving due to incomplete combustion of fossil fuels, is also responsible for environmental damage. Hence intense research is going on to replace these fossil fuels with alternatives that are renewable and environmental friendly. One of the best alternatives to the internal combustion engine fuels such as diesel and petrol are electrolytic fuel cells[2] and Li air batteries. These fuel cells are of various types which uses hydrogen and oxygen as raw materials and the byproducts of these are water.

1.2. Fuel cell technology

A fuel cell is an electrochemical device which converts the chemical energy into electricity through a chemical reaction of a fuel with oxygen or another oxidizing agent[3]. A fuel cell employs hydrogen as the most common fuel. Fuel cells can produce electricity continuously as long as the fuel and oxygen are supplied. In this, the source is hydrogen and is generally referred to as the fuel so it derives its name fuel cell. Fuel cells were invented as early as 1839 by William Groove. Fuel cells did not find any practical application until NASA used them as power generators in Gemini and Apollo space programmes. Since then fuel cells are used as main power generators in fields of stationary power generators, transportation and other power generators. There are several kinds of fuel cells but the basic unit of typical fuel cell consists of three parts viz anode, cathode and electrolyte giving three different segments. In order to increase the rate of reaction at the electrodes, a catalyst is often used to speed up the reactions at the electrodes. Hydrogen-based gaseous fuels are fed continuously to the anode compartment and oxygen from air as oxidant is fed continuously to the cathode compartment and two chemical reactions occur at each electrode and the net result is that the fuel is consumed. The products formed are water, carbon dioxide (in the case of methanol oxidation type of fuel cell), electric current and it is this electric current that can be used to power electrical devices. At anode a catalyst converts the hydrogen into a proton and electron

as shown in the Fig 1.1 and the electrolyte is specially designed in such a way that it is permeable only to ions but not to electrons and these electrons travel through a wire creating the electric current. On reaching near the cathode, water is generated by reaction among proton, electron and oxygen.

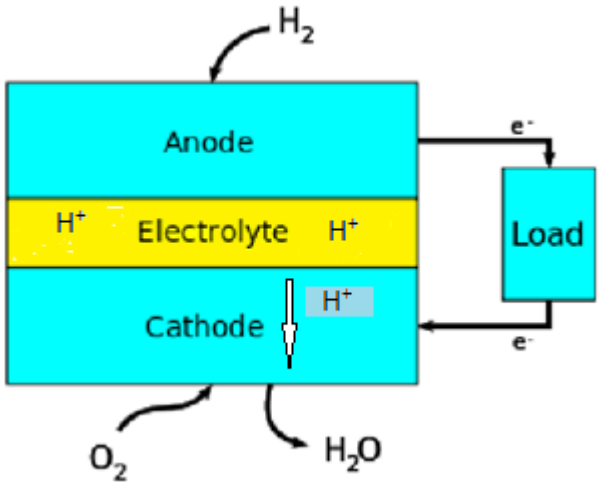

Fig 1.1: schemat of typical fuel cell

Fuel cell systems have different variables such as [4]

1) Type of the exchanged ion through the electrolyte,

2) Type of the electrolyte used in fuel cell,

3) Type of the reactants (e.g. primary fuels and oxidants),

4) Operating temperature and pressure,

5) Direct and indirect usage of the primary fuels in fuel cell system and

6) finally the primary and regenerative system

1.2.1. Types of fuel cells

Fuel cells are classified based on the nature of electrolyte used. Therefore, based on this classification, fuel cells include the following different types:

1) Proton exchange membrane fuel cells
2) Phosphoric acid fuel cell
3) Solid oxide fuel cells
4) Molten carbonate fuel cells

5) Direct methanol Fuel Cells
6) Alkaline fuel Cells

1.2.2. Proton exchange membrane fuel cells

It was popularly called as "solid polymer electrolyte fuel cell" (SPEFC) in the early 1970s, but ever since the mechanism of proton exchange was understood it was renamed as proton exchange membrane fuel cells[5]. In this, a proton-conducting polymer membrane separates the anode and cathode as shown in Fig 1.2. Near the anode hydrogen diffuses to the anode catalyst where it dissociates into protons and electrons. These newly formed protons are conducted through the membrane to the cathode, but since the membrane is electrically insulating, the electrons are forced to travel in an external circuit. Near the cathode catalyst side, oxygen molecules react with protons and the electrons that travelled through the external circuit to form water. Relatively low temperature conditions around 80 °C is sufficient to operate PEM fuel cells. Proton exchange membrane fuel cells are primarily used for transportation applications and some domestic applications particularly in passenger vehicles, cars and buses due to their fast startup time, low sensitivity to orientation, and favorable power-to-weight ratio.

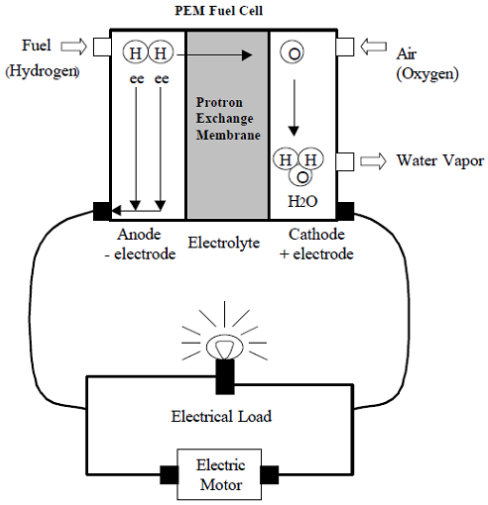

Fig 1.2: Schematic illustration of proton exchange membrane

The main important reactions of fuel cell are

Anode: $H_2 \rightarrow 2H^+ + 2e^-$ (Hydrogen oxidation reaction)

Cathode: $1/2O_2 + 2H^+ + 2e^- \rightarrow H_2O$ (Oxygen reduction reaction)

Pt supported on mesoporus carbon is the main catalyst that is used to catalyze this reaction. Pt has attracted because it offers high catalytic activity, chemical stability, high exchange current density and superior work function[6]. Since this Pt is a rare earth metal with limited reserves, its choice to use it as electrocatalyst makes the PEMFCs most expensive. This Pt based electorcatalyst is used both for anodic and cathodic reactions. The rate of cathodic reaction where oxygen reduction will take place, is extremely slow by several orders of magnitude than anodic reaction and demand high catalyst loading[7]. Apart from this, another major disadvantage with this fuel cell is during operation the catalyst layer undergoes degradation. The catalyst will undergo degradation due to Pt agglomeration or may be due to loss of activation sites [8] and also affected by the CO poisoning as shown in Fig 1.3

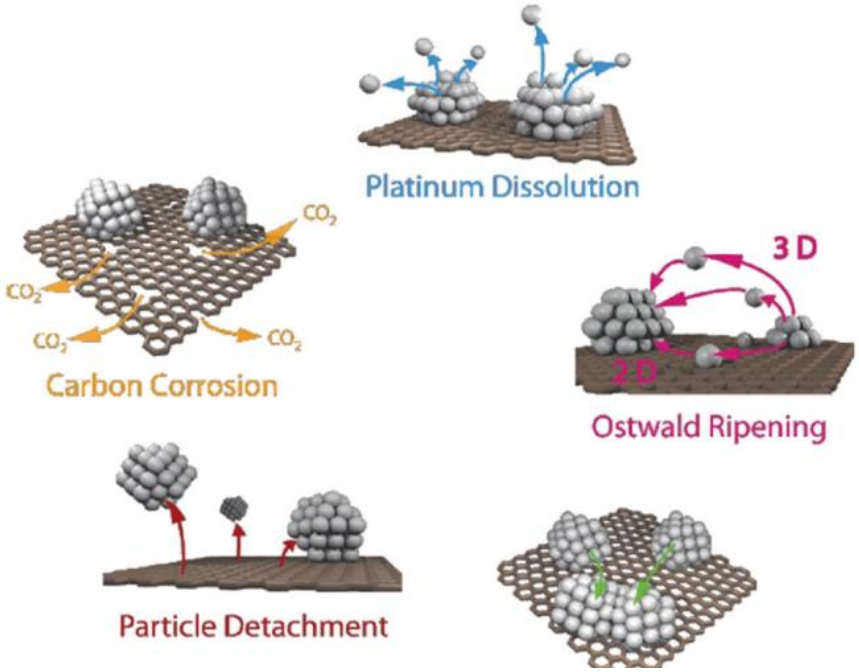

Fig 1.3: Schematic representation of catalyst degradation during fuel startup and shut down

(Figure adapted from ***Beilstein, J. Nanotechnol. 2014, 5, 44–67*****)**

1.3. Li air battery:

With the advancement in technology across globe especially in transportation sector, there was a huge increase in energy consumption which leads to raise in carbon foot print. Around 80 % of energy consumption is from transportation sector because of which there are numerous environmental problems such as emission of carbon dioxide and green house gases. With continuous depletion in fuels, special emphasis on alternatives for energy consumption in

transportation sector is highly recommended[9]. So it would highly benefit if there is a transition from use of fossil fuels to use of hybrid electric vehicles and subsequently to pure electric vehicles. The use of hybrid vehicles is already beginning in the market. Pure electric vehicles also started to offer high efficiency as high as 1.14 Km/MJ, 2 times higher than Toyota Prius hybrid. Hence to reduce CO_2 emissions and green house gases, a transition towards the usage of alternate energy sources such as solar, and wind power is highly demanded. In this scenario, use of Li air battery would be a viable option. There are various metal air batteries such as zinc-air battery, aluminum air battery, magnesium- air battery, iron-air battery. But of all these, the theoretical capacity of Li air battery is high, 11680 Wh/Kg[10] as shown in Fig 1.4, almost close to gasoline. Metal air battery was first discovered by Leclanche in 1868. Zinc air battery was first discovered by Heise and Schumacher in 1932.

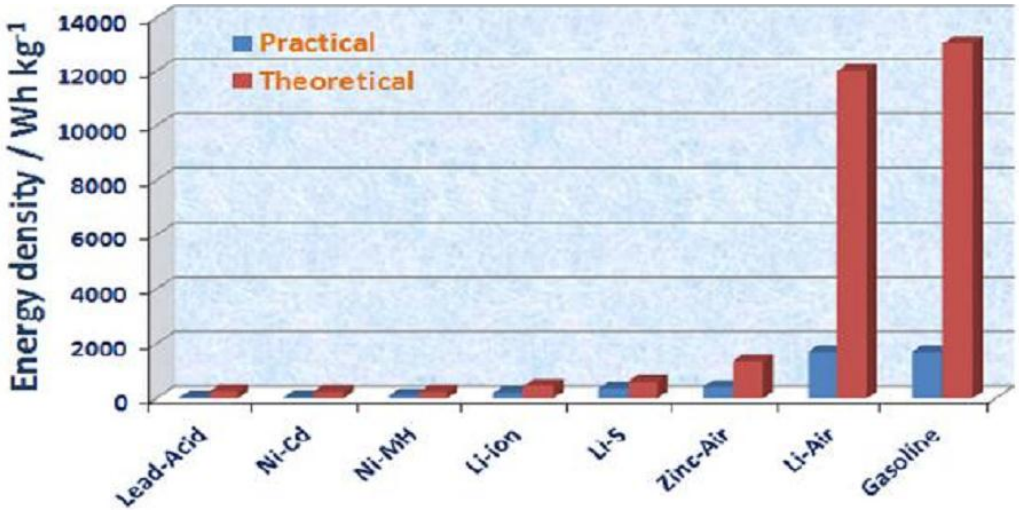

Fig 1.4: Comparision of energy densities of various batteries with gasoline (figure adopted from ***Nano Energy*, 2013, 2, 443–467)**

These metal air batteries consist of metal based anode and cathode which continuously draws oxygen from ambient air, called as air-cathode. Depending on the metal used, different metal air batteries were characterized. Li air battery is an advanced energy storage system which converts chemical energy to electrical energy during discharge and stores chemical energy during charge[11]. Depending on the type of electrolyte used, 4 different types of Li-O_2 batteries have been developed. They are aprotic, aqueous, solid-state, and hybrid aqueous/ aprotic batteries. Fig 1.5 shows the schematic representation of different types of Li air batteries.

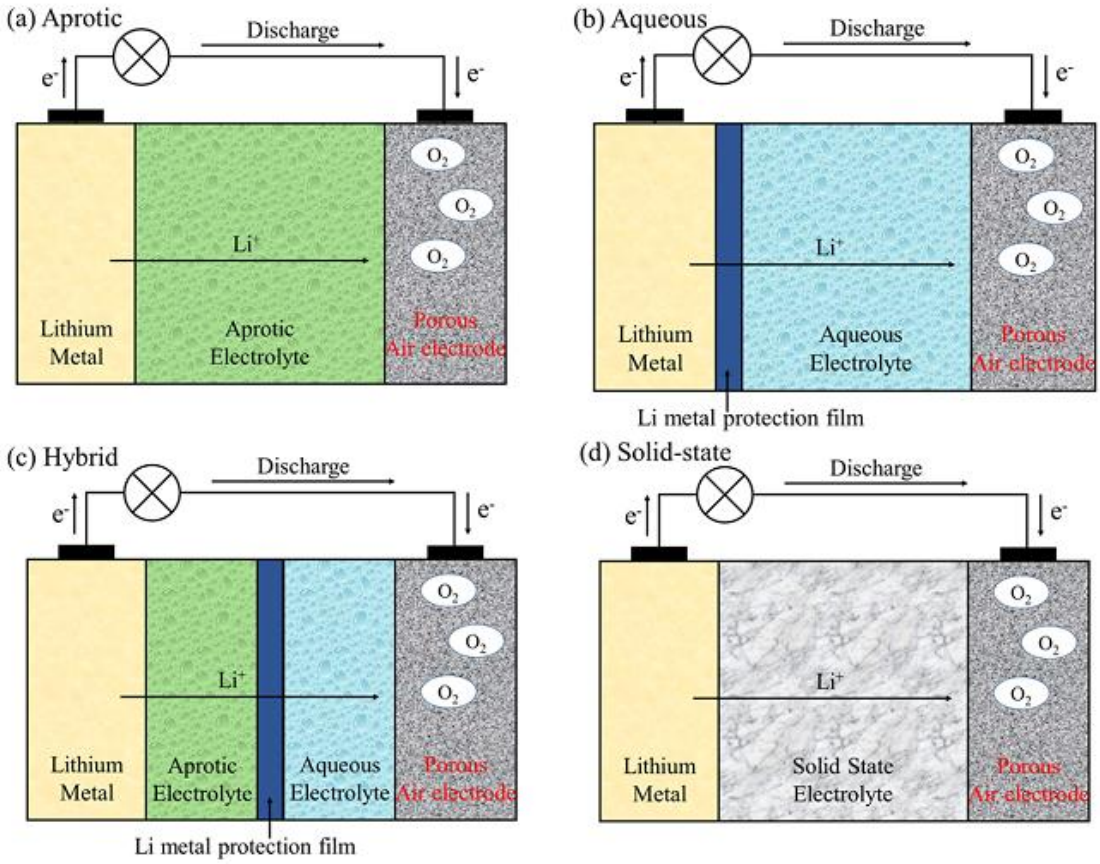

Fig 1.5: Schematic representation of different types of Li-air batteries (Figure adopted from ***Chem. Rev.*, 2014, 114, 5611–5640**)

Irrespective of the electrolyte used, the fundamental reaction are as follows.

Anode:

$Li \rightarrow Li^+ + e^-$ equation 1

Cathode: Non aqueous: $2Li^+ + 2e^- + O_2 \leftrightarrow Li_2O_2$ (E_0= 2.96 V vs Li/Li^+) equation 2

Alkaline: $O_2 + 2H_2O + 4e^- \leftrightarrow 4OH^-$ (E_0= 3.43 V vs Li/Li^+) equation 3

Acid: $O_2 + 4e^- + 4H^+ \leftrightarrow 2H_2O$ (E_0= 4.26 V vs Li/Li^+) equation 4

Li air batteries are superior to fuel cells and Li ion batteries. It has no fuel infrastructure issues, as in the case of fuel cells and its energy density and specific energy are much higher than lithium ion batteries. From the equations 3 and 4, many modelling systems have proved that for Li air batteries nonaqueous electrolyte system provides high energy density than aqueous electrolyte system. This batteries also have some challenges such as improvement in energy density and energy efficiency, cyclability, lithium metal anode incompatibility with electrolyte and air, dendrite formation on electrode, instability of electrolytes in oxygen atmosphere, evaporation of electrolytes[12], conductivity and so on. A major challenge is to understand the oxygen reduction reaction kinetics. Currently Li−air batteries can only be discharged/charged at a current density of 0.1−0.5 mA/cm^2 when compared to >10 mA/cm^2 for a Li ion battery and >1500 mA/cm^2 for PEMFCs. This inefficiency is due to the sluggish oxygen reduction kinetics, many side reactions of Li-O_2 systems.

ORR and OER in nonaqueous systems follows the following mechanisms.

ORR:

$$O_2 + e^- \rightarrow O_2^-$$

$$O_2^- + Li^+ \rightarrow LiO_2$$

$$2LiO_2 \rightarrow Li_2O_2 + O_2$$

OER:

$$Li_2O_2 \rightarrow 2Li^+ + O_2 + 2e^-$$

It was found that Li^+ containing nonaqueous electrolyte first forms O_2^-, which then binds to Li^+, forming LiO_2 on the surface of the electrode. LiO_2 is unstable and disproportionates to more stable Li_2O_2[13]. During discharge OER will take place with the direct involvement of Li_2O_2 instead of LiO_2 showing that the mechanisms of OER and ORR are different because of different over potentials for charge and discharge[14].

1.3.1. Effect of electrolyte:

Indeed the choice of electrolyte plays an important role in Li air batteries. Electrolytes that are employed in the batteries should be stable against the superoxide radical (O^{2-}) which is developed during the oxygen reduction reaction upon charge[15]. So far many electrolytes were tested and used in Li ion batteries. But they were tested in closed environment in absence of environment. To use the same electrolytes for Li air batteries, they need to be tested thoroughly in

oxygen rich enviornments. Apart from stability, the electrolyte should have the following requirements[15].

1) stability toward reaction with lithium metal since this is the choice of the metal electrode for Li−O_2 cells
2) high boiling point and low volatility due to the open cell system
3) high oxygen solubility and diffusivity to facilitate the oxygen reduction and oxygen evolution reactions on the air electrode
4) low viscosity to improve the rate performance of the oxygen electrode

Carbonate based electrolytes especially polypropylene carbonates have been extensively used owing to several advantages such as wide potential window, low volatility but these electrolytes are not stable against many side products that are formed during the oxygen kinetics such as O_2^-, O_2^{2-}, LiO_2, and LiO_2 . Read et al[16] and Aurbach et al[17] were the first to find out the effect of carbonate electrolytes.

Later the focus of investigation was shifted to ether based electrolytes such as 1,2 dimethoxyethane (DME) and tetraethylene glycol dimethyl ether ("tetraglyme" or TEGDME) as these are stable to super oxide radicals, inflammable, low cost and highy thermally stable. It was proved that ether based electrolytes show good stability and excellent rate capability.

1.3.2. Effect of lithium salt:

Many lithium salts such as $LiPF_6$, lithium bis[(trifluoromethyl)sulfonyl]imide (LiTFSI), $LiClO_4$, $LiCF_3SO_3$, $LiBF_4$, LiCl, and lithium bis(oxalato)borate (LiBOB) were used as supporting electrolyte. Lithium salt for lithium air battery should meet the following requirements such as[9]

1) the salt should have high enough solubility in the solvent to support the ion transport
2) the anion of the salt should be inert to the solvent and other cell components, such as current collectors and separators. In addition to these basic requirements, the salt

used in the Li−O_2 system should be inert to the aggressive oxygen reduction species, such as Li_2O_2 and O_2^- radical.

1.4. Introduction to oxygen reduction reaction:

Oxygen is the most important element in earth's crust. Oxygen reduction is the most important reaction in life process such as biological respiration, photosynthesis, corrosion and corrosion inhibition apart from energy converting systems such as fuel cells and metal air batteries.

1.4.1. Mechanism of ORR:

ORR is quite complicated reaction and involves many intermediates and these intermediates depend on catalyst, electrode material and electrolyte used. ORR mechanism in different medium along with thermodynamic potential is presented in Table 1.1.

Table 1.1: Thermodynamic electrode potentials of electrochemical oxygen reduction reaction.

Electrolyte	ORR reactions	Thermodynamic electrode potential at standard conditions, V
Acidic aqueous solution	$O_2 + 4H^+ + 4e^- \rightarrow H_2O$	1.229
	$O_2 + 2H^+ + 2e^- \rightarrow H_2O_2$	0.70
	$H_2O_2 + 2H^+ + 2e^- \rightarrow 2H_2O$	1.76
Alkaline aqueous solution	$O_2 + H_2O + 4e^- \rightarrow 4OH^-$	0.401
	$O_2 + H_2O + 2e^- \rightarrow HO_2^- + OH^-$	–0.065
	$HO_2^- + H_2O + 2e^- \rightarrow 3OH^-$	0.867
Non-aqueous aprotic solvents	$O_2 + e^- \rightarrow O_2^-$	a
	$O_2^- + e^- \rightarrow O_2^{2-}$	b

Oxygen reduction reaction (ORR) can either be reduced to water by 4 e^- process or it can be reduced to hydrogen peroxide by 2e^- process. In fuel cells 4e^- pathway is preferred. The 2e^- reduction pathway is preferred in industry for H_2O_2 production.

Conductive carbons with high surface area are used as fuel cell electrocatalyst supports to ensure large electrochemical surface[6] and in the similar lines many carbon supports were used. It is worth to understand the mechanism of ORR on these carbon materials.

1.4.2. Mechanism of ORR on carbon materials:

1.4.2.1. ORR on graphite and glassy carbon: The following mechanism have been proposed on carbon catalyst. The following mechanism have been proposed.

$O_2 \rightarrow O_{2(ads)}$ equation 1

$O_2 + e^- \rightarrow [O_{2(ads)}]^-$ equation 2

$O_{2\,(ads)} \rightarrow O_{2\,[ads]}$ - equation 3

$O^-_{2(ads)} + H_2O \rightarrow HO_2 + OH^-$ equation 4

$HO_2 + e^- \rightarrow HO^-_{2(ads)}$ equation 5

$HO^-_{2(ads)} \rightarrow HO^-_2$ equation 6

The subscript *ads* indicated that corresponding species adsorbed on the electrode surface. The reactant and product in Reaction 3 are two different forms of the superoxide ion on the carbon surface. The left one is a relatively inert form adsorbed on an inert graphite site, and the right one is the same species, but migrating to an active site according to Reaction 3. It was confirmed that Reaction 3 was the rate determining step. But it was found out that the rate determining step was dependent on pH[18]. At pH > 10, Reaction 3 was the rate determining step, and at pH < 10, Reaction 2 was the rate determining step

1.4.2.2. ORR on carbon nanotubes:

Ever since the discovery of carbon nanotubes, they were found to be useful in many applications. They are also found to catalyze ORR and catalytic activity also depends on preparation method. When $MWCNT_S$ were synthesized in dihexadyl hydrogen phosphate method on glassy carbon electrode, it was found that CNT_S could catalyse ORR by $2e^-$ process[19]. When MWCNTs were synthesized by poly(diallyldimethyl ammonium chloride), electron transfer number was found to be in between 3-3.5[20].

1.4.2.3. ORR on heteroatom doped carbon atoms

It was found that ORR activity on carbon atoms can be greatly improved by doping with heteroatom such as nitrogen. Studies found that by doping nitrogen on carbon fiber, nearly 70 mV shift in ORR was observed with electron transfer number close to 4[21]. Apart from doping with nitrogen, other atoms such as boron, sulfur, fluorine and phosphorus can be doped into carbon to

improve ORR activity. Although the exact mechanism is not clear, it was predicted that inclusion of heteroatom in carbon will create active sites in carbon next to heteroatom and facilitates O=O bond breakage in O_2.

1.4.2.4. ORR on pretreated carbon surface:

It was found that by pretreating the electrode, ORR can be greatly improved. There are various methods to pretreat the electrode surface such as vaccum heat treatment, polishing the electrode, radio frequency plasma treatment, in-situ laser treatment, heating at low pressures and electrochemical oxidation. Studies found that pretreatment improves surface area[22], create more functional groups, defects and expose fresh edges.

1.4.2.5. ORR activity on precious metals:

Platinum (Pt) was found to be more active metal in catalyzing ORR. So far no other metal had shown equalent activity when compare with Pt. The mechanism of ORR activity of Pt is not very clear but many elementary steps with many intermediates were predicted as shown in Fig 1.6. It was shown that oxygen will get reduced to water completely by consuming 4 electrons without any intermediate formation.

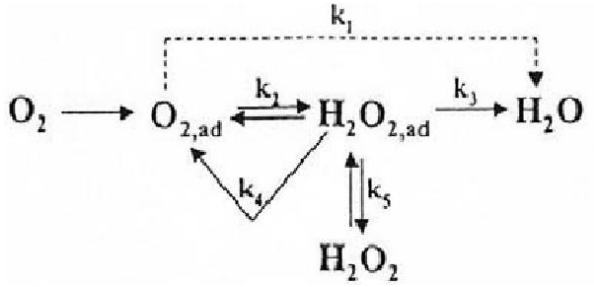

Fig 1.6: Mechanism of ORR on Pt

As we see in Fig 1.6, O_2 can be directly reduced to H_2O with the rate constant K_1 or can be reduced with an intermediate formation, H_2O_2 with the rate constant K_2. Further this intermediate can be reduced to H_2O with rate constant K_3 or can be desorbed in electrolyte with rate constant K_5 or can decompose at electrolyte surface with rate constant K_4. But is widely accepted that the most favorable pathway is to form water directly with electron transfer number 4.

Based on electronic energy and by using DFT calculations two mechanisms were proposed. They are associative mechanism and dissociative mechanism. Associative mechanism is for high

current density region. In this, molecular O_2 is adsorbed onto electrode surface followed by transfer of proton/electron to it and to OOH, which breaks into O and OH.

Dissociative mechanism is for low current density region and in this the O–O bond in O_2 splits and the hydrogenation of atomic O to OH and to H_2O takes place[23]. ORR on other metal such as Au, Cu, Pd, Ir, Rh can also take place but no other metal is as active as Pt.

Pt shows high activity because

1) High work function (4.6 eV)
2) Good resistance to corrosion and metal dissolution
3) High exchange current density (10^{-8} mA/cm^2)

1.4.2.6. ORR activity by transition metal chalcogenides:

Transition metal chalcogenides became more prominent towards ORR especially after discovery by N. Alonoso vante and H. Tributsch[24]. Based on structure they are classified in two types

A) Chevrel phase ($Mo_4Ru_2Se_8$) and B) amorphous phase (Ru_xS_y)[24]

Ruthenium based chalcogenides are most intensively studied [24]. Cheveral phase was synthesized by treating Ru and chalcogene elements at high temperature and pressure. Subsequently chemical reduction of $RuCl_3 \cdot xH_2O$ and SeO_2 by $NaBH_4$ at ~80 °C temperature was developed[23].

Depending on the type of chalcogenide used, ORR can be catalyzed either by 4 e^- or by 2 e^- transfer. $Mo_4Ru_2Se_8$, $Ru_{1.92}Mo_{0.08}SeO_4$, $Ru_xS_y(CO)_n$, Ru_xSe_y, etc. catalyze ORR via 4-electron transfer while W-Co-Se catalyzes a ORR by 2 e^- process as shown in Fig 1.7.

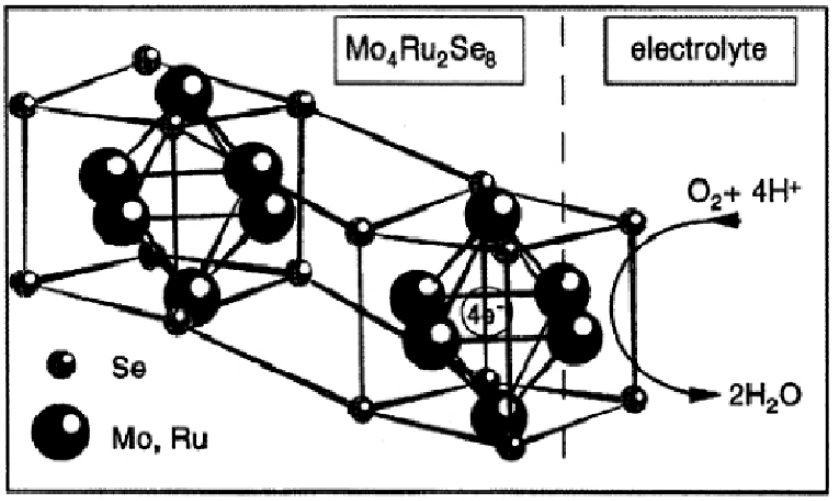

Fig 1.7: Structure of $Mo_4Ru_2Se_8$ and interaction of O_2 at the Chevrel phase clusters electrolyte interface

1.4.2.7. Special emphasis on Pt based catalysts:

ORR is very sensitive reaction and strongly dependent on electronic properties of surface and atomic arrangement. Hence the catalytic properties of Pt can be greatly improved by altering the surface electronic properties and by modyifng the atomic arrangement[25]. This engineering the surface properties also improves the durability[26]. There are four ways to engineer the surface properties of Pt i) preparation of single facet Pt which has maximum activity towards ORR, ii) utilising the Pt in conjunction with another metal forming multimetallic catalyst. This way of modification has dual advantages deriving the benefits that are associated with each metal along with new properties because of synergistic effect from both metals[27]. iii) it is also possible to alter the properties of Pt by introducing the foreign species such as metal clusters, molecules, ions, organic or inorganic compounds. This strategy also help in improving the additional properties such as hydrophilicity. iv) one another approach is to combine catalyst which has high corrosion resistance to improve durability[28].

1.4.2.8. Facet controlled catalysis

Inorder to achieve high performance in ORR, facet controlled ORR has grabbed extensive attention from researches across globe. Studies regarding low index Pt nanosurfaces are well established in perchloric acid. In weakly absorbing electrolyte such as perchloric acid activity follows the order Pt (100) << Pt (111)~Pt (110). When sulfuric acid was used as electrolyte, Pt (100) was found to be more active than Pt (111). This is mainly because of the surface coverage of Pt (111) by bisulfate ion[29]. Pt (100) and Pt (111) both differ in their properties due to different facets and Pt (111) could adsorb bisulfate ions more strongly and activity reduces. Following this work, it was further confirmed that a catalytic performance is dependent on the surface atom arrangement, that is, morphologic characteristics. Therefore, ''transfer'' of the active catalytic surface from a single crystal to more practical nanophase by establishing a shape-control synthesis strategy is a promising route to boost Pt activity towards ORR. El-Sayed et al made considerable efforts in synthesizing the different facets of Pt and was successful in their pursuit and suggested shape-controlled synthesis of single Pt nanocrystals, consisting of nanotetrahedra with (111) and nanocubes with (100), and ''near spherical'' nanocrystals containing a mixture of {111} and {100} facets[30].

Sun *et al* reported a high temperature method for the synthesis of single facet Pt nanocubes (100) and showed 2 times superior activity for ORR activity than commercially available Pt catalyst. This group also proved that 7 nm (100) Pt nanocubes show better activity than other morphological form of nanoparticles, demonstrating the importance of facet along with shape dependency[31]. Studies were extended towards investigation about the high index planes towards ORR activity. Sun and co-workers have synthesized high-index facets, such as {730}, {210} and {520} by applying a square-wave potential to polycrystalline Pt microspheres supported on a glassy carbon electrode and obtained materials showed higher activity than low index facets.

Xia et al. have synthesized Pt concave nanocubes with high-index facets including {510}, {720}, and {830} and showed higher electrocatalytic activity per unit surface area when compared to other morphological forms such as Pt cubes, cuboctahedra, and commercial Pt/C catalysts with low-index planes such as {100} and {111}[32]. Though these higher facets have shown higher activity but the mechanism is still unclear. Moreover these high facet nanocrystal have less mass activity when compared with other highly active ORR catalysts. Also they were found to be

unsuitable to fuel cell operations especially those with high-index planes and unsaturated atomic steps, edges and kinks, all of which are active sites for crystal growth.

1.4.2.9. Effect of particle size and shape on ORR activity:

Following the interesting observations that were made that higher facet planes are more active than (111)>> (100) focus shifted towards shape and its effect on ORR. It was found that octahedral Pt nanoparticles (111) are more actve than nanoparticles with cubic ones (100)[33]. Nanoparticles with tetrahexahedron (hk0), trapexezohedron (hkk) trisoctahedron (hhk) showed more ORR activity than (111) or (100)[34]. The activity enhancement was attributed to the presence of low coordinated atoms on kinks, edges and steps. Since the nanoparticles will tend to grow thermodynamically, stability becomes an issue toward ORR condition.

The effect of particle size on ORR has been a long standing problem which needs to be resolved. It was observed that as the particle reduces from 5 nm to 1 nm, (111) and (100) facets decreases and edges and kinks with low coordination number increases. Since these edges and kinks have stronger binding energy to oxygen, ORR activity is lower. So the specific activity decreases drastically when the nanoparticles size is smaller than 3 nm. In the similar lines many researchers argue that specific activity does not decrease even when the particle size is in the range 1-5 nm[35].

It was found that when Pt nanoparticles with size ranging from 1-5 nm, are dispersed on carbon, the change of specific activity was negligible. This is because reaction pathway changes as the particle size decreases. When the particle size decreases the oxygen binding energy increases and so the rate determining step is breaking of O-O bond rather than proton and electron transfer[36]. It was found that ORR activity also depends on interparticle distance. When the interparticle distance decreases ORR activity increases. The interparticle distance overlapps with the double layer formation which leads to decrease in potenitial drop and consequently to weaker adsorption energy on Pt surfaces. This effect of interparticle size dependency was also seen when Pt nanoparticles were dispersed on carbon. It was also found that H_2O_2 reduction was more pronounced when Pt nanoparticles were dispersed on carbon[37].

Studies were also conducted on Pt nanocluster that are not used in fuel cells. For example Pt_{12} showed 10 times higher activity when compare to TKK catalyst. When the number atoms increased from Pt_{12} to Pt_{13}, ORR activity decreased. This decrease in ORR activity is due to

structural modification from C_{2v} to icosahedral which has much stronger binding energy than C_{2v} Pt_{12}. By adding more atoms to icosahedral Pt_{13}, it will be converted to Pt_{17} and Pt_{19}. These two showed an activity enhancement towards ORR. This study proved that icosahedral Pt_{13} is not active towards ORR.

It is difficult to establish a relationship between ORR activity and particle size and shape effect. Even on the well defined octahedron structure, TEM revealed surface defects and appearance of steps instead of smooth surface. There is a need to study the role of these stepped surface atom to understand fully about size and shape effect.

1.4.2.10. Improved ORR activity with Pt alloys preparation:

Since the use of Pt based catalysts incurs high cost, an alternative to this was investigated and one important finding out of such investigation was to utilize Pt in the form of alloys. These alloys have higher activity than Pt alone. Ever since the idea of utilizing Pt in the form of alloys, it has been executed and the results showed superior activity. Synthesis of Pt alloys became prominent and they were considered as "second generation catalysts". Toyata mirai used these alloys as catalysts in their fuel cell vehicles[38].

These alloy catalyst which consists of lower Pt content can be cost effective and also showed superior activity than monometallic activity. The superior activity can be due to extra properties that are derived from both the mixture as well as individual constituents. In recent past many alloy systems consisting of Pt in conjunction with other metals such as Cu, Ni, Fe, Co. Ag, Au, W, Pd have been studied[26].

Studies were also conducted by incorporating 3d such as Ni, CO, Fe, Ti, V and found that they showed volcano type behavior[39] as shown in Fig 1.8. Stamenkovic et al have done investigations with 3d metals and gave understanding about the role of good catalyst. A better catalyst for ORR should bind oxygen less strongly than Pt to increase the removal rate of oxygen-containing intermediates. In their studies it was found that a better catalyst should lower the binding energy by 0.2 eV compared to Pt and found that Ni, CO, Fe, Ti, V are suitable for alloying to lower binding energies.

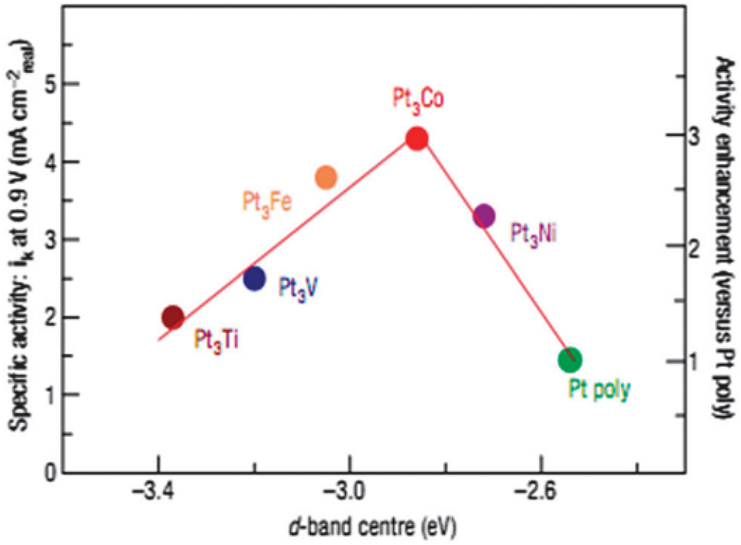

Fig 1.8: Activity trend of 3d elements towards ORR

(Figure adapted from ***Nat. Mater., 2007, 6, 241–247)***

Han et al discovered that ORR activity of Pt alloys depends on dissolution potential of alloying metals. If the dissolution potential is higher, then the alloying metal dissolves and the resultant activity is only from Pt mono metal itself. It was also investigated that post treatment of Pt alloys improves ORR activity. During ORR measurments, many nonnoble metals dissolutes resulting in exposure of Pt which is called as Pt skeleton. When the same alloys were annealed at higher temperature close to 1000 K then Pt atoms seggrate on surface whereas alloying metals will move beneath the Pt layer. This is called as Pt skin. It was found that specific activity was found to be enhanced by 5 times in annealed alloy when compared to non annealed one. Hence fine tuning and engineering the surface structures of Pt plays an important role for ORR activity. The Pt atom segregation was also found when the samples were annealed at 727 °C in case on Pt_3Co. With the help of scanning transmission electron microscopy (STEM) it was found that Pt was on surface covering the Co beneath[40]. Effect of thermal annealing was also found on surface reorientation of different facets. It was found that after thermal annealing, in Pt-Ni before thermal annealing (111) was only 25% but after thermal annealing (111) facet was 35% with a two folds enhancement in activity[41] as depicted in Fig 1.9.

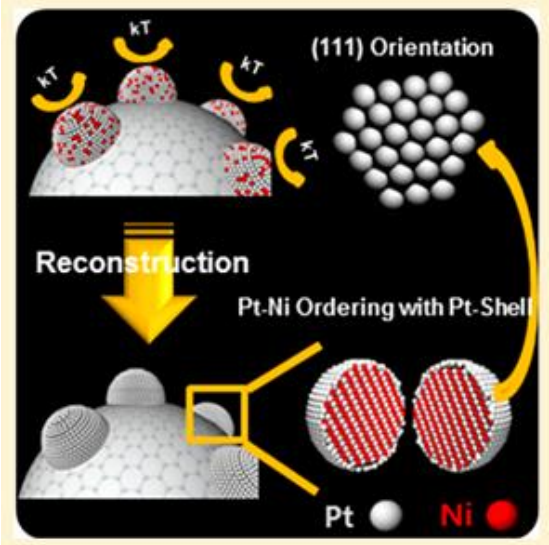

Fig 1.9: Surface reorientation of Pt and Co atoms upon thermal annealing

(Figure adapted from ***J. Phys. Chem. C, 2014,* 118, *9939–9945*)**

It is also possible to prepare alloys with more than one metal calling as binary and ternary and quaternary alloys. In binary alloys, there will be two metals apart from primary metal (In this case Pt) and in ternary alloys there will be three metals. Because multiple metals are introduced ternary and quaternary alloys showed higher activity than binary alloy. Almost all the metals such as Fe, Ni, Co, Ti, V, Ag, Au, Sn, Cr, Mn, Mo, Pd and Ir with various combinations were studied. Studies were extended even to include transition metals such as Y, Sc, Hf, Ga, Ce, La, and Gd. The activity of these early transition metal alloys was even higher than late transition metals. It was shown that Pt_3La showed higher activity. Later it was proved that Pt_5La, Pt_5Ce, Pt_5Gd showed higher activity than Pt_3La[42]. Fig 1.10 shows trends in ORR activity of transition metals.

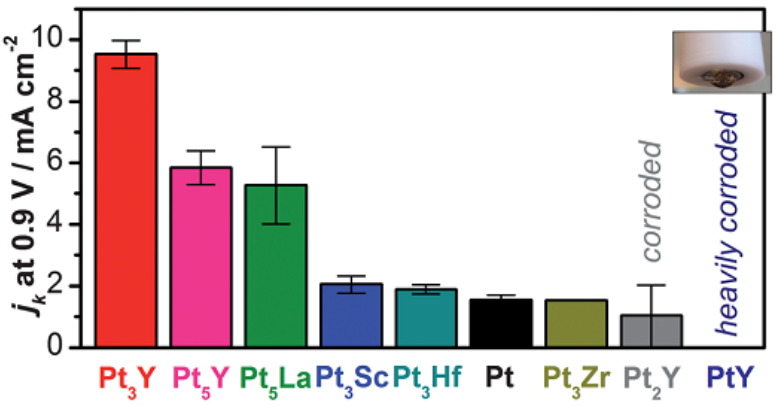

Fig 1.10: Trends of ORR activity of transition metals

(Figure adapted from ***energy Environ. Sci. 2012, 6744–6762)***

1.4.2.11. Mechanisms for enhancing the activity of these alloys:

Numerous reasons were given for activity enhancement of these alloys. The enhancement may be due to modification of electronic structure due to decrease in Pt-Pt bond distance which impose strain, down shifting of d-band center, surface roughness which is caused due to metal dissolution, delay in formation of oxide species formation.

1.4.2.12. Disadvantages of Pt- alloy systems:

The main disadvantage with this is alloy is dissolution when comes in contact with acidic electrolyte. When an alloy catalyst comes in contact with electrolyte for ORR activity, the non Pt metal leaches or dissolutes and as a result the activity is compromised. The disadvantages of these alloy systems can be overcome by engineering the nano structure of these dual metal systems in the form of core and shell nanoparticles**.**

1.5. Introduction to core shell nanoparticles:

Composite nanomaterials that are synthesized at nano scale consisting of inner material as **core**, covered by outer material as **shell** is defined as core shell nano particles[43]. The inner material and outer material is separated completely with a distinct boundary. In these core shell nanoparticles Pt plays an important role to meet the requirements, demands and targets of automobile industries and world energy organizations such as DOE, USA and NEDO, Japan[44]. Pt core shell nanoparticles

consists of a shell enriched with Pt surrounding a core which is made of metal or alloy. These core shell preparation offers enormous impediments such as controlling shell thick ness, size and shape of core and shell, core composition etc. Due to altering in surface geometry and electronic effects, these core shell nanoparticles derives its benefits. One of the key parameters for ORR activity is Pt shell thickness. With the increase in shell thickness ORR activity drops and this is because the particle behaves similar to Pt nanoparticles. When the shell thickness increases, particles aggregate because of Ostwalds ripening. Intense ORR activity can only be seen when the shell thickness is small and covers the core in monolayer formation. Apart from this shell, core also plays an important role in enhancing ORR activity. Core should be stable under fuel cell operating conditions and should be stable when it comes in contact with acid electrolyte. It was found that 3d metals such as Fe, Ni, Co, Cu offer high ORR activity. This is because of difference in d band energies, acceptor and donor interactions as well as increased lattice mismatch. But these 3d metals are dissolved when comes in contact with acids. The stability of the core depends on oxophilicity of the metal, segregation behavior of metal due to temperature and electrochemical conditions. When a core has strong affinity for oxygen, it migrates towards shell and leaches, dissolves in acid[45]. Hence an alternative to this is to utilize tungestin and molybdenum carbides to minimize Pt content and also to enhance ORR activity and durability[46]. To achieve more stability, it is advised to use a metal which has high corrosion resistance. Usually smaller particles show less ORR activity because of strong oxophilic character i. e strong affinity for oxygen. Because of this they have high binding affinity for oxygen and as result it is difficult to get access for oxygen reactants. On contrary large particles show high ORR specific activity and durability[47]. Gibbs Thomson gives the relation between dissolution rate and particle size. Larger particles have low Gibbs Thomson energy and low dissolution rate. Smaller particles will have high Gibbs Thomson energy and dissolves easily. Hence selecting an appropriate core which has high corrosion resistance is important. Further by controlling Pt shell thickness, controlling particle size and shape, it is possible to optimize electronic effects and strain between core shell nanoparticles with which higher ORR activity can be achieved.

1.5.1. Synthesis of core shell nanoparticles:

There are various strategies for core shell nanoparticle synthesis. They are as follows

1) Select a core metal and deposit shell over this already formed core.
2) Removing a component from an alloy
3) Treatment of an alloy in such a way that one of the alloy component segregates toward the surface to form shell.

With the above mentioned strategies there are various different methods for core shell nano particles such as electrochemical dealloying, electrochemical leaching, thermal induced seggregation or adsorbate induced segregation, deposition methods and Fig 1.11 gives the schematic illustration.

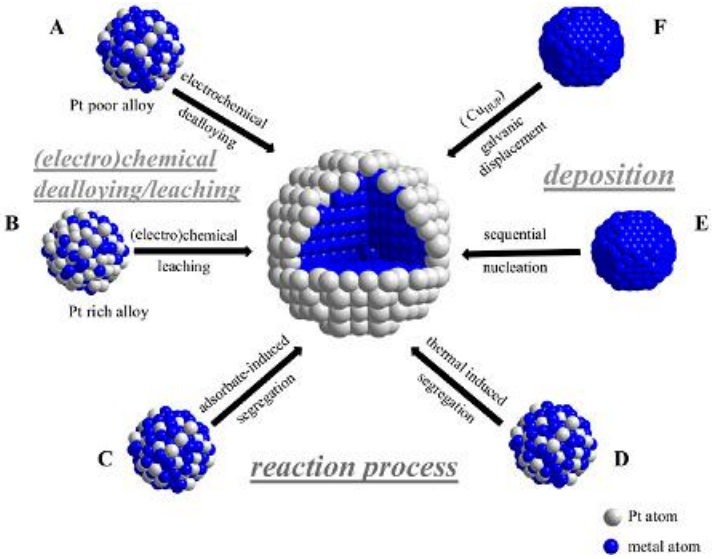

Fig 1.11: various synthesis methods for core shell nanoparticles

(Figure adapted from ***J. Phys. Chem. Lett., 2013, 4, 3273–3291)***

1.5.2. Electrochemical dealloying:

Dealloying is a phenomenon where dissolution of less noble metals takes place from a uniform multimetallic alloy leading to the formation of Pt enriched surface. In this process Pt shell of various layers are formed over a core. various core shell nano particles of Cu-Pt[48], Pt-

Ni[49], and Cu-Pd[50] were prepared and studied extensively with this method and characterized by X-ray techniques.

1.5.3. Electrochemical leaching:

In this nonprecious metal as soon as comes in contact with acid dissolves from near surface region leaving behind Pt vacancies. Thereby fast diffusing Pt atoms gradually enrich the surface. The rough Pt enriched surface is called as Pt skeleton.

1.5.4. Colloidal synthesis:

This process provides a facile method of synthesizing Pt shell over already synthesized cores or seeds. With this method it is possible to deposit Pt shell over core in monolayer or multilayer fashion and easy to achieve monodispersity[51]. Many core shell nanoparticle such as Au-Pt[52], Cu-Pt[53] can be prepared in this manner. Solvents, reducing agents, capping agents play a strong role in deposition of shell over core and also in determining the active sites and catalytic activities.

1.5.5. Under potential deposition:

In this under potential deposition technique, Cu will be used as a sacrificial layer for the formation of shell. In this technique, first Cu will be deposited over a selected core by applying a potential slightly less negative than equilibrium potential of metal that is intended to form shell. Later by applying the reduction potential, Pt will be deposited by removing the Cu. Adzic and coworkers have pioneered this technique. It is possible to deposit Pt shell in the form of thin layer which results in high mass activity[54].

1.5.6. Physical vapor deposition:

This is used by many surface scientists. At elevated temperature and at high vaccum conditions, a pure vaporized metal will be deposited on to a support material by condensation. This method is rarely used when compared to above mentioned methods.

1.6. Electorcatalytic ORR activity on various carbon supports:

Till today carbon decorated with Pt nanoparticles remained as state of art catalyst for ORR

activity. But during fuel cell operating condition this carbon black undergoes corrosion as discussed earlier. Hence this carbon black was replaced with several other carbon materials such as CNTs, graphite, carbon nano fibers etc. But the problem still remained and yet to be completely mitigated. Hence in this similar lines semiconducting metal was looked as support materials. These semiconducting systems offer advantages such as high corrosion resistance, cocatalytic activity and high specific surface area. Several semiconducting material such as WO_3 [55], SnO_2[56], NbO_2, TiO_2, RuO_2-SiO_2, TaB_2, TiC were employed. Many studies have proved that strong metal substrate interaction (SMSI) between Pt nanoparticles and these semiconducting materials would be the reason for enhanced activity. It is very well known that the SMSI between the support materials and Pt nanoparticles alter the electronic properties of Pt nanoparticles either by up shift or down shift because of which there will be enhanced activity and durability. Hwang et al have decorated Pt nanoparticles on $Ti_{0.7}Mo_{0.3}O_2$ as support and found superior activity than commercially available catalyst as shown in Fig 1.12. Electron transfer from this support to Pt thereby shifting d-band center could be the reason for enhancement and durability[57].

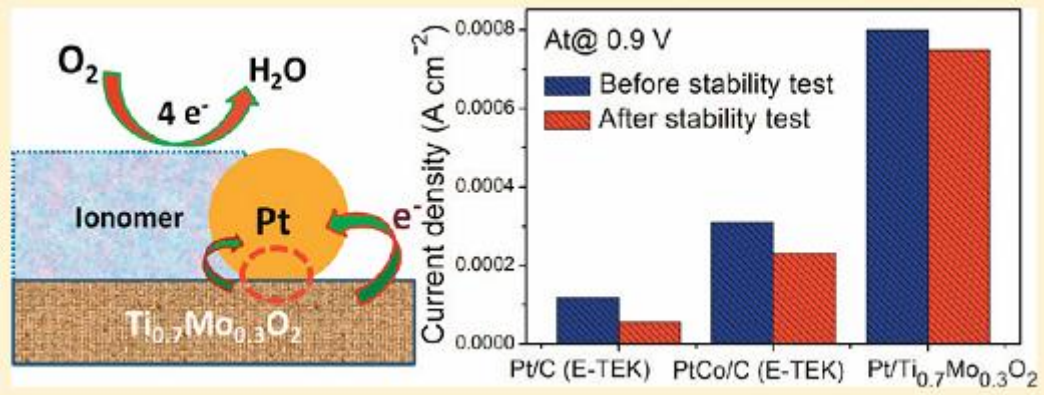

Fig 1.12: Comparision of $Ti_{0.7}$ $Mo_{0.3}O_2$ with commericial catalyst

(Figure adapted from **J. Am. Chem. Soc., 2011, 133, 11716–11724*)***

Of the semiconducting materials that were used above, TiO_2 has edge over others as it possess high mechanical strength, environmental safety and stabiity to electrochemical and electrocatalytic acitivity. This TiO_2 is available in varied morphological forms such as nanoparticles, nanorods, nanoplates and nanotubes. Of all the forms, nanotubes will have extra advantages such as high orientation and uniformity, facile preparation method (anodization method). These nanotubes provide precise design control for decoration of nanoparticles, and demand lower Pt loading[58],[6].

1.7. Introduction to titania nanotubes (TNTs):

Titania nanotubes have many important properties such as easy preparation, low cost preparation, high surface to volume ratio. It was used in many application such as photocatalysis, solar cells, for hydrogen, sensors, storage device, and also as catalyst support, waste water treatment, biomedical applications.

There are various methods for the synthesis of nanotubes such as hydrothermal method, sol-gel method, anodization method, template method.

1.7.1. Hydrothermal method:

In this requsite amounts of anatase TiO_2 nanopowders were mixed with 10 M NaOH in a perfluoroalkoxy (PFA) bottle and stirred for 1 h. Then the mixture was poured into a Teflon-lined stainless steel autoclave and heated at 110 °C under autogenous pressure for 90 h. There after the mixture was cooled to room temperature. The resultant precipitate was separated by centrifugation and rinsed with diluted HCl aqueous solution and deionized water numerous times till the pH 7 is obtained. The collected precipitate was dried at 110 °C overnight in an oven. There after sample will be annealed at 400 °C[59].

1.7.2. Solvothermal method:

This method is similar to hydrothermal synthesis except here only nonaqueous solvents are used and here the reaction is performed at even high temperatures. It is easy to control size, shape and crystallinity. This method is mainly used for synthesis of nanoparticles.

1.7.3. Sol- gel method:

In this a sol is prepared by polymerizing and hydrolyzing metal oxides. This sol is converted to gel after complete polymerization and hydrolysis. Complete polymerization and loss of solvent leads to the transition from the liquid sol into a solid gel phase. Thin films can be produced on a piece of substrate by spin-coating or dip-coating. A wet gel will form when the sol is cast into a mold, and the wet gel is converted into a dense ceramic with further drying and heat treatment. A highly porous and extremely low density material called an aerogel is obtained if the solvent in a wet gel is removed under a supercritical condition. Ceramic fibers can be drawn from the sol when the viscosity of a sol is adjusted into a proper viscosity range. Ultrafine and uniform ceramic powders are formed by precipitation, spray pyrolysis, or emulsion techniques. Under proper conditions, nanomaterials can be obtained[60].

1.7.4. Anodization method:

Of all the methods that were mentioned above, anodization method is most easy, cost effective method. It is easy to control tube length and diameter with this method. This method consists of two electrode system in which titaniaum foil acts as working electrode and platinum foil as counter electrode as illustrated in Fig 1.13.

1.7.5. Formation mechanism of TNT:

In this, fluoride ion plays an important role. It acts as a dissoluting agent of oxide layer[61]. Initially oxidation of metal takes place from Ti to Ti^{4+} according to equation A

$Ti \rightarrow Ti^{4+} + 4e^-$ **equation A**

$Ti^{4+} + 2H_2O \rightarrow TiO_2 + 4H^+$ **equation B**

$TiO_2 + 6F^- + 4H^+ \rightarrow (TiF_6)^{2-} + 2H_2O$ **equation C**

Ti^{4+} will react with O^{2-} of H_2O and forms an oxide layer. H^+ ions are created according to equation B and F^- ions migrates to the sites of H^+ to maintain electroneutrality and further compete with O^{2-} and where there are no longer H^+ sites are available, F^- reacts with oxide layer and form fluoride complex by dissolving TiO_2. This creates negatively charged cation vacancies at the oxide and would migrate to the metal/oxide interface due to the potential gradient across gradient. Because of these cation vacancies, Ti^{4+} ions occupy these vacant sites and would facilitate the reaction A. During this state nanopores were nucleated on the oxide surface. Since the initial small pores are very narrow, a mass of H^+ ions are generated at the bottom of the pore, where the Ti came out of the metal and dissolved in the solution and the concentration of HF inside the pores increases rapidly. High concentration of HF makes the wall of pores dissolves until the adjacent pore walls disappear. At the same time, the integration by small pores resulted in the appearance of larger pores. Simultaneously, the enhanced electric field-assisted dissolution at the pore bottom leads to deepening of the pore and the voids starts forming. Due to the applied electric field, the Ti–O bond undergoes polarization and is weakened which promotes the dissolution of the metal oxide. The entire process of formation of nanotubes is illustrated in Fig 1.14.

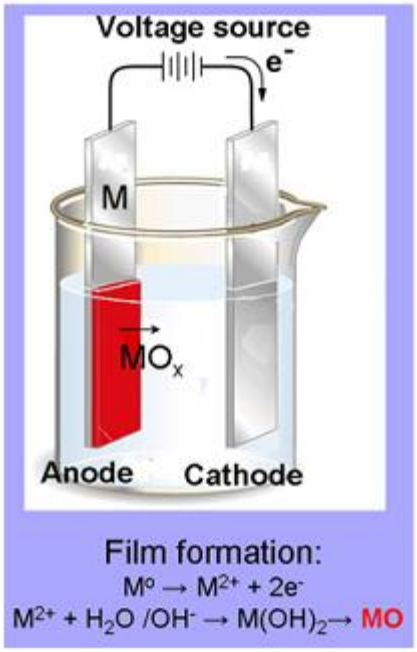

Fig 1.13: Illustration showing the experimental set up for anodization method.

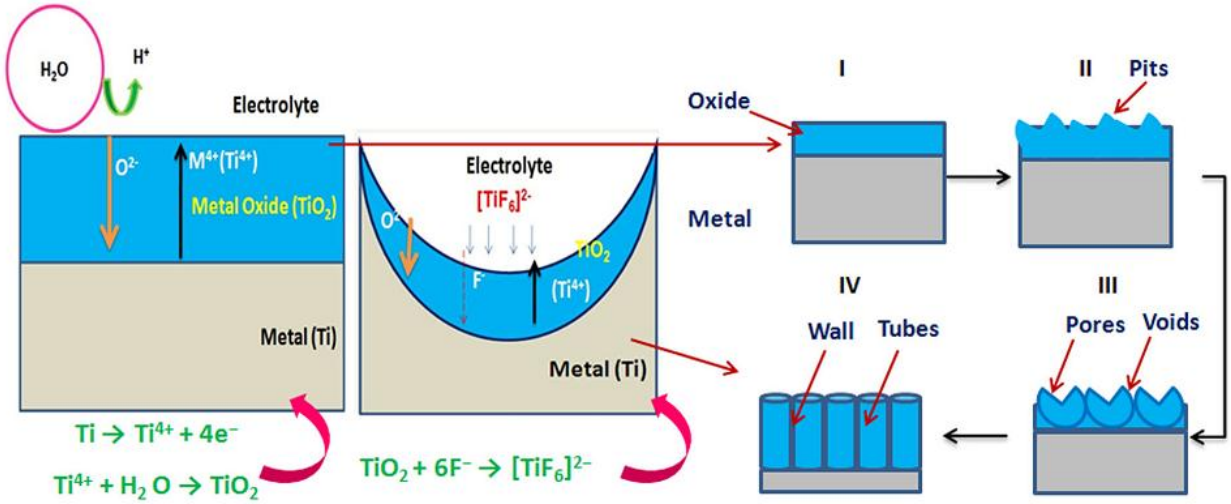

Fig 1.14: Illustration showing the formation mechanism of titania nanotubes.

(Figure adapted from ***J. Bio- Tribo-Corrosion, 2015, 1, 28***)

1.7.6. Influence of various factors on titania nanotubes:

1.7.6.1 Anodization:

One of the key factors that influence the nanotube formation is anodization. When the applied voltage is in the range of 1 to 25 V, nanotube diameter was found to be in the range of 15-20 nm. Nanotubes were obtained even when the applied potential was as low as 1 V but the morphology was found to be web like instead of clear tubular morphology. When electrolyte containing glycerol water system, nanotube diameter was grown from 20 to 300 within the potential range 2 and 40 V[62]. If the anodization is only for short period of time then tubes will be connected with each other through the side walls. If the anodization is continued for longer time then tubes will be separated with each other through the dissolution of side walls.

1.7.6.2. Effect of electrolytes:

Two types of electrolytes are used for TNT synthesis. They are organic/neutral electrolyte and aqueous/acidic electrolytes. Aqueous electrolytes will have high water content and organic electrolytes will have low water content. In organic electrolytes such as $(NH_4)H_2PO_4/NH_4F$ and $(NH_4)_2SO_4/NH_4F$ nanotubes with longer length and well organized layers will be obtained. Where as in acidic electrolytes thin layered nanotubes will be obtained[61].

1.7.6.3. Effect pf pH

The pH of the electrolytes will determine the aspect ratio and self organization behavior of TNT. Oxide dissolution rate is higher at low pH than the higher pH and therefore thinner tubes are obtained at low pH. During the anodization process, the pH of the electrolyte will be altered due to the hydrolysis reaction. Due to this hydrolysis there will be local acidification which leads to TiO_2 dissolution. Thereby providing more protective environment against dissolution, longer tubes will be obtained.

1.7.6.4 Effect of voltage:

Pore diameter and thickness will be controlled by voltage. At low applied voltage, shorter nanotubes with few nm in diameter will be obtained.

1.7.6.5. Effect of temperature:

With the increase in temperature during the anodization, then pore formation will be promoted. This is because at higher temperature viscocity of the electrolyte will decrease and therefore the etching rate will be high. At low temperatures, viscocity will be lower and the etching rate is low. Hence nanotubes with less pore size will be formed.

1.8. Introduction to important parameters in electrochemical studies:

Electrochemistry is a branch of chemical sciences which deals with the links between electricity and chemical reactions. It is the study of chemical changes that occurs by

1) The passage of electric current across a medium,

2) The production of electric energy by chemical reactions,

and also deals with the electrolyte solutions and the chemical equilibria that occur in them. Electrochemical techniques are nothing but the measurement of current, potential, charge and their relationship. It is an interplay between current and chemistry.

1.8.1. Mass transport

Mass transport occurs in an electrochemical cell when the material moves from the bulk liquid phase to the electrode surface. This mass transport can happen in the following three ways.

1) *Convection*- The material moves from the bulk liquid phase to the electrode surface due to stirring a solution, rotating an electrode.

2) *Migration*- Due to the interaction of molecules with the electric field that exists near the electrode as shown in the Fig 1.15.

3) *Diffusion*-This is the simplest method when the chemical potential is not uniform, molecules move from a region of higher potential to a region of lower potential.

Diffusion is effected by one or more permeable or semi permeable phase boundaries that exist in the solution. In electrochemistry, the electrode usually acts as an impermeable phase boundary. Sometimes the diffusion barrier interact with the solute via an electrochemical reaction. Rate of mass transport is measured in terms of Flux. This is an important parameter because of its relationship to electrode current.

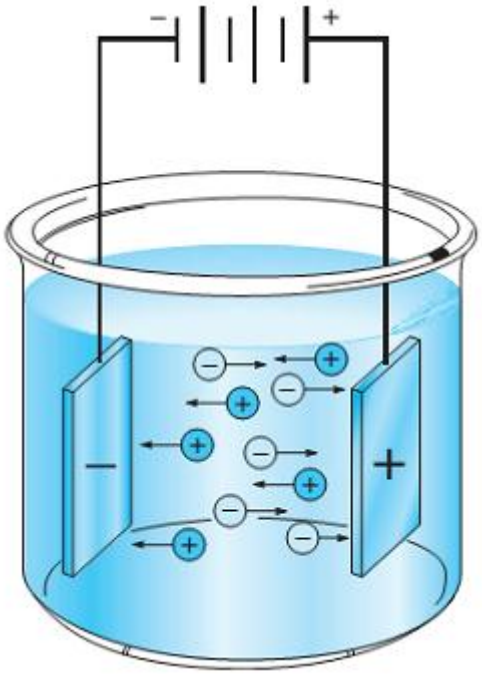

Fig 1.15: Illustration showing the migration of ions in presence of electric field

1.8.2. Electrochemical measurements

1.8.2.1. Voltammetry

Voltammetry is an important technique in electrochemistry. It combines a group of techniques which gives the information about analyte derived from the measurement of current as a function of applied potential under conditions that promote polarization of an indicator, or working electrode. Voltammetry is widely used in the fields of physical, chemical, and biological fields for non analytical purposes including the fundamentals of oxidation and reduction process. The voltammetric measurements are done in an unstirred solution. The scan begins at a potential E_i at which no reaction is taking place and then continues through the standard electrode potential. The diffusion layer will not be effected during electrolysis of the solute, because the electrode is stationary.

1.8.2.2. Cyclic Voltammetry*:*

Cyclic voltammetry which is also known as "CV" is most popularly used and extensively studied among voltammetric techniques. Cyclic voltammetry has wide applications in the study of oxidation/reduction reactions, in finding the reaction intermediates and also in observing the products formed near the electrodes[63]. It is also like linear sweep voltammetry where the working electrode potential is ramped linearly versus time as depicted in Fig 1.16. In this, first the applied potential is swept in one direction and the current is measured. This is called forward scan. After this, the potential is inverted and the current is measured. This is called as reverse scan. A cyclic voltammetric measurement may make use of one full cycle, a half cycle or multiple cycles.

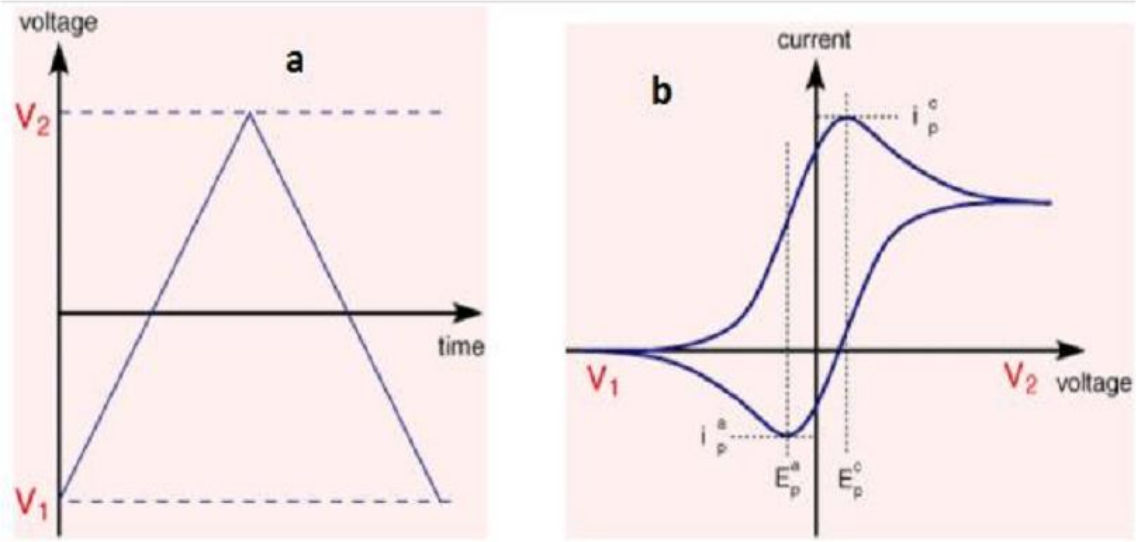

Fig 1.16: (a) Potential as a function of time and (b) current as a function of voltage for cyclic voltammetry

1.8.2.3. Rotating disc electrode:

In the year 1925, Dr Benjamin Levich for the first time described the theory of mass transport current for the first time at rotating disc electrode (RDE). Fig 1.17 gives the schematic illustration of RDE. This rotating disc is used to avoid the effect of convection of molecules. In this technique the solution under observation will be stirred at a desired speed. Because of laminar flow, material will be conveyed to electrode surface from bulk solution in a steady state. In this technique the portion of solution that is close to electrode rotates along with electrode so when viewed from electrode keeping it as frame of reference and solution remains as stagnant. The thickness of this stagnant layer can be approximated with the formula

$$\delta_H = 3.6\left(\frac{\vartheta}{\omega}\right)^{\frac{1}{2}}$$

where ϑ is kinematic viscocity, ω is rotation speed of electrode.

In this technique the movement of ions from bulk to stagnant layer occurs by convection and to electrode surface solely by diffusion. Thus through this method convection can be completely avoided. This diffusion layer also has certain thickness which can be measured by

$$\delta_f = 1.61\left(D_f\right)^{\frac{1}{3}}(\vartheta)^{\frac{1}{6}}(\omega)^{\frac{-1}{2}}$$

With the levich equation it is possible to find the limiting current as follows

$$i_l = 0.0620FAD^{\frac{2}{3}}(\vartheta)^{\frac{-1}{6}}(\omega)^{\frac{-1}{2}}C_o$$

A plot of inverse of current density and inverse of RPM provides information on kinetics of reaction.

$$\frac{1}{l} = \frac{1}{l_k} + \frac{1}{i_l} = \frac{1}{l_k} + \frac{1}{0.62nFAC\omega^{\frac{1}{2}}V^{\frac{-1}{6}}D^{\frac{2}{3}}}$$

Where I_L = Diffusion Limiting Current (A)

n= number of electrons transferred to oxygen

I_L= Diffusion Limiting Current (A)

F = Faraday constant (C/mol)

A =electrode area (cm^2)

D= diffusion coefficient (cm^2/s)

W= angular rotation rate of the electrode (rad/s)

V= kinematic viscosity (cm^2/s)

C= analyte concentration (mol/cm^3)

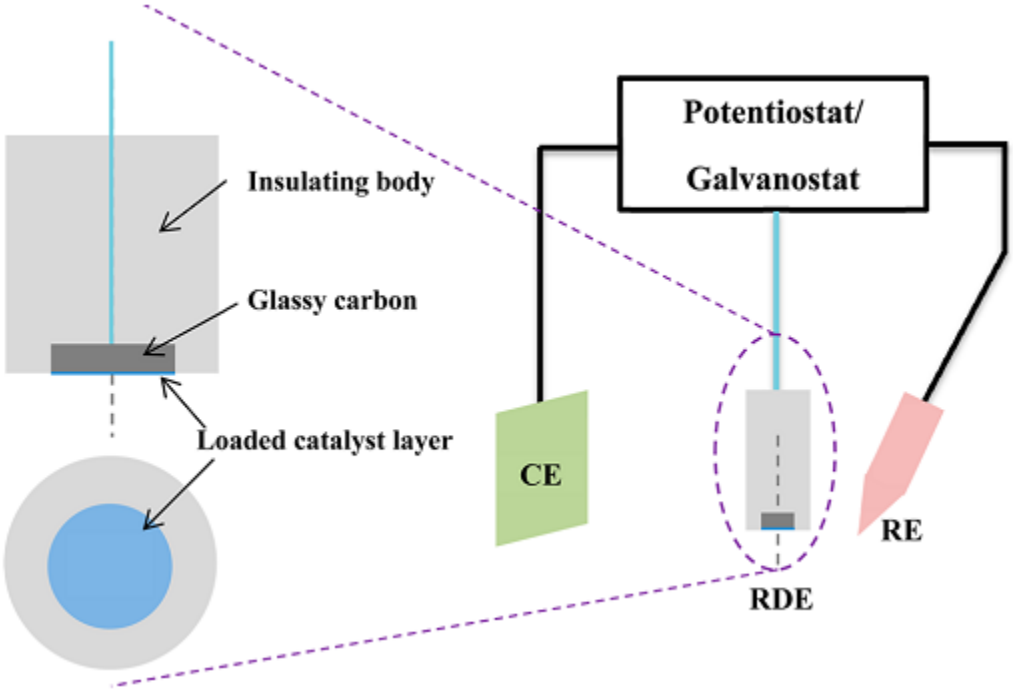

Fig 1.17: Schematic illustration of the typical RDE

1.9. Research Outlook:

The above mentioned work inspires me to work towards the utilization of an alternative support material to carbon owing to its problems such as cost, corrosion and aggregation of nanoparticles. In this work I utilized titania nanotubes as support material for decoration of nanoparticles. Using this as support material I aim to decorate the titania nanotubes with core shell nanoparticles of platinum and gold in ultrafast manner. Also I utilized titania nanotubes in conjuncton with functionalized acetylene black as composite material for deocartion of Pt nano particles and utilized as electrocatalyst materials for ORR in both aqueous and nonaqueous medium.

References:

1 E. Delarue, H. Lamberts and D. Ã. William, *Energy*, 2007, **32**, 1299–1309.

2 G. G. Harding, *J. Power Sources*, 1999, **78**, 193–198.

3 C. Eric, *Fuel cell technology handbook*, 2003, CRC Press.

4 S. J. Peighambardoust, S. Rowshanzamir and M. Amjadi, *Review of the proton exchange membranes for fuel cell applications*, Elsevier Ltd, 2010, 35.

5 A. Dupuis, *Prog. Mater. Sci.*, 2011, **56**, 289–327.

6 M. Manikandan, R. Vedarajan, R. Kodiyath, H. Abe, S. Ueda, A. Dakshnamoorthy, N. Rajalakshmi, K. S. Dhathathreyan and G. V Ramesh, *J. Nanosci. Nanotechnol.*, 2016, **16**, 8269-8278.

7 I. Mahesh and A. Sarkar, *ChemElectroChem*, 2016, **5**, 836–845.

8 J. C. Meier, C. Galeano, I. Katsounaros, J. Witte, H. J. Bongard, A. A. Topalov, C. Baldizzone, S. Mezzavilla, F. Schüth and K. J. J. Mayrhofer, *J. Nanotecnol*, 2014, **5**,44–67.

9 J. Lu, L. Li, J. B. Park, Y. K. Sun, F. Wu and K. Amine, *Chem. Rev.*, 2014, **114**, 5611–5640.

10 J. Wang, Y. Li and X. S. A, *Nano Energy*, 2013, **2**, 443–467.

11 Y. Shao, S. Park, J. Xiao, J. G. Zhang, Y. Wang and J. Liu, *ACS Catal.*, 2012, **2**, 844–857.

12 L. L. Zhang, Z. L. Wang, D. Xu, X. B. Zhang and L. M. Wang, *Int. J. Smart Nano Mater.*, 2013, **4**, 27–46.

13 Z. Peng, S. A. Freunberger, L. J. Hardwick, Y. Chen, V. Giordani, F. Barde, P. Novak, D. Graham, J. M. Tarascon and P. G. Bruce, *Angew. Chem. Int. Ed.*, 2011, **50**, 6351–6355.

14 J. S. Hummelshoj, J. Blomqvist, S. Datta, T. Vegge, J. Rossmeisl, K. S. Thygesen, A. C. Luntz, K. W. Jacobsen and J. K. Nørskov, *J. Chem. Phys.*, J. Chem. Phys., 2010, **132**, 071101-071105.

15 K. Xu, *Chem. Rev.*, 2004, **104**, 4303–4417.

16 J. Read, K. Mutolo, M. Ervin, W. Behl, J. Wolfenstine, A. Driedger and D. Foster, *J. Electrochem. Soc.*, 2003, **150**, A1351-A1356.

17 D. Aurbach, *J. Electrochem. Soc.*, 1989, **136**, 3198-3205.

18 R. J. Taylor and A. A. Humffray, *J. Electroanal. Chem*, 1975, **64**, 63–84.

19 M. Zhang, Y. Yan, K. Gong, L. Mao, Z. Guo and Y. Chen, *Langmuir*, 2004, **20**, 8781–8785.

20 G. Ju and K. Tammeveski, *J. Electroanal. Chem.*, 2006, **597**, 119–126.

21 S. Maldonado and K. J. Stevenson, *J. Phys. Chem. B.*, 2005, **109** (110) 4707–4716.

22 M. G. Sullivan, R. Kotz and O. Haas, *J. Electrochem. Soc*., 2000, **147**, 308–317.

23 A. E. Russell, *Faraday Discuss.*, 2009, **140**, 9–10.

24 N. A. Vante and H. Tributsch, *Nature*, 1986, **323**, 431–432.

25 P. Strasser, S. Koh, T. Anniyev, J. Greeley, K. More, C. Yu, Z. Liu, S. Kaya, D. Nordlund, H. Ogasawara, M. F. Toney and A. Nilsson, *Nat. Chem.*, 2010, **2**, 454–460.

26 Y. Nie, L. Li and Z. Wei, *Chem. Soc. Rev.*, 2015, **44**, 2168–2201.

27 C. Campbell, *Annu. Rev. Phys. Chem.*, 1990, **41**, 775–837.

28 S. J. Tauster, S. C. Fung, R. T. K. Baker and J. A. Horsley, *Science*, 1981, **211**, 1121–1125.

29 J. Perez, H. M. Villullas and E. R. Gonzalez, *J. Electroanal. Chem.*, 1997, **435**, 179–187.

30 R. Narayanan and M. A. El-Sayed, *J. Phys. Chem. B*, 2005, **109**, 12663–12676.

31 C. Wang, H. Daimon, T. Onodera, T. Koda and S. Sun, *Angew. Chem. Int. Ed.*, 2008, **120**, 3644–3647.

32 T. Yu, D. Y. Kim, H. Zhang and Y. Xia, *Angew. Chem. Int. Ed.*, 2011, **50**, 2773–2777.

33 V. R. Stamenkovic, B. Fowler, B. S. Mun, G. Wang, P. N. Ross, C. A. Lucas and N. M.

Markovic, *Science.*, 2007, **315**, 493-497.

34 M. D. Macia, J. M. Campiña, E. Herrero and J. M. Feliu, *J. Electroanal. Chem.*, 2004, **564**, 141–150.

35 M. Nesselberger, S. Ashton, J. C. Meier, I. Katsounaros, K. J. J. Mayrhofer and M. Arenz, *J. Am. Chem. Soc.*, 2011, **133**, 17428–17433.

36 Y. Kawamura and R. Jinnouchi, *ECS Trans.,* 2013, **50**, 1321–1331.

37 E. Fabbri, S. Taylor, A. Rabis, P. Levecque, O. Conrad, R. Kötz and T. J. Schmidt, *ChemCatChem*, 2014, **6**, 1410–1418.

38 M. Shao, Q. Chang, J.-P. Dodelet and R. Chenitz, *Chem. Rev.*, 2016, **116**, 3594–3657.

39 V. R. Stamenkovic, B. S. Mun, M. Arenz, K. J. J. Mayrhofer, C. A. Lucas, G. Wang, P. N. Ross and N. M. Markovic, *Nat. Mater.*, 2007, **6**, 241–247.

40 S. Chen, P. J. Ferreira, W. Sheng, N. Yabuuchi, L. F. Allard and Y. Shao-Horn, *J. Am. Chem. Soc.*, 2008, **130**, 13818–13819.

41 Y. H. Chung, D. Y. Chung, N. Jung, H. Y. Park, S. J. Yoo, J. H. Jang and Y. E. Sung, *J. Phys. Chem. C*, 2014, **118**, 9939–9945.

42 I. E. L. Stephens, A. S. Bondarenko, U. Grønbjerg and I. Chorkendorff, *Energy Environ. Sci.*, 2012, **5**, 6744–6762.

43 H. Wang, L. Chen, Y. Feng and H. Chen, *Acc. Chem. Res.*, 2013, **46**, 1636–1646.

44 M. Oezaslan, F. Hasché and P. Strasser, *J. Phys. Chem. Lett.*, 2013, **4**, 3273–3291.

45 G. E. Ramírez-Caballero, Y. Ma, R. Callejas-Tovar and P. B. Balbuena, *Phys. Chem. Chem. Phys.*, 2010, **12**, 22092-2218.

46 D. V. Esposito, S. T. Hunt, Y. C. Kimmel and J. G. Chen, *J. Am. Chem. Soc.*, 2012, **134**, 3025–3033.

47 E. F. Holby, W. Sheng, Y. Shao-Horn and D. Morgan, *Energy Environ. Sci.*, 2009, **2**, 865-871

48 R. Yang, P. Strasser and M. F. Toney, *J. Phys. Chem. C*, 2011, **115**, 9074–9080.

49 Y. Liu, C. M. Hangarter, U. Bertocci and T. P. Moffat, *J. Phys. Chem. C*, 2012, **116**, 7848–7862.

50 H. Borchert, E. V. Shevchenko, A. Robert, I. Mekis, A. Kornowski, G. Grübel and H. Weller, *Langmuir*, 2005, **21**, 1931–1936.

51 M. H. Lee and J. S. Do, *J. Power Sources*, 2009, **188**, 353–358.

52 D. Zhao and B. Q. Xu, *Angew. Chem. Int. Ed.*, 2006, **45**, 4955–4959.

53 S. Zhou, B. Varughese, B. Eichhorn, G. Jackson and K. McIlwrath, *Angew. Chem. Int. Ed.*, 2005, **44**, 4539–4543.

54 J. X. X. J. X. Wang, H. Inada, L. Wu, Y. Zhu, Y. Y. M. M. Choi, P. Liu, W. P. P. W. P. Zhou and R. R. R. R. Adzic, *J. Am. Chem. Soc.*, 2009, **131**, 17298–17302.

55 H. Chhina, S. Campbell and O. Kesler, *J. Electrochem. Soc.*, 2007, **154**, B533-B539.

56 N. R. Elezovic, V. R. Radmilovic, J. Kovac, B. M. Babic, L. M. Gaijic-Krstajic and N. V. Krstajic, *RSC Adv.*, 2015, **5**, 15923–15929.

57 V. T. T. Ho, C. J. Pan, J. Rick, W. N. Su and B. J. Hwang, *J. Am. Chem. Soc.*, 2011, **133**, 11716–11724.

58 L. Yang, W. Yang and Q. Cai, *J. Phys. Chem. C*, 2007, **111**, 16613–16617.

59 L. B. Fen, T. K. Han, N. M. Nee, B. C. Ang and M. R. Johan, *Appl. Surf. Sci.*, 2011, **258**, 431–435.

60 M. Malekshahi Byranvand, A. N. Kharat, L. Fatholahi and Z. M. Beiranvand, *JNS*, 2013, **3**, 1–9.

61 K. Indira, U. K. Mudali, T. Nishimura and N. Rajendran, *J. Bio- Tribo-Corrosion*, 2015, **1**, 28-50.

62 J. M. Macak, H. Tsuchiya, A. Ghicov, K. Yasuda, R. Hahn, S. Bauer and P. Schmuki, *Curr. Opin. Solid State Mater. Sci.*, 2007, **11**, 3–18.

63 A. J. Bard, L. R. Faulkner, N. York, C. @bullet, W. Brisbane and S. E. Toronto, *ELECTROCHEMICAL METHODS Fundamentals and Applications*, 1944.

Chapter 2

Ultrafast Electrochemical Deposition of Core Shell Metal Nanoparticles on TiO_2 Nanotubes for Electrocatalytic Applications

2.1. Abstract:

In this work, we report a rapid and reliable electrochemical synthetic method for decoration of core shell nanoparticles of Pt and Au over titania nanotubes (TNTs). The decoration was achieved in an ultrafast manner within a span of 60 sec without using any reducing agents or any use of further thermal of chemical treatments. The successful formation of double shell nanoparticles such as AuPt@Pt-TNT, PtAu@Au-TNT and single shell nanoparticles such as Pt@Au-TNT was characterized by using transmission electron microscopy (TEM), X-ray photo electron spectroscopy (XPS), energy dispersive X-ray spectroscopy (EDS) and high-angle annular dark-field scanning transmission electron microscopy (HAADF-STEM) techniques. The synthesized core shell nanoparticles showed good electrocatalytic activity towards aqueous and non-aqueous ORR applications.

2.2. Introduction:

Development of new energy sources, energy storage and energy conversion device has become most pressing issue because of continuous depletion in fossil fuels[1]. One of the promising technologies that can serve as an alternative to fossil fuels is fuel cell technology which can provide clean and efficient energy[2]. Recently there has been a continuous special interest in development of Polymer Electrolyte Membrane Fuel Cells (PEMFCs) which employs hydrogen as fuel[3]. Efficient catalysts facilitate oxidation of hydrogen and reduction of oxygen thereby generating electrical energy and water. At present, Pt-based materials are the most widely used catalysts for oxygen reduction reaction (ORR) in PEMFCs as these materials offer high chemical stability, high catalytic activity, superior work function and high exchange current density[4]. In PEMFCs, conductive porous materials are commonly employed as support materials as they provide maximum utilization of Pt and also reduce charge transfer resistance. Conventionally, carbon materials are used as support materials for Pt as they provide high surface area. However under operating fuel cell conditions, carbon support undergoes severe corrosion which results in Pt aggregation and detachment leading to rapid degradation in performance. Hence, there is a need to search for alternatives which can act as support materials. Semiconducting metal oxides such as titanium dioxide[5,6] , cerium oxide[7], molybdenum oxide[8], tungsten oxide[9] or tin oxide[10] can be alternatives to carbon based supports as they are corrosion resistant and offer strong metal substrate interaction[11]. Of these metal oxides, TiO_2 can be a potential alternative as they are environmentally friendly, highly stable and resistant to corrosion and possess high mechanical strength and very interesting with its strong metal substrate interaction. Of the various morphological forms of TiO_2 such as nanoparticles, nanorods, nanoplates and nanotubes, nanotubes play a crucial role due to ease of synthesis, size tunability, good chemical inertness[12], cost effectiveness and high surface area[13]. Fabrication of 1D titania nanotubes, by electrochemical anodization appears to be most suitable approach[14]. The second critical issue that needs to be dealt with is the scarcity of the Pt metal because of which the fuel cell prices are sky rocketing and difficult to bring in to market and meet future demands. Also, Pt is vulnerable to CO poisoning which makes the catalytic activity goes down[15]. Thus several strategies have been developed to reduce the amount of Pt such as utilizing Pt in the form of alloys, minimizing Pt content in the form of core shell structures or replacing Pt completely with less expensive metals[16]. Of these, modification of Pt in the form of core shell nanoparticles proved to be a viable option to decrease Pt content and to increase durability. There are wide variety of metals that are available that can be used with Pt such as Co[17], Ni[18], Fe[19] and Au but of these Au can be more reliable as Au is more

abundant in nature, corrosion resistant and dissolution resistant during fuel cell operating conditions[20]. Therefore utilizing Au and Pt, there is an abundant opportunity to minimize Pt content and also to enhance catalytic activity. A vast amount of literature is available for synthesis of core shell nanoparticles on carbon by various methods such as wet chemical method[21], spontaneous deposition[20], redox displacement of copper by under potential deposition[16], but all these methods are either thermally driven which requires high temperatures, tedious, time consuming, involves use of surfactants and also involves use of gases such as Ar, N_2 and H_2. Further synthesis has been done on carbon which is prone for corrosion. Till date under potential deposition of Pt by galvanic replacement of Cu for achieving decoration of Pt on Au in monolayer fashion is widely examined. But recent studies by Russel et al suggested that 1) Cu may not yield uniform shell[22] and 2) also random selection of potential just above where bulk deposition occurs may lead to non-uniform coverage over core[23], 3) preparation of core material is time consuming. Figure 2.1 gives glimpse of different core shell nanoparticles along with time that is required to prepare core shell nanoparticles. Table 2.1 gives the required, chemicals needed with reaction conditions to prepare core shell nanoparticles.

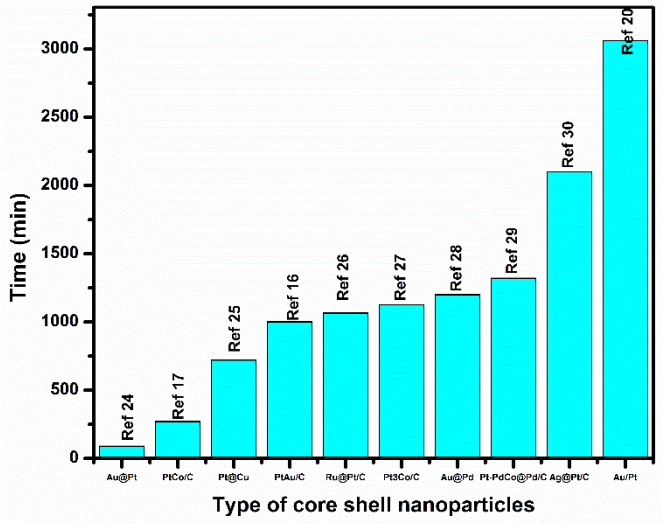

Fig 2.1: Different types of core shell nanoparticles along with time required for synthesis.

Table 2.1: The details of preparation of various core shell nanoparticles with different reaction conditions along with time

Type of synthesis	Type of core shell	Chemicals and High temparature	Time required for synthesis (min)	References
Wet chemical method	Au@Pt	$HAuCl_4$, Trisodium citrate, $NaBH_4$, Ascorbic acid, H_2PtCl_6	90	24
Impregnation method	PtCo/C	$H_2PtCl_6.6H_2O$, $CoCl_2.6H_2O$, H_2/N_2 (gases) 700 °C, Vulcan XC 72	270	17
Galvanic displacement	Pt@Cu	$CuSo_4.5H_2O$	720	25
Wet chemical and galvanic displacement	PtAu/C	$HAuCl_4$, Tetraoctyl ammonium bromide, Decane thiols, $NaBH_4$, Carbon Black, H_2SO_4 $CuSO_4$, K_2PtCl_4, H_2/N_2 (gases), 300 °C	1002	16
Polyol method	Ru@Pt/C	$Ru(acac)_2$, PVP, $H_2PtCl_6.6H_2O$, Ethylene Glycol, Vulcan XC 72 R, HNO_3	1065	26
Impregnation method	Pt_3Co/C	$H_2PtCl_6.6H_2O$, $CoCl_2.6H_2O$, Vulcan XC 72 R, H_2/N_2 (gases), 700 °C	1125	27
Wet chemical method	Au@Pd	$HAuCl_4.3H_2O$, Olelyamine, $Pd(acac)_2$	1200	28
Impregnation and Spontaneous method	Pt-PdCo@Pd/C	$CoCl_2.6H_2O$, $PdCl_2$, K_2PtCl_4, Vulcan XC 72 R, H_2/N_2 (gases), 500 °C	1320	29
Chemical Method	Ag@Pt/C	Formaldehyde, Ethylene glycol, $AgNO_3$,Vulcan XC 72 R, NH_4OH, $NaPtCl_6$	2100	30
Spontaneous deposition	Au/Pt	$HAuCl_4$, $NaBH_4$, Vulcan XC 72 R, K_2PtCl_4	3060	20

Some researchers such as Tada et al have synthesized supported core shell nanoparticles of Au core and Pt shell on TiO_2 particles by two step method which involves wet chemical method and photocatalytic method[31] and Sung et al reported decoration of core shell nanoparticles on TNTs which involves time consuming reduction process [32]. Therefore, there is a great demand to deposit core shell nanoparticles on titania nanotubes in easy, nontoxic and sustainable method for electrocatalytic applications and also for longevity[33]. Towards this end, we present a simple and clean method for decoration of core shell nanoparticles without using any extraneous reagents by electrochemical deposition. The formation of core shell was confirmed by STEM-HAADF and EDS mapping. In this study highly ordered TNTs which were synthesized by electrochemical anodization were employed. Electrochemically deposited metal nanoparticles of very high purity, were formed rapidly, and have good adhesion to the TNT. Three variants of this electrodeposition can be envisioned from Pt and Au, as bimetallic core shell nanoparticles with variation in shell

and core composition. This work throws light upon synthesis of three different core shell nano particles. The novelty of this work lies in synthesis and decoration of core shell nanoparticles over TNT within a short span of 60 sec without any further purification process.

2.3. Experimental:

2.3.1. Synthesis of titania nanotubes:

Synthesis of titania nanotubes was carried out by anodization as reported previously[34]. Ti foils of high purity were obtained from Nilaco corporation. Prior to anodization, these foils were polished with sandpapers of different grades ranging from P-220, P-600, P-800, P-1200 and chemically etched in solution containing HF: HNO_3: H_2O in 1:3:16 volume ratio, respectively. Later they were washed in acetone, methanol, isopropanol and deionized water and dried in air. Then anodization procedure was carried out by two electrode set up with Pt as counter electrode and Ti as working electrode in ethylene glycol (Kanto chemical, Tokyo, Japan) and water (90:10) containing 0.5 wt % ammonium fluoride (Kanto chemical, Tokyo, Japan). Anodization was carried out at room temperature under ultrasonication by applying constant potential of 50 V for 150 min by using a DC power supply (Kikusui PAS60-6). After completion of anodization, these TNTs were annealed at 300° C for 90 min to obtain anatase phase.

2.3.2. Deposition of core shell nanoparticles on TNTs by electrochemical reduction:

Electrochemical reduction was carried out in 0.5 M NaCl aq. 5 mg of aqueous metal precursors ($H_2PtCl_6.6H_2O$ (TCI) and $AuCl_3$ (Sigma Aldrich)) were added in 50 ml of 0.5 M NaCl aq. and a potential of -2.0 V for 30 sec and 60 sec respectively was applied using computer controlled potentiostat (Bio-logic SAS model: VSP s/n.1198). The electroreduction was carried out using conventional three electrode system with Ag/AgCl as reference electrode, platinum as counter electrode and TNT chip as working electrode in 0.5 M NaCl aq. electrolyte. Three different core shell nano structures have been prepared (Table 2.2).

Table 2.2: Various types of catalyst prepared with metal precursor: 5 mg, Applied Voltage : -2.0 V, Time: 30 s, for Pt and 60 s for Au.

No	Sample	Core	shell
1	Pt@Au-TNT	Au	Pt
2	PtAu@Au-TNT	Au	Pt, Au
3	AuPt@Pt-TNT	Pt	Au, Pt

Preparation of Pt@Au-TNT: To deposit Au core on TNTs, first 5 mg of aqueous metal precursor ($AuCl_3$) was added to 0.5 M NaCl aq. (50 ml) and potential of -2.0 V for 60 sec was applied. As a result Au core was deposited on TNT. Further Pt shell was deposited by adding 5 mg of aqueous metal precursor ($H_2PtCl_6.6H_2O$) to the freshly prepared 50 ml of 0.5 M NaCl aq. and a potential of -2.0 V for 30 sec was applied using already prepared Au-TNT as working electrode.

Preparation of PtAu@Au-TNT: To deposit Au core on TNTs, first 5 mg of aqueous metal precursor ($AuCl_3$) was added in 0.5 M NaCl aq. (50 ml) and potential of -2.0 V for 60 sec was applied. As a result Au core was deposited on TNT. Further Pt, Au shell was deposited by adding 5 mg of aqueous metal precursor ($H_2PtCl_6.6H_2O$) to the freshly prepared 50 ml of 0.5 M NaCl aq in which 5 mg of $AuCl_3$ was also added and a potential of -2.0 V was applied for 30 sec by using already prepared Au-TNT as working electrode.

Preparation of AuPt@Pt-TNT: To deposit Pt core on TNTs, first 5 mg of aqueous metal precursor ($H_2PtCl_6.6H_2O$) was added in 0.5 M NaCl aq. (50 ml) and potential of -2.0 V for 30 sec was applied. As a result Pt core was deposited on TNT. Further, both Pt and Au shell was deposited by adding 5 mg of aqueous metal precursor ($AuCl_3$) to the freshly prepared 50 ml of 0.5 M NaCl aq. in which 5 mg of $H_2PtCl_6.6H_2O$ was also added and a potential of -2.0 V was applied for 60 sec using already prepared Pt-TNT as working electrode.

Fig 2.2 depicts the methodology of core shell nanoparticles decoration on TNTs.

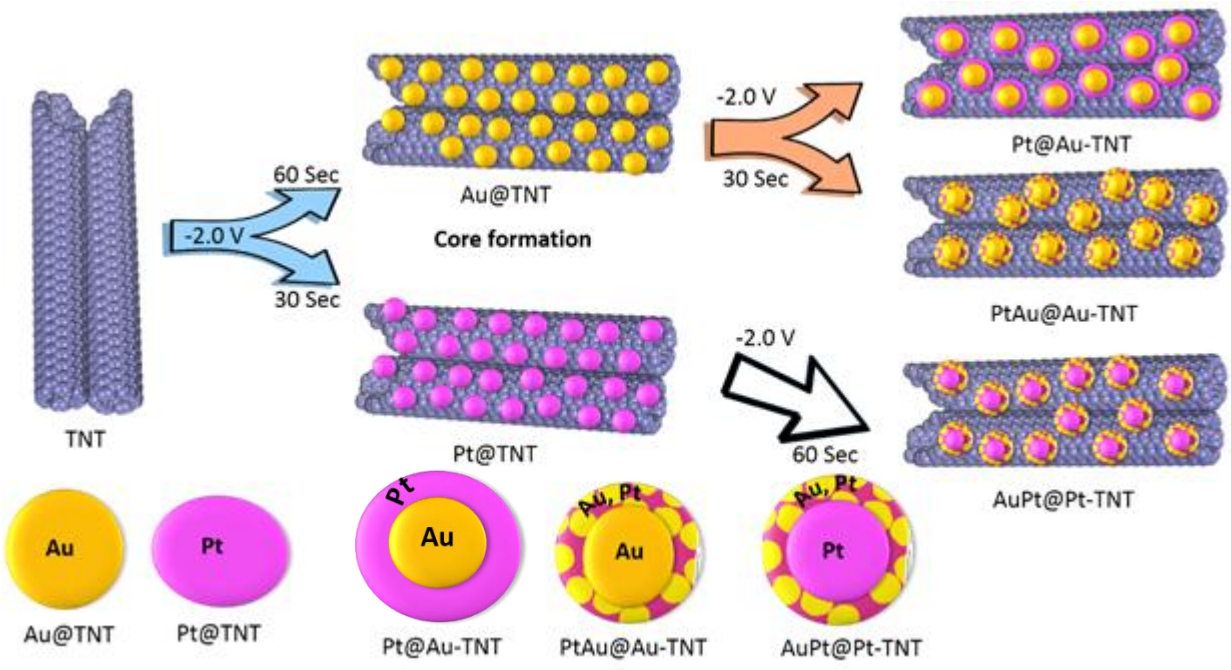

Fig 2.2: Schematic illustration of core shell nanoparticles formation on TNTs by applying potential.

2.3.3. Material characterization:

The surface morphology of titania nanotubes was characterized by scanning electron microscope (Hitachi model S-4500 Tokyo, Japan) and transmission electron microscope (Hitachi model H-7100 Tokyo, Japan). The surface properties of the samples were studied by X-ray photoelectron spectroscopy using S-probe TM 2803 instrument. The core shell morphology was studied by energy dispersive X-ray spectroscopy (EDS), scanning transmission electron microscopy equipped with high angle annular dark field detector (STEM-HAADF) using JEM-ARM200F, JEOL model. Elemental mapping and line profile studies were performed to observe core shell structure and uniformity of Pt and Au elements.

2.3.4. Electrochemical characterization:

Electrochemical performance of different core shell nanoparticles were characterized by cyclic voltammetry (CV) and linear sweep voltammetry (LSV) coupled with rotating disk electrode (RDE) using Biologic VSP electrochemical work station. Electrochemical characterizations were carried out using conventional three electrode system. Mirror polished glassy carbon electrode coated with catalyst was used as working electrode, Pt wire as counter electrode and Hg/HgO in 0.1 M $KOH_{(aq)}$ as reference electrode at 30 °C. ORR studies were also carried out in nonaqueous medium with various core shell nanoparticles. 0.1M LiTFSI in tetraethyleneglycoldimethylether (TEGDME) was used as electrolyte. Ether based electrolytes have attracted significant attention recently since they have high resistance towards the superoxide radical which is a side product formed during oxygen reduction. Hence in this studies TEGDME was choosen. LiTFSI was choosen as supporting electrolyte since this is most compatible supporting electrolyte with TEGDME.

Catalyst ink was prepared by dispersing nanotubes with core shell nanoparticles in distilled water, isopropyl alcohol along with 5 wt% nafion. Ink was drop casted in such a way that 4.6 $\mu g/cm^2$ of Pt was loaded on GC.

2.4. Results and discussion:

Surface morphology of self-organized TNT array was characterized by SEM. Fig 2.3 shows the surface morphology of self-organized TNT prepared according to literature[26]. This TNTs were characterized by SEM in which each pore was found to have diameter of 130 nm. This SEM image clearly reveals honey comb like pore formation of TNTs on Ti substrate.

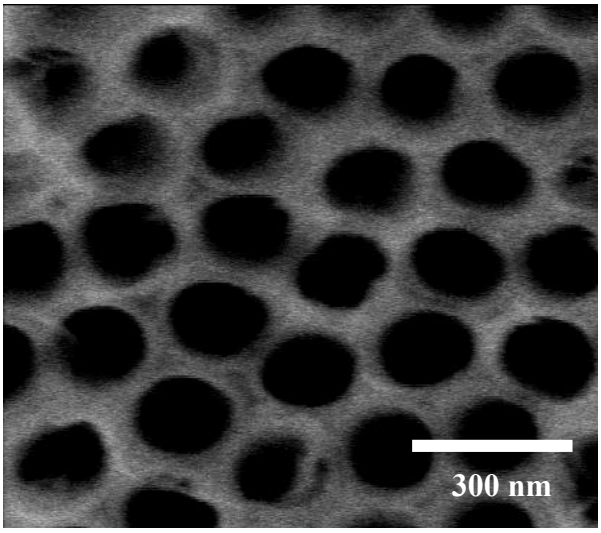

Fig 2.3: SEM image of self-organized TNTs

Once these TNTs were synthesized, they were decorated with nanoparticles (Au and Pt) by applying a potential of -2.0 V for 30 sec for Pt and -2.0 V for 60 sec for Au. The successful decoration of nanoparticles on TNTs was characterized by TEM. Fig 2.4 (A) and 2.4 (B) show the successful deposition of Pt nanoparticles and Au nanoparticles, respectively. These TEM images reveal the decoration of Pt and Au nanoparticles on TNTs with size of approximately 5 nm and 20 nm, respectively.

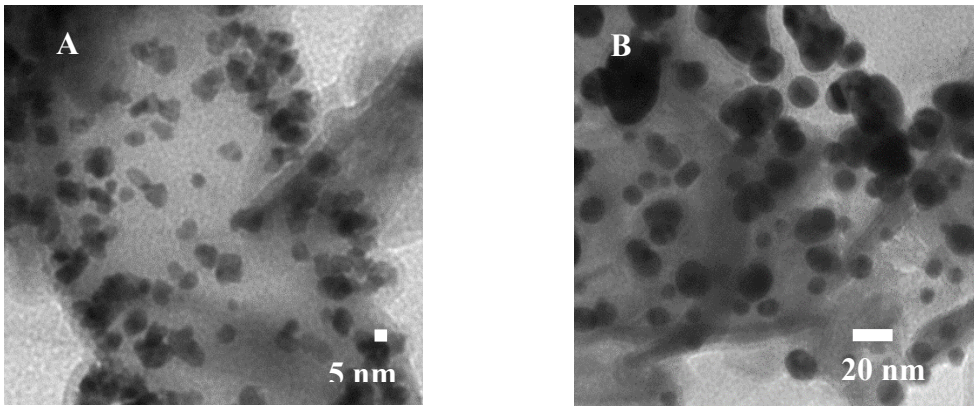

Fig 2. 4 (A-B): TEM images of Pt (Left) and Au (Right) nanoparticles on TNT

To deposit bimetallic nanoparticles, TNTs decorated with monometallic nanoparticles (shown above) were used as substrates for deposition of second metal by applying potential of -2.0 V for 30/ 60 sec. Fig 2.5 (A-C) shows TEM images of Pt@Au-TNT, AuPt@Pt-TNT, PtAu@Au-TNT, respectively. These TEM images indicate that bimetallic nanoparticles were

uniformly decorated on TNT by this electrochemical decoration method and the size of these nanoparticles were ~20 nm.

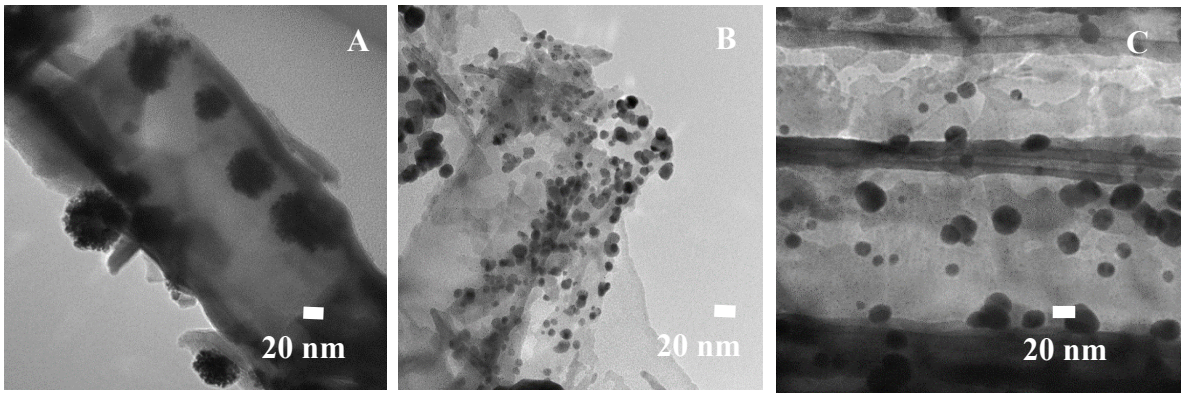

Fig 2.5 (A-C): TEM images of A) Pt@Au-TNT B) AuPt@Pt-TNT C) PtAu@Au-TNT

To understand the core shell nature of decorated nanoparticles, the samples were analysed by STEM-HAADF to observe EDS elemental mapping and line profiling. The observed images are represented in Fig 2.6, 2.7, 2.8. Fig 2.6 (A) gives the STEM-HAADF image of titania nanotubes decorated with nanoparticles with inset at higher magnification of single nanoparticle for AuPt@Pt-TNT. A closer look at the inset of this image shows less pronounced dark and bright contrast due to the close atomic numbers (Z) for Au and Pt, 79 and 78, respectively. STEM-HAADF signal intensity and contrast are largely dependent on atomic number. Hence large contrast difference will be seen only in case of metals with large atomic number difference[35-37]. Since the atomic numbers of Au and Pt are close, the difference in contrast is less pronounced. Fig 2.6 (B-E) shows the EDS elemental mapping images for titania nanotubes (Fig 2.6 B), Pt (Fig 2.6 C), Au (Fig 2.6 D) and overlaid image with inset at higher magnification of single nanoparticle (Fig 2.6 E) respectively. Thus the overlaid Fig 2.6 (E) reveals a dense core of Pt which is covered by rich shell containing Pt and Au. This indicates that these particles have core shell structures.

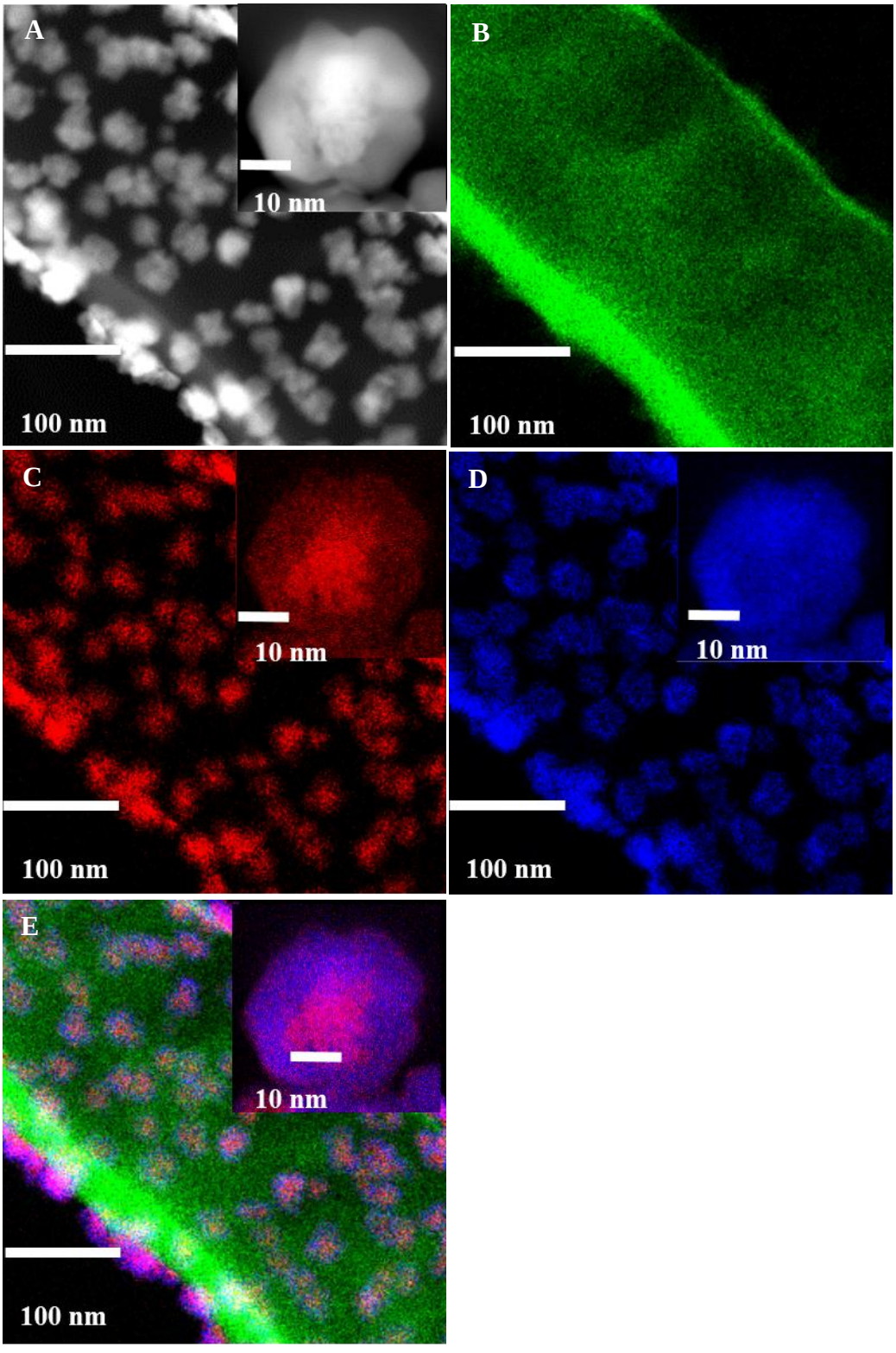

Fig 2.6 A: STEM-HAADF, **B-E:**EDS elemental mapping images of TNTs, Pt and Au in AuPt@Pt-TNT **B)** Ti K **C)** Pt L **D)** Au L **E)** overlay

Fig 2.7 (A) shows the STEM-HAADF images for PtAu@Au-TNT. Fig 2.7 (B-E) shows the EDS elemental mapping images for titania nanotubes (Fig 2.7 B), Pt (Fig 2.7 C), Au (Fig 2.7 D) and overlaid image (Fig 2.7 E), respectively. These mapping images show nanotube (green colour coding) was decorated with nanoparticles (red and blue colour coding) revealing a dense core (Au: blue colour coding) which is covered by rich shell made of two metals, Pt and Au (Pt: red colour, Au: blue colour). Hence these particles are core shell structures with shell made of both Pt and Au metals and core made of single metal (Au).

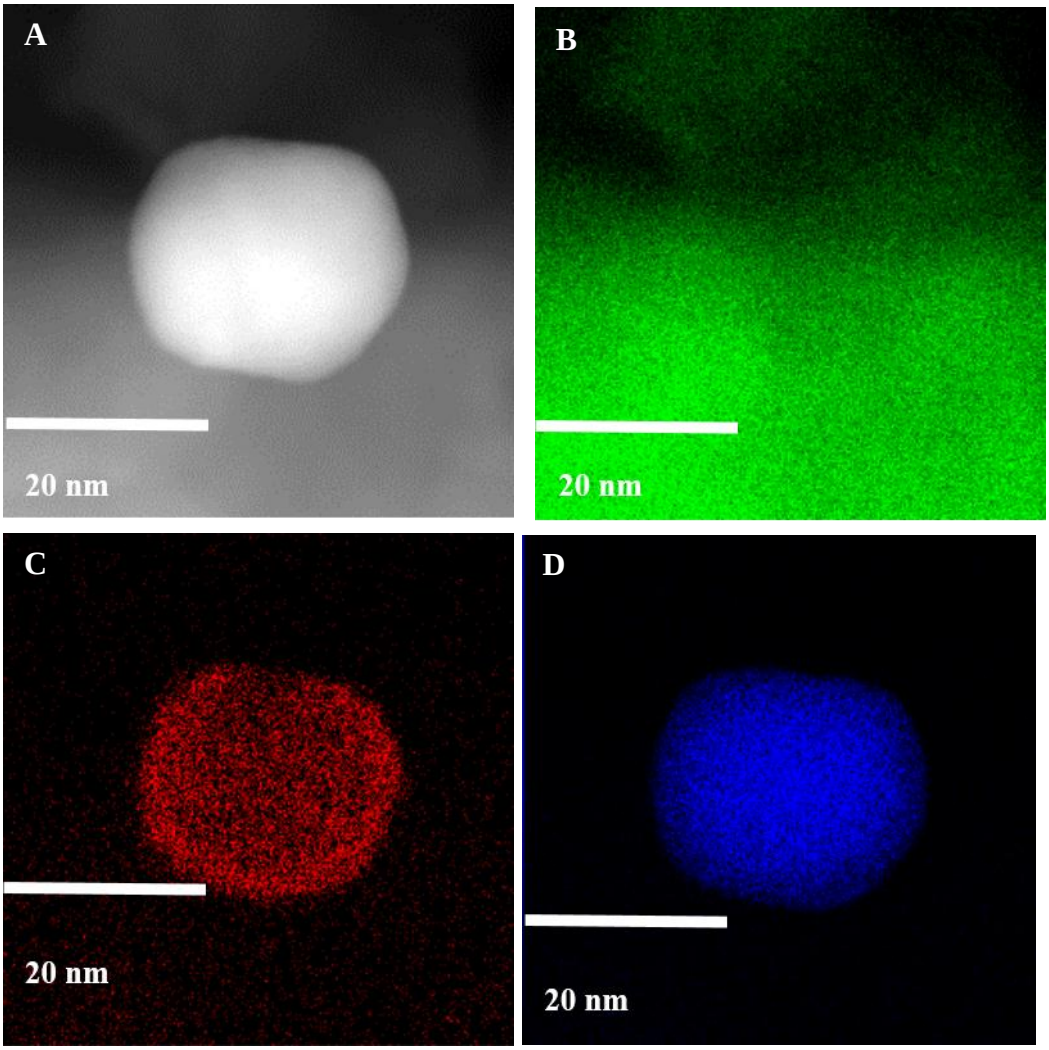

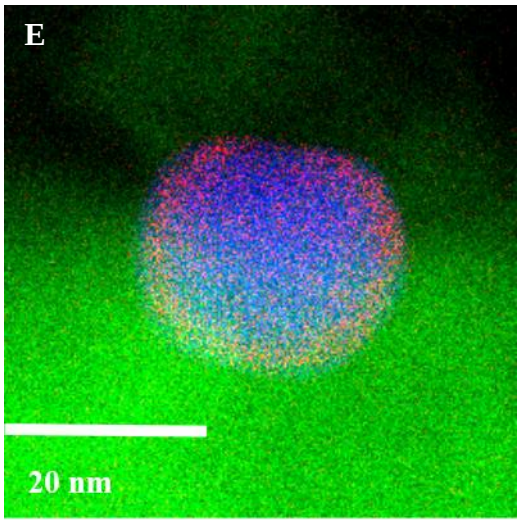

Fig 2.7 A: STEM-HAADF, **B-E:** EDS elemental mapping images of Pt and Au in PtAu@Au-TNT **B)** Ti K**C)** Pt L edge **D)** Au L **E)** overlay

Fig 2.8 (A) shows the STEM-HAADF image for Pt@Au-TNT. Fig 2. 8 (B-D) shows the EDS elemental mapping images for Au (Fig 2. 8 B), Pt (Fig 2. 8 C) and overlaid image (Fig 2. 8 D), respectively. These mapping images shows a dense core (Au: blue colour coding) which is covered by rich shell (Pt: red colour coding) thus revealing the formation of single Au core and single Pt shell.

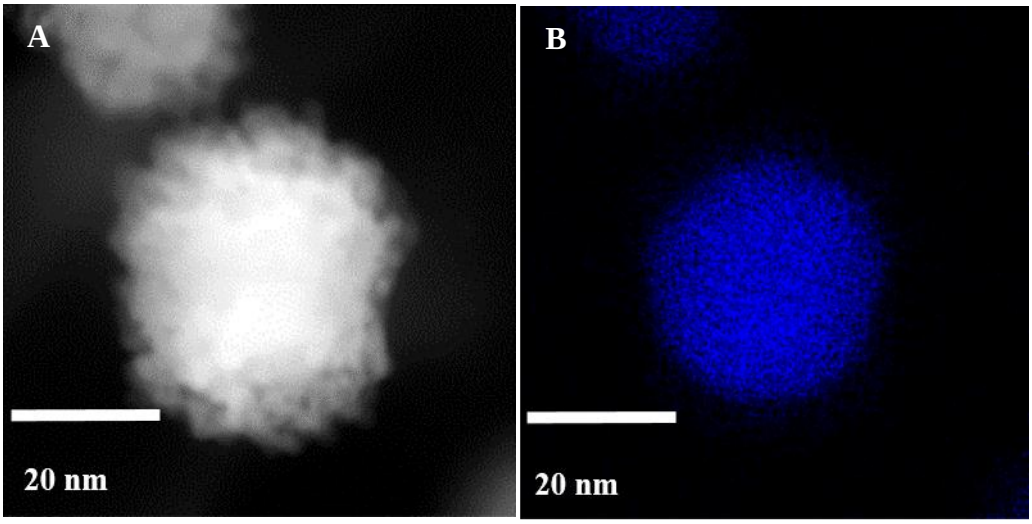

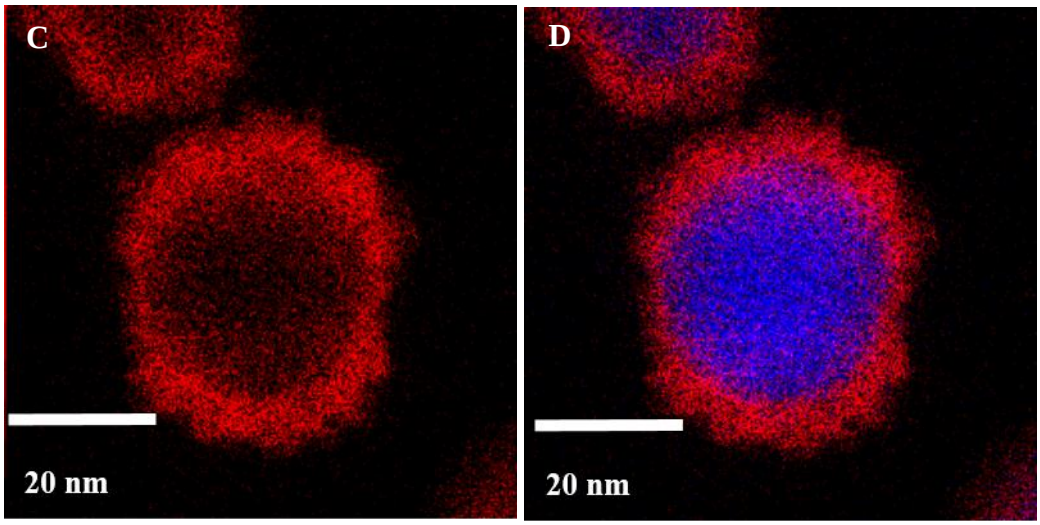

Fig 2.8 A: STEM-HAADF, **B-D:** EDS elemental mapping images of Pt and Au for Pt@Au-TNT **B)** Au L **C)** Pt L

Fig 2.9 shows the STEM-HAADF and EDS line profiles of the core shell nanoparticles (AuPt@Pt-TNT). The image on the left shows the line profiling region and the line profile on right shows the elemental distribution along the studied line. As seen from center (right image) the particle is rich in Pt at the center. Traversing away from the center, either of which gains intensity in Au. This evinces an Au rich shell. When further travelling towards the edge, a clear definite peak for Pt is seen. The thickness of shell was found to be 11 nm and thickness of core was found to be 18 nm. This kind of electrochemical decoration provides a uniform distribution of Pt and Au as shell all around the Pt core.

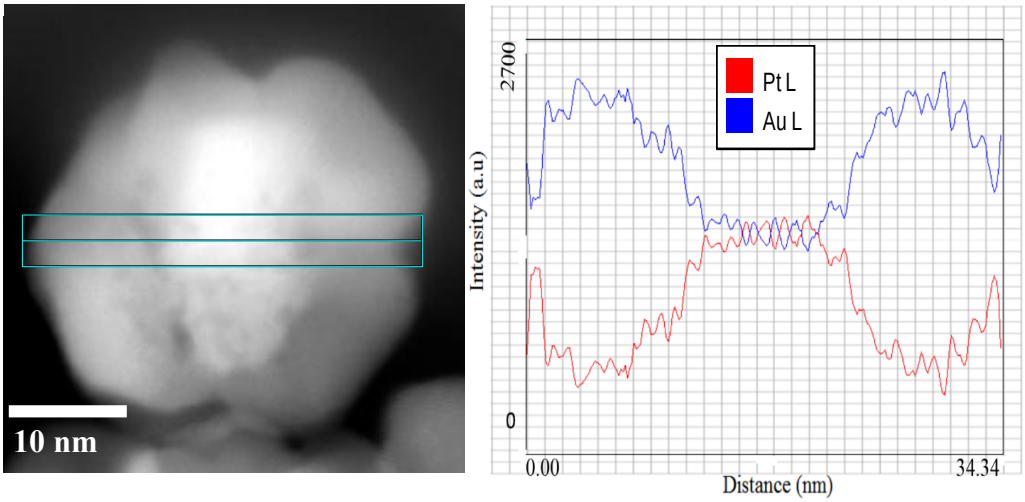

Fig 2.9: STEM-HAADF (left) and EDS line spectra (right) for AuPt@Pt-TNT

Fig 2.10 shows the STEM-HAADF and EDS line profiles of the core shell nanoparticle (Pt@Au-TNT). The image on the left shows the line profiling region and the line profile on right shows the elemental distribution along the studied line. As seen from center (right image) the particle is rich in Au at the center. Traversing away from the center, either of which gains intensity in Pt. This evinces an Pt rich shell covering Au rich core.

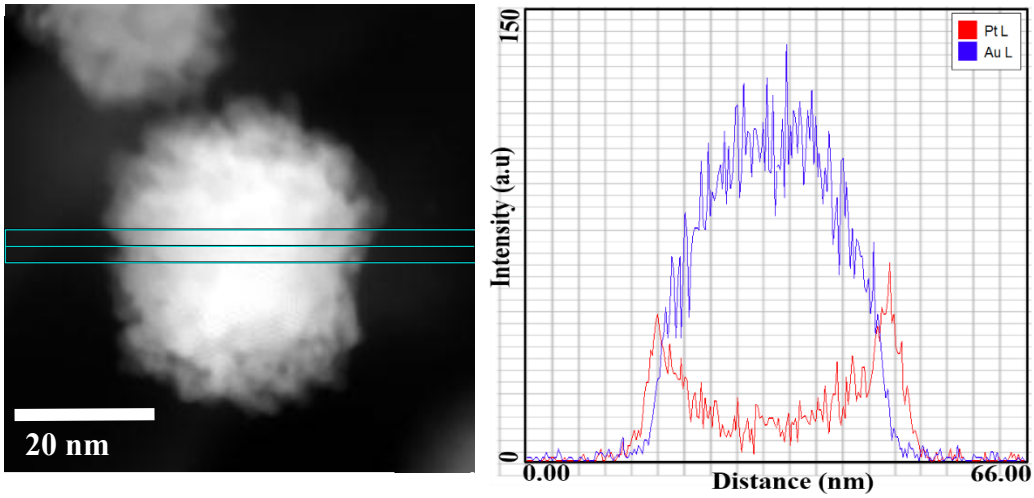

Fig 2.10: STEM-HAADF (left) and EDS line spectra (right) for Pt@Au-TNT

Fig 2.11 shows the STEM-HAADF and EDS line profiles of the core shell nanoparticle (PtAu@Au-TNT). The image on the left shows the line profiling region and the line profile on right shows the elemental distribution along the studied line. As seen from center (right image) the particle is rich in Au at the center. Traversing away from the center, either of which gains intensity in Pt with some intensity of Au as well. This evinces an that shell consists of Pt and Au and core consists of Au.

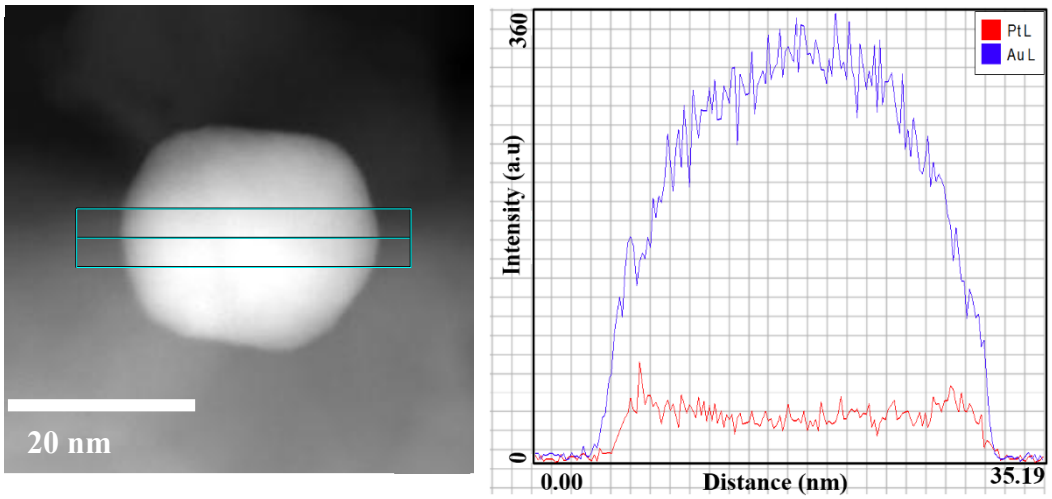

Fig 2.11: STEM-HAADF (left) and EDS line spectra (right) for PtAu@Au-TNT

For quantitative analysis including valence state of elements, XPS measurements were performed. Fig 2.12 (A-C) gives the full survey spectra of AuPt@Pt-TNT, PtAu@Au-TNT and Pt@Au-TNT. In these samples major elements such as Ti 2p, C 1s, O 1s, Pt 4f, and Au 4f were found. Binding energies were calibrated with respective to binding energy of carbon 284.6 eV. Pt content in AuPt@Pt-TNT, PtAu@Au-TNT and Pt@Au-TNT was found to be 13.12 wt% and 16.7 wt%, 12.4 wt% respectively and the Au content for the same nanoparticle was 67.0 wt%, 5.2 wt % and 27.6 wt %, respectively. Further high resolution spectra of Pt 4f and Au 4f region of AuPt@Pt-TNT, PtAu@Au-TNT and Pt@Au-TNT were deconvoluted. Three different oxidation states such as Pt (0), Pt (II), Pt (IV) were found in all the cases with Shirley background by maintaining the Lorentzain-Guassian ratio of 7:3. In AuPt@Pt-TNT, Pt (0), Pt (II), Pt (IV), binding energies were found to be 69.79, 70.46, 72.35 eV with relative concentrations of 32.90%, 42.40%, 17.67%, respectively. In PtAu@Au-TNT, Pt (0), Pt (II), Pt (IV) binding energies were 69.74, 70.38, 71.31 eV with relative concentrations of 32.90%, 24.50%, 42.50%, respectively. In Pt@Au-TNT, Pt (0), Pt (II), Pt (IV), binding energies were found to be 70.27, 71.2, 72.93 eV with relative concentrations of 38.80%, 35.30%, 25.80%, respectively. Additionally high resolution peak of Au 4f was deconvoluted for AuPt@Pt-TNT, PtAu@Au-TNT and Pt@Au-TNT and found two oxidation states Au (0) and Au (I). In AuPt@Pt-TNT, Au (0), Au (I) binding energies were found to be 83.03, 83.26 eV with relative concentrations of 64%, 36%, respectively. In PtAu@Au-TNT, Au (0), Au (I) binding energies were found to be 83.62, 83.82 eV with relative concentrations of 56%, 44%, respectively. In Pt@Au-TNT, Au (0), Au (I) binding energies were found to be 83.30, 84.07 eV with relative concentrations of 92 %, 8 %, respectively. The existence of two oxidation states for Au shows that it was oxidised in air which is a common phenomena when Au nanoparticles were deposited on TiO_2 support[38].

The comparative binding energy values of Pt and Au of core shell nanoparticles are presented in Table 2.3. It is clear from the Table that binding energy of Au is largely effected due to the presence of Pt.

Table 2.3: Binding energy values of Au 4f and Pt 4f of Pt@Au-TNT, PtAu@Au-TNT, AuPt@Pt-TNT

No	Sample	Core	shell	Pt binding energy (eV)	Au (0) Binding energy (eV)
1	Pt@Au-TNT	Au	Pt	70.27	83.30
2	PtAu@Au-TNT	Au	Pt, Au	69.74	83.62
3	AuPt@Pt-TNT	Pt	Au, Pt	69.79	83.03

The shift in binding energy values of Au is due to electron transfer from Pt to Au. In both AuPt@Pt-TNT and PtAu@Au-TNT, core determines the electron transfer. In AuPt@Pt-TNT core is Pt which means the electron transfer from Pt to Au occurs both from core and neighbouring Pt atoms from shell leading to increase in the electron on Au. Hence least binding energy for Au (0) was observed. In case of PtAu@Au-TNT, Au is present in both core and shell, whereas Pt is present only in shell in coordination with Au, therefore the binding energy was high. In case of Pt@Au-TNT the shell consists of only. The charge transfer predominantly occurs at the interface of Pt shell and Au core. Hence the binding energy of Au (0) in Pt@Au-TNT can be expected to be between PtAu@Au-TNT and AuPt@Pt-TNT. This was in accordance with the observation.

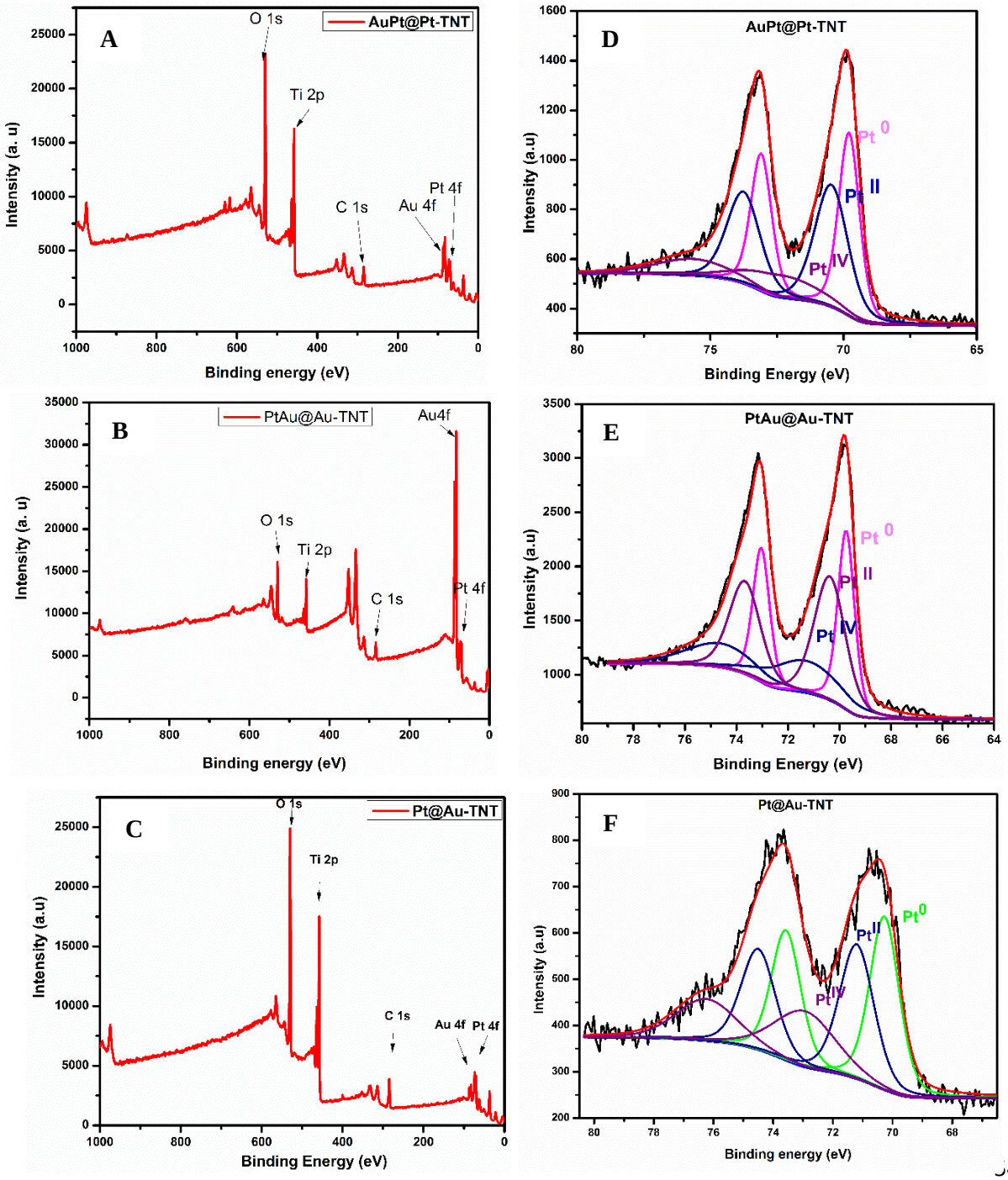

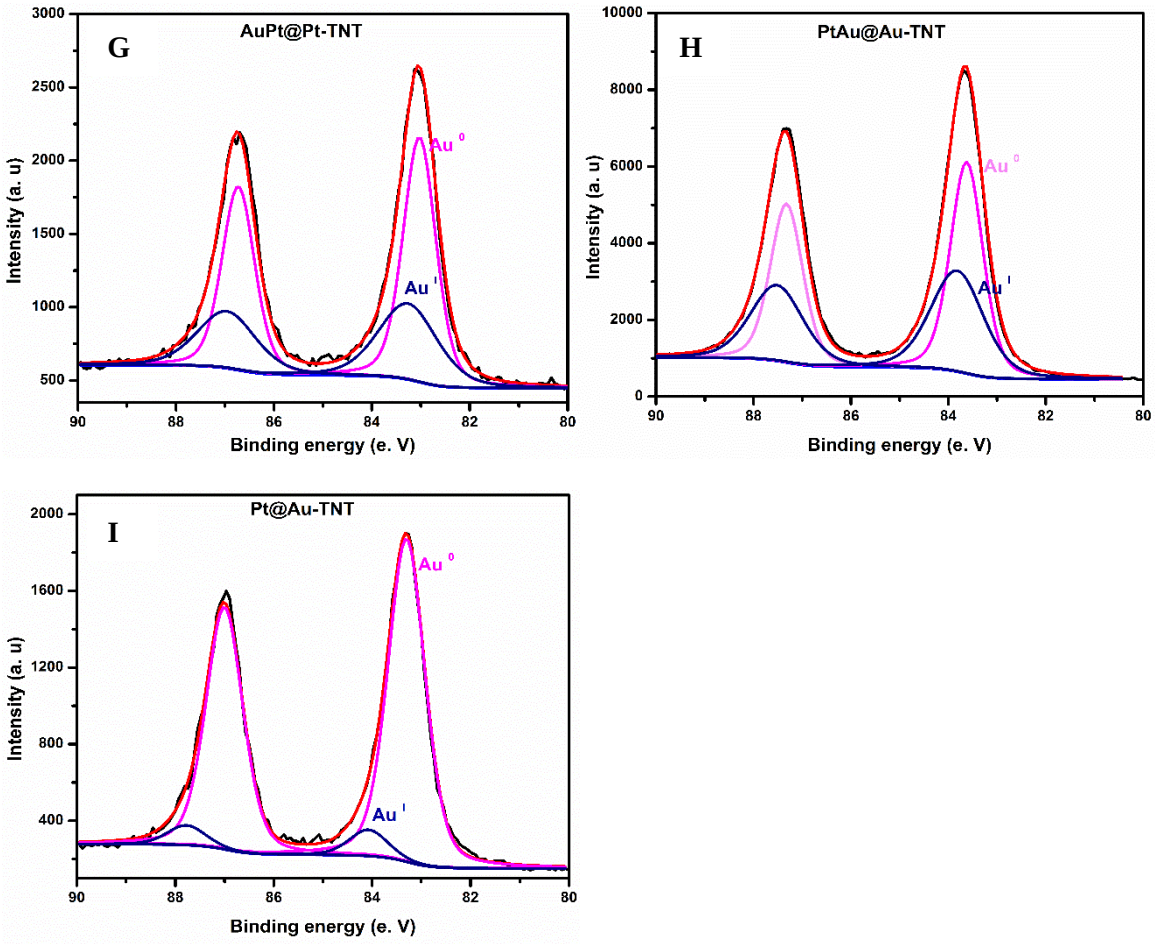

Fig 2. 12: Survey scan profiles of A) AuPt@Pt-TNT, B) PtAu@Au-TNT C) Pt@Au-TNT and corresponding deconvoluted high resolution spectra of Pt region for D) AuPt@Pt-TNT, E) PtAu@Au-TNT F) Pt@Au-TNT and Au region for G) AuPt@Pt-TNT H) PtAu@Au-TNT I) Pt@Au-TNT

To test the electrochemical activity of materials under study cyclic voltammetry (CV) and linear sweep voltammetry (LSV) using rotating disc electrode (RDE) were studied. Fig 2.13 gives cyclic voltammograms of all 3 materials showing ORR peaks. Table 2.4 gives ORR current intensity values for each of different core shell nanoparticle.

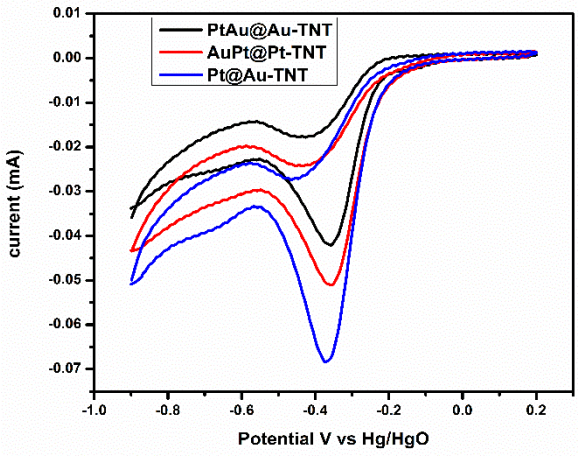

Fig 2.13: Cyclic voltammograms of different core shell nanoparticles in 0.1 M KOH at a scan rate of 100 mv/s.

Table 2.4 Various types of core shell nanoparticles and corresponding peak current for ORR

Sample	**Metal**	**Core**	**Shell**	**Peak current (mA)**
Pt@Au-TNT	Pt, Au	Au	Pt	-0.068
AuPt@Pt-TNT	Pt, Au	Pt	Au, Pt	-0.051
PtAu@Au-TNT	Pt, Au	Au	Au, Pt	-0.041

Further to assess the ORR Kinetic parameters, rotation dependent polarization measurements were carried out at various rotation speeds from 400 to 2500 RPM with RDE. Polarization curves are given in Fig 2.14 for various core shell nanoparticles. By utilizing Koutecky-Levich equation,

$$\frac{1}{l} = \frac{1}{l_k} + \frac{1}{i_l} = \frac{1}{l_k} + \frac{1}{0.62nFAC\omega^{\frac{1}{2}} V^{\frac{-1}{6}} D^{\frac{2}{3}}}$$

Where I_L = Diffusion Limiting Current (A)

n= number of electrons transferred to oxygen

I_L= Diffusion Limiting Current (A)

F = Faraday constant (C/mol)

A =electrode area (cm^2)

D= diffusion coefficient (cm^2/s)

W= angular rotation rate of the electrode (rad/s)

V= kinematic viscosity (cm^2/s)

C= analyte concentration (mol/cm^3)

the number of electrons involved in the ORR was analyzed. It was found to be ~4 electron transfer at -0.3 V for Pt@Au-TNT (inset of Fig 2. 14 A) and AuPt@Pt-TNT (inset of Fig 2.14 B) and ~2 electron transfer at -0.3 V for PtAu@Au-TNT (inset of Fig 2.14 C). This is because of predominant Au present in both core and shell.

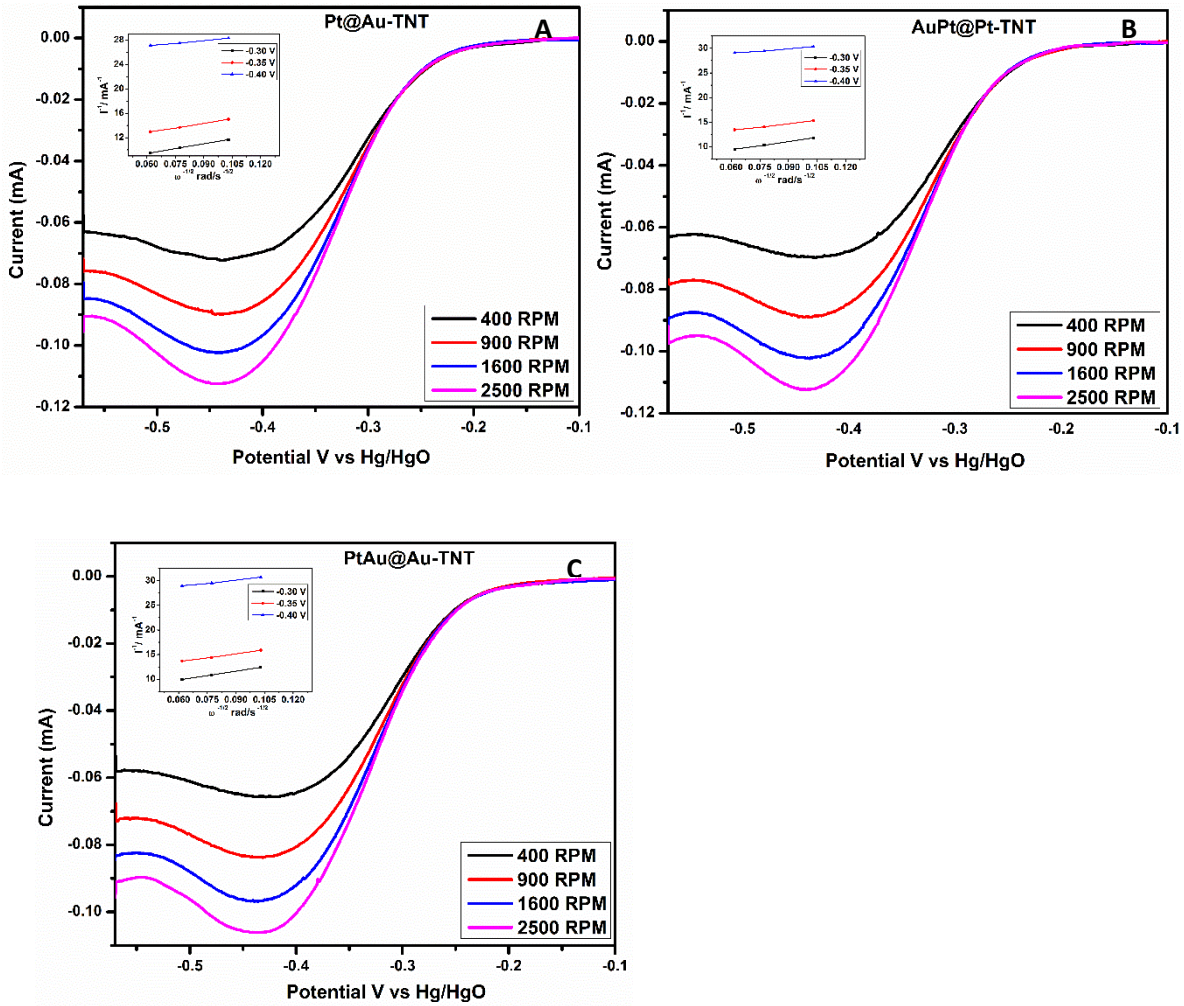

Fig 2.14: Linear sweep voltammograms for A) Pt@Au-TNT B) AuPt@Pt-TNT C) PtAu@Au-TNT with RDE at a scan rate of 5 mV/s in oxygen atmosphere at different RPM in 0.1 M KOH (aq) with KL plots in inset at -3.0, -0.35 and -0.40 V

It is very important to get a correlation between the structural composition of core-shell nanoparticle and their catalytic activity. It is also well known that the electrocatalytic activity is majorly determined by the availability of electron density on the metal catalyst. It is clearly seen from the STEM EDS mapping that the shell of Pt@Au-TNT comprises of Pt alone. Hence, a Pt like high activity is seen. Alongside, a Pt like highly active 4 electron ORR process was seen. It was clearly seen in XPS that the Au binding energy is largely affected varying the core. In case of AuPt@Pt-TNT, it is clearly visible that Pt being in both core and shell the binding energy of Au is least. In other words, the electronic structure of Au is highly affected and the electron density on Au becomes high. The increase in the electronic density of Au reflected in achieving 4 electron ORR process and higher ORR activity than that of PtAu@Au-TNT. In case of PtAu@Au-TNT, as the Pt is available only in shell, the electron cloud on Au is least in case of PtAu@Au-TNT. Hence, it showed 2 electron ORR process and least activity in the order.

The charge transfer phenomena between core shell nanoparticles and titania nanotubes for ORR is depicted in Fig 2.15

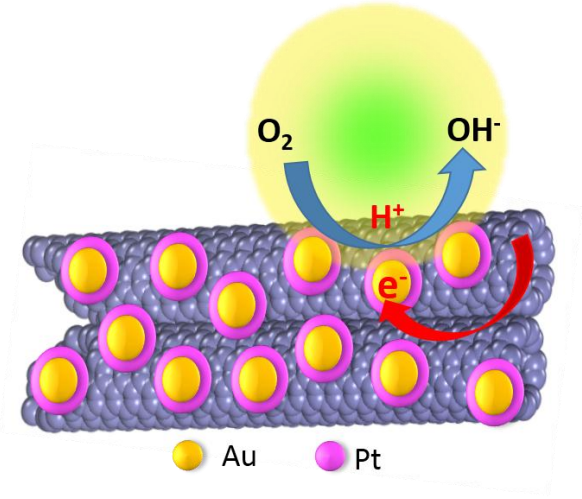

Fig 2.15: charge transfer phenomena between core shell nanoparticles and titania nanotubes for ORR

2.4.1. Electrochemical ORR studies in nonaqueous medium:

Fig 2.16 shows the cyclic voltammogram of materials under study in non-aqueous environment. The voltammograms reveals two distinct peaks. One at around. -1.17 V corresponding to ORR, where in oxygen is reduced by Li ions to form lithium oxides (Li_xO_2). The second peak at 1.37 corresponds to oxygen evolution reaction where in Li_xO_2 is dissociated into Li ions and molecular oxygen. The order of ORR activity in nonaqueous medium was also found to be in the same order of aq ORR. The presence of both ORR and OER indicate the applicability of current materials in rechargeable metal air batteries. Peak current corresponding to Pt@Au-TNT is higher than AuPt@Pt-TNT and PtAu@Au-TNT. This is due to the fact that in Pt@Au-TNT, shell is covered by Pt and it being more active towards ORR showed higher current.

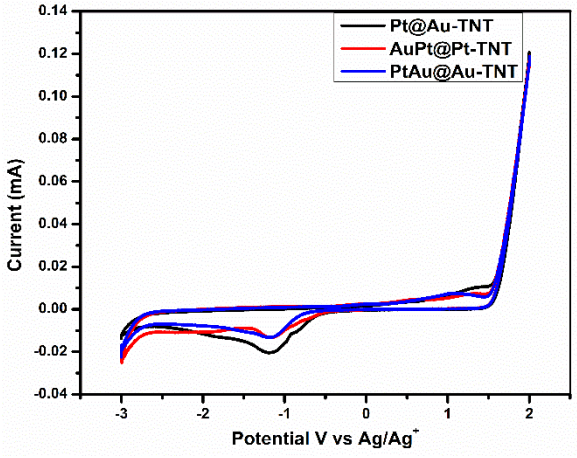

Fig 2.16: Cyclic voltammograms of core shell nanoaprticles in oxygen saturated 0.1 M LiTFSI in TEGDME at 25 mV/s

2.5. Conclusions:

In summary we decorated various core shell nanoparticles of Pt and Au on titania nanoubes in ultrafast manner within a short span of 60 sec. Novelty of this synthesis lies in decoration over TNTs at room temperature without using any surfactants and without need of any further purification. The formation of core shell structures was characterized by STEM-HAADF and EDS mapping and line profiling. This type of synthesis helps in maintaining the uniform shell composition of Au and Pt. All these core shell nanoparticles were electrochemically characterized in terms of aqueous ORR and non aqueous ORR applications. Pt@Au-TNT was found to show relatively high activity as the shell is predominantly covered with Pt.

References:

1. M. Granovskii, I. Dincer and M. A. Rosen, *J. Power Sources.*, **157**, 411-421 (2006).

2. L. Dai , Y. Xue, L. Qu, H. J. Choi and J. B. Baek, *Chem. Rev.*, **115** (11), 4823–4892 (2015).

3. F. Ando, T. Tanabe, T. Gunji, T. Tsuda, S. Kaneko, T. Takeda, T. Ohsaka, F. Matsumoto, *Electrochim. Acta.*, **232**, 404-413 (2017).

4. M. Manikandan, R. Vedarajan, R. Kodiyath, H. Abe, S. Ueda, A. Dakshnamoorthy, N. Rajalakshmi, K. S. Dhathathreyan and G. V. Ramesh, *J. Nanoscience and Nanotechnology.*, **16**, 8269–8278 (2016).

5. C.T. Lin, H. J. Huang, J. Yang and M. H. Shiao, *Microelecton. Eng.*, **88,** 2644–2646 (2011).

6. T. Gunji, K Sasaki, A. J. Jeevagan, T. Tanabe, S. Kaneko and F. Matsumoto, *ECS Trans.*, **66** (39), 1-8 (2015)**.**

7. D. M. Gu, Y. Y. Chu, Z. B. Wang, Z. Z. Jiang, G. P. Yin and Y. Liu, *Appl. Catal., B,* **102**, 9–18 (2011).

8. N. R. Elezovic, B. M. Babic, V. R. Radmilovic, L. M. Vracar and N. V. Krstajic, *Electrochim. Acta.*, **54**, 2404–2409 (2009).

9. H. Chhina, S. Campbell and O. Kesler, *J. Electrochem. Soc.*, **154** (6), B533-B539 (2007).

10. N. R. Elezovic, V. R. Radmilovic, J. Kovac, B. M. Babic, L. M. G. Krstajic and N. V. Krstajic, *RSC Adv.*, **5**, 15923-15929 (2015).

11. X. L. Sui, Z. B. Wang, Y. F. Xia, M. Yang, L. Zhao and D. M. Gu, *RSC Adv.*, **5**, 35518-35523 (2015).

12. M. Tian, M. Malig, S. Chen and A. Chen, *Electrochem. Commun.*, **13**, 370–373 (2011).

13. J. M. Macak, B. G. Gong, M. Hueppe and P. Schmuki, *Adv. Mater.*, **19**, 3027–3031 (2007).

14. F. X. Xiao, *RSC Adv.*, **2**, 12699-12701 (2012).

15. L. Su, W. Jia, C. M. Li and Y. Lei, Chem Sus Chem., **7** (2), 361-78 (2014).

16. M. Shao, A. Peles, K. Shoemaker, M. Gummalla, P. N. Njoki, J. Luo and C. J. Zhong, *J. Phys. Chem. Lett.*, **2** (2), 67–72 (2011).

17. D. Wang, H. L. Xin, R. Hovden, H. Wang, Y. Yu, D. A. Muller, F. J. DiSalvo and H. D. Abruna, *Nat. Mater.*, **12**, 81–87 (2013).

18. Y. Chen, Z. Liang, F. Yang, Y. Liu, and S. Chen, *J. Phys. Chem. C.*, **115** (49), 24073–24079 (2011**)**.

19. J. H. Jang, E. Lee, J. Park, G. Kim, S. Hong and Y. U. Kwon, *Sci. Rep.*, **3**, 2872-2879 (2013).

20. Y. Dai and S. Chen, *ACS Appl. Mater. Interfaces.*, **7**, 823−829 (2015).

21. J. Fennell, D. He, A. M. Tanyi, A. J. Logsdail, R. L. Johnston, Z. Y. Li, and S. L. Horswell, *J. Am. Chem. Soc.*, **135** (17), 6554–6561 (2013).

22. S. W. T. Price, J. D. Speed, P. Kannan, and A. E. Russell, *J. Am. Chem. Soc.*, **133** (48), 19448–19458 (2011).

23. Y. Yu, Y. Hu, X. Liu, W. Deng and X.Wang, *Electrochim. Acta.*, **54**, 3092–3097 (2009).

24. S. Wang, N. Kristian, S. Jiang and X. Wang, Nanotechnology, **20**, 025605-025613 (2009).

25. A. Sarkar, A. Manthiram, *J. Phys. Chem. C*, **114** (10), 4725–4732 (2010).

26. A. Jackson, A. Strickler, D. Higgins, T. F. Jaramillo, *Nanomaterials*, **8**, 38-52 (2018).

27. Y. Xiong, L. Xiao, Y. Yang, F. J. DiSalvo, and H. D. Abruna, *Chem. Mater.*, **30** (5), 1532–1539 (2018).

28. D. Chen, C. Li, H. Liu, F. Fe, J. Yang, *Sci Rep*, **5**, 11949-11957 (2015).

29. D. Wang, H. L. Xin, Y. Yu, H. Wang, E. Rus, D. A. Muller and H. D. Abruna *j. am. chem. Soc*, **132**, 17664–17666 (2010).

30. J. Cao, M. Guo, J. Wu, J. Xu, W. Wang, Z. Chen, *J. of Power Sources*, **277**, 155-160 (2015).

31. H. Tada, F. Suzuki, S. Ito, T. Akita, K. Tanaka, T. Kawahara, and H. Kobayashi, *J. Phys. Chem. B.*, **106**, 8714-8720 (2002).

32. S. F. Hung, Y. C. Yu, N. T. Suen, G. Q. Tzeng, C.W. Tung, Y.Y. Hsu, C. S. Hsu, C. K. Chang, T. S. Chan, H. S. Sheu, J. F. Lee and H. M. Chen, *Chem. Commun.*, **52**, 1567 **(**2016).

33. S. Chen, M. Malig, M. Tian and A. Chen, *J. Phys. Chem. C.*, **116**, 3298−3304 (2012).

34. R. Vedarajan, S. Ikeda and N. Matsumi, *Nanoscale Res. Lett.*, **9**, 1–5 (2014).

35. R. Esparza, A.F.Garcia-Ruiz and J. J. V. Salazar, *J Nanopart Res*., **15** (1342) (2012).

36. S. Kamimura, T. Miyazaki, M. Zhang, Y. Li, T. Tsubota and T. Ohno, *Appl. Catal., B.*, **180**, 255–262 (2016).

37. D. G. Gutierrez, C. G. Wing, M. M. Yoshida and M. J. Yacaman, *Appl. Phys. A.*, **79**, 481–487 (2004).

38. M. P. Casaletto, A. Longo, A. Martorana, A. Prestianni and A. M. Venezia, *Surf. Interface Anal*., **38**, 215–218 (2006).

Chapter 3

TiO_2 Nanotubes/Functionalized Acetylene Black Composite Decorated with Pt Nanoparticles as Efficient Electrocatalyst for ORR

3.1. ABSTRACT:

Despite extensive work on Pt/C based catalyst materials for fuel cells towards oxygen reduction reaction, the high cost of catalyst is still a major problem for efficient use of fuel cells in daily life. This demands at designing a new electrocatalyst with high catalytic activity for oxygen reduction reaction. In this regard, we present a novel composite material consisting of functionalized acetylene black and TiO_2 nanotube (FAB/TNT) as the substrate for Pt as catalyst. Using this novel composite, Pt was decorated using photo-reduction process. Due to the presence of photo-electrons all over the conducting part of the material, H_2PtCl_6 was photo-reduced to Pt nanoparticles with extremely small size ~ 1.6 nm. The material demonstrated that even with as less as 3.5 wt% of Pt, mass activity and specific activity was found to be 519 A/g and 10.4 A/m^2 respectively which is 4.7 times higher than commercial catalyst, Pt Vulcan XC- 72 (mass activity and specific activity was found to be 111 A/g and 8.50 A/m^2, respectively) at 0.6 V vs RHE.

3.2. Introduction:

The global warming and exhaustion of fossil fuels raised an alarm among the scientific community[1] to look for alternative energy sources. This led to the development in the outlook towards alternative energy storage and conversion devices. Fuel cell and Li air battery are the leading devices in the fields of energy conversion and storage[2, 3, 4]. Fuel cell has been commercialized in automobile industry and Li air battery is the upcoming technology. The principle reaction in both these technologies is oxygen reduction reaction (ORR) at cathode[5] and sluggish reaction kinetics makes ORR, the rate determining reaction. Platinum based carbon catalysts are generally employed as the catalysts for ORR[6]. Pt being a rare metal, it makes up the major cost of the fuel cell[7]. To reduce the cost of ORR catalyst without compromising on catalytic activity and increasing the durability is the major focus of many researchers in this field[8, 9]. There have been various strategies to reduce the amount of Pt used, by alloying with other transition metals[10], making Pt skins[11] or skeletons[12] to increase the active surface area[13]. But, all these aforementioned catalysts either have a very limited durability or the preparation method is not commercially viable. Among other strategies, metal free catalysis is one of the hot topics in the recent years[14]. Heteroatom doped graphene based materials are the front runners in this area. However, these materials are active only in basic medium with large over-potential[15]. On the other hand, reducing the size of the Pt particles was found to be another workable strategy for increasing specific surface area[7]. With this methodology the available active sites for ORR increases along with the surface area. In most of the available Pt/C preparation methods involving reducing agents like polyols or other inorganic agents rely on the nucleation sites on the carbon to reduce the particle size. But, it is well known factor that, as increasing the defects in the carbon structure, the durability is reduced by oxidation of carbon in stringent ORR conditions. Hence, a simple method for preparation of ultra-small nanoparticle is urgently needed.

Our recent report on various ORR catalysts introduced a novel photo-reduction method[16], where TiO_2 was used as photo-catalyst for the reduction of platinum salt to generate platinum nanoparticles of small size (1-3 nms) on conventional carbon substrates. Due to the presence of conduction band of carbon marginally lower to that of TiO_2, the spillover of photo electrons onto the conducting carbon is possible. This spillover of electrons in the presence of any platinum salt precursor can generate Pt nanoparticles. Here, it is worth noting that the photoelectrons are available all over the substrate of the conducting carbon. This also indicates that there is a large

possibility of formation of nanoparticles whereever the electrons are available. As the electrons are available all over the substrate, there will be numerous nucleation sites to form small nanoparticles.

Therefore utilization of TiO_2 with carbon is in high demand. TiO_2 is available in many morphological forms such as in nanoparticles, nanorods, nanoplates, and nanotubes. Of the various morphological forms, titania nanotubes (TNT) has an extra advantage because of high surface area[17]. Among other factors that determine the activity of the ORR catalyst, absorption of electrolyte to reduce the charge transfer boundary plays a major role. Recently our report on functionalized acetylene black (FAB) showed high ORR activity due to its high solvent absorption properties. Moreover, FAB itself has ORR activity due to its defective sites[18]. Hence there is a tremendous opportunity to obtain a novel substrate utilizing FAB in conjunction with TiO_2. This substrate will offer enhanced interaction at two interfaces. One at catalyst-electrolyte interface and the other at substrate-Pt. To the best of our knowledge, utilization of FAB with TNT as composite substrate and subsequent decoration of Pt nanoparticles over this substrate with photoreduction method (using formic acid as hole scavenger) is for the first time and not studied before.

The interaction between carbon substrates and Pt are well studied[19]. Most of these reports shows that the carbon interacts with coordinative or covalent type of bonding. As FAB contains oxygen functional groups along with conducting C=C, the interaction will probably be both coordinative or covalent between carbon and Pt. In case of FAB the presence of polar functional groups will attract polar platinum precursor at these polar functional groups during the reaction process which will further act as nucleation sites. TNT also consists of oxygen functionalities in the form of surface hydroxyl groups. These functionalities also offer coordinative or covalent interactions with Pt. This can be termed as strong metal substrate interaction (SMSI)[20]. These interactions will result in pertubation of electronic structure due to charge transfer between nanoparticles and TiO_2 resulting in three major effects which are geometric, electronic and bifunctional ones. These effects weaker interaction of electrocatalyst with oxide intermediates that are formed during ORR facilitating the availability of more active sites on electrocatalyst. Moreover it is well known fact that by utilizing TiO_2 in conjunction with carbon, it is possible to achieve anti corrosion and anti-poisoning properties whereby the overall performance of elelctrocatalyts can be enhanced[21]. Further the strong anchoring of Pt nanoparticles on TiO_2 inhibits the aggregation and migration of nanoparticles with which the durability was enhanced[22].

The present work demonstrates that by utilizing strategies by 1) having ultra-small nanoparticles 2) strong metal substrate interaction (SMSI) and 3) with good absorptive properties of substrate (FAB) highly active and durable ORR catalyst can be attained. To achieve the aforementioned strategies, photo-catalytic activity of TiO_2 nanotubes (TNT) and the absorptive properties of FAB were utilized to make highly ORR active Pt-TNT-FAB with just 3.5 wt% of Pt amount.

3.3. Experimental:

3.3.1. Synthesis of TNT:

Synthesis of TNT was carried out by general anodization method[23]. Briefly, anodization was carried out by two electrode set up with Pt as counter electrode and Ti as working electrode in ethylene glycol (Kanto chemical, Tokyo, Japan) and water (90:10) containing 0.5 wt % ammonium fluoride (Kanto chemical, Tokyo, Japan). Anodization was carried by applying constant voltage of 50 V for 150 min by using a DC power supply (Kikusui PAS60-6) under continuous ultrasonication at room temperature. The obtained TNT array on Ti chip was washed with water and methanol before dispersing in methanol. The methanol was evaporated and TNT was obtained.

3.3.2. Synthesis of FAB:

Synthesis of FAB was carried out as described elsewhere[18]. In short, 1 gm. of acetylene black (AB) was taken in a round bottom flask. To this H_2SO_4 and HNO_3 (3:1 vol/vol) were added and made sure that all the AB was immersed in the acid mixture. This mixture was ultrasonicated for 3 hrs at room temperature. This dispersion was slowly added to crushed ice. Later, the mixture was filtered using nylon filter membrane with 0.1 μm pore size and washed with copious amount of water. The resulted FAB was then dried at 100 ^{o}C in a vacuum oven for 2 hrs.

3.3.3. Synthesis of TNT/FAB composite:

Synthesis of composite was carried out by following the procedure described elsewhere[24]. TNTs and FAB (1:1 wt ratio) was dispersed in water and ultrasonicated and then the mixture was stirred at room temperature for 24 hrs. Later this mixture was heated at 80 °C for 3 hrs. Then the mixture was centrifuged and powder obtained was dried at 80 °C for 3 hrs followed by calcination at 300 °C for 90 min to obtain successful composite.

3.3.4. Photochemical deposition of Pt nanoparticles over composite:

10 mg of composite was dispersed in 10 ml water and ultrasonicated for 1 hr. Then 270 µl of formic acid and 80 µl of 0.045 M $H_2PtCl_6.6H_2O$ were added to the dispersion. Further, it was irradiated by a simulated solar light (Peccel, PEC-L15 solar simulator) with a maximum of 1 sun intensity (100 $mWcm^{-1}$) for 5 hrs under constant stirring. The solution was continuously bubbled with N_2 to maintain inert atmosphere. After 5 hrs the reaction mixture was filtered, washed with deionized water and dried under vacuum overnight at room temperature.

For comparison purpose, 10 mg of only TNTs were dispersed in 10 ml water and ultrasonicated for 1 hr. Then 270 µl of formic acid and 80 µl of 0.045 M $H_2PtCl_6.6H_2O$ were added to the dispersion. Further, it was irradiated by a simulated solar light (Peccel, PEC-L15 solar simulator) with a maximum of 1 sun intensity (100 $mWcm^{-1}$) for 5 hrs under constant stirring. The solution was continuously bubbled with N_2 to maintain inert atmosphere. After 5 hrs the reaction mixture was filtered, washed with deionized water and dried under vacuum overnight at room temperature.

3.3.5. Material characterization:

The as prepared TNT/FAB and Pt-TNT/FAB were systematically characterized by various techniques. The quantitative elemental composition for both the materials was studied by SEM-EDS (Hitachi TM3030 plus). XPS (S-probe TM 2803, Fisons Instruments) was used for understanding the chemical and electronic states of elements in the materias. TEM (Hitachi model H-7100) was employed to understand the morphology of the composite and size and distribution of Pt nanoparticles.

3.3.6. Electrochemical characterization:

Electrochemical performance of composite was characterized by cyclic voltammetry (CV) and linear sweep voltammetry (LSV) coupled with rotating disk electrode (RDE) using Biologic VSP electrochemical work station. Electrochemical characterizations were carried out using conventional three electrode system, electrocatalyst coated on mirror polished glassy carbon electrode (area: 0.0706 cm^2) as working electrode, Pt wire as counter and Ag/AgCl (sat. KCl) as reference electrodes at 30 °C in 0.1 M $HClO_4$ aq. However all potentials in this study refer to that of reversible hydrogen electrode (RHE) [Potential values from Ag/AgCl were converted to RHE suing the equation

$E_{RHE} = E_{Ag/AgCl} + 0.059\ P^H + E°_{Ag/AgCl}$. (pH=1)]. The Pt loading on the working electrode was maintained at 4.6 µg/cm^2. Catalyst ink was prepared by dispersing 1.5 mg of catalyst in 300 µl distilled water, and to this 450 µl of isopropyl alcohol along with 30 µl of 5 wt% nafion was added. Commercially available 20 wt% Pt/C (Pt-Vulcan XC-72 which was procured from Sigma Aldrich) was used for comparison purpose. The Pt loading of 20 wt% Pt-Vulcan XC-72 was maintained at 4.6 µg/cm^2 on the working electrode. CV was performed at 30 °C in nitrogen saturated 0.1 M $HClO_4$ (aq) in the potential range of 0.05-1.2 V Vs RHE at a scan rate of 50 mV/s. ECSA was calculated by using the charge under the hydrogen desorption curve in the potential range of 0.05-0.4 V vs RHE. LSV was performed at 30 °C in oxygen saturated 0.1 M $HClO_4$ (aq) at a scan rate of 5 mV/s. Durability tests were performed by cycling the catalyst in the potential range of 0.6-1.0 V vs RHE with a scan rate of 100 mV/s in oxygen saturated 0.1 M $HClO_4$ (aq) at 30 °C.

3.4. Results and discussion:

SEM-EDS technique was used for the quantitative elemental analysis of both TNT/FAB and Pt-TNT/FAB. The presence of Ti, C, O, Pt and absence of Cl confirms the successful decoration of Pt (Table 3. 1). It showed that the Pt-TNT/FAB composite consists of 3.5 wt% of Pt.

Table 3. 1: Quantitative analysis of Pt on TNT/FAB by SEM-EDS

Element	Weight percent
Ti	20.07
C	55.88
O	16.13
Pt	3.51

For better understanding of the chemical and electronic states of elements in the composite, XPS measurements were performed. Fig 3.1 (A-D) shows the survey spectra of FAB, TNT, FAB/TNT and Pt-FAB/TNT respectively. Spectra show the presence of finger print peaks at respective binding energies for C 1s, O 1s, Ti 2p and Pt 4f. The absence of Cl 2p peak in the Pt-

TNT/FAB confirms that all the Pt salt has been successfully reduced to Pt^0 during the photo-reduction process. The wide scan spectra shows the presence of F 1s at 690 eV. As NH_4F was used during the preparation of TNT by anodization method, F 1s contamination is very commonly seen in anodization process. To understand chemical and electronic states, core-level high resolution spectra were analysed by deconvolution. C 1s core level spectra of TNT/FAB (Fig 3.2) revealed that along with the peaks representing C=C, C-OH, C=O of related to FAB (Fig 3.3), a new peak at binding energy of 283.6 eV was observed. This represented direct bonding of Ti-C which enhances the electronic interaction between TNT and FAB[25]. This Ti-C peak confirms the successful formation of composite of TNT-FAB. Further, the high resolution spectra of Pt 4f (Fig 3.4) showed that the peak can be deconvoluted into three peaks representing metallic Pt^0, Pt^{II} and Pt^{IV} at 70.5, 71.6 and 73.2 eV respectively. It was also found that Pt^0 was the predominant oxidation state. It is worth noting here that the Pt^0 peak has been considerably shifted to lower binding energy i.e by ~0.5 eV in comparision with Pt/C[26, 16]. The shift in the binding energy can be ascribed to strong metal substrate interaction[27]. The shift shows that the availability of electron density in the Pt that can enhance the interaction of available oxygen in the electrolyte and also eases the electron transfer to oxygen molecule. Hence, the SMSI will enhance the catalytic activity. On the other hand, SMSI also confirms that the Pt nanoparticles are not just physically adsorbed on the substrate but are electronically connected. This electronic interaction helps in anchoring the nanoparticles to the substrate. This anchoring will reduce the dissociation or displacement of nanoparticles to form aggregates which eventually leads to low surface area. Hence, SMSI will enhance the electrocatalytic activity and the durability when used for longer duration at high voltages[28].

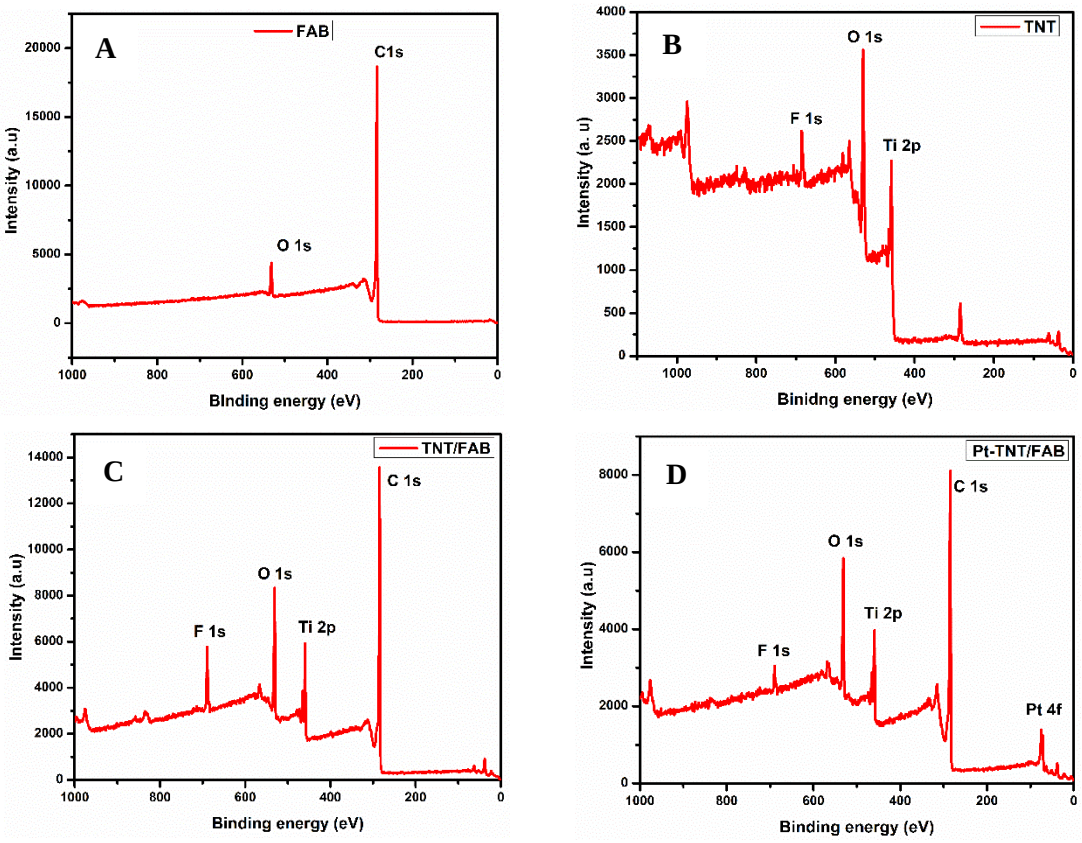

Fig 3.1: XPS survey spectra for A) FAB B) TNT C) TNT/FAB D) Pt-TNT/FAB.

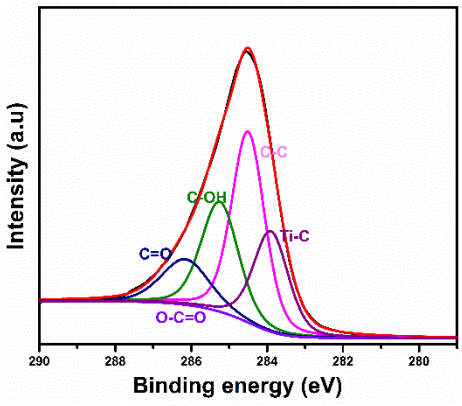

Fig 3.2: XPS deconvolution for HR spectra of C 1s in the TNT/FAB

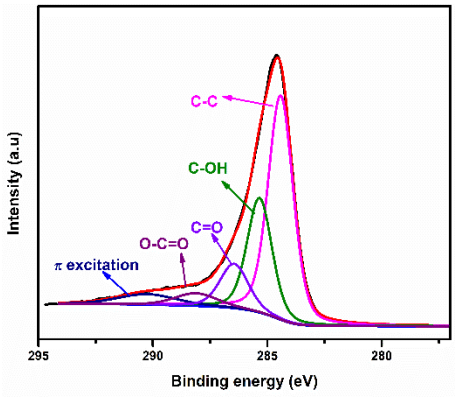

Fig 3.3: XPS deconvolution of C 1s of FAB

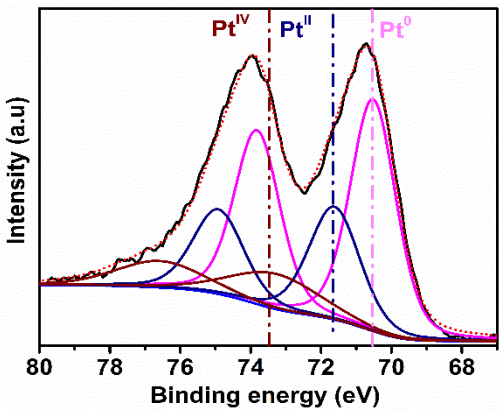

Fig 3.4: XPS HR spectra of Pt 4f in Pt-TNT/FAB.

Morphological characterization was done by TEM. Fig 3.5 shows the TEM micrographs of FAB, TNT, TNT/FAB, Pt-TNT/FAB and Pt-TNT. Fig 3.5 A. shows the interconnected nature of FAB with the grain size of around ~50 nm. Fig 3.5 B. shows the array of TNT, the tube diameter was found to be around 120 nm. The surface can be seen as smooth and without any particle like structures with contrast difference. On contrary Fig 3.5 C. shows that the rough surface of TNT with interconnecting FAB over the surface. This indirectly indicates the covalent connection between TNT and FAB through Ti-C bond formation during the composite preparation method. Figure 3.5 D. confirms the formation of ultrasmall nanoparticles evenly distributed over the surface of FAB with the average size of 1.6 ±0.2 nm. It was also observed that there is no agglomeration of Pt nanoparticles. Hence, the surface area of the nanoparticles could be very high. Whereas Pt nanoparticles on TNTs (control sample) was found to be irregular with a particle size of 3.6 nm as shown in Fig 3.5 E.

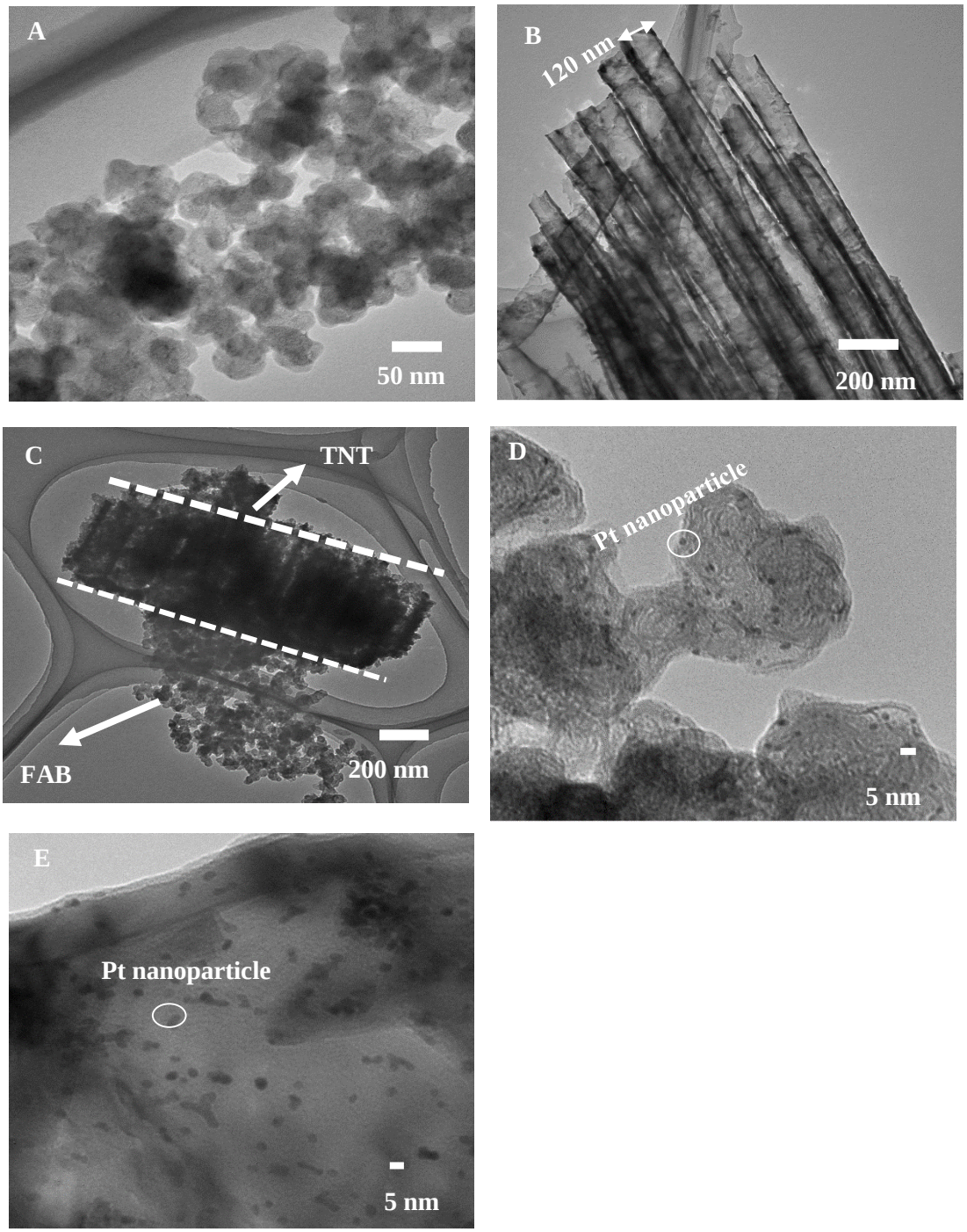

Fig 3.5: TEM images for **A)** FAB showing interconnected nature **B)** TNT array **C)** TNT/FAB with FAB over the surface of TNT **D)** Pt - TNT/FAB with nanoparticles of around 1.6 nm **E)** Pt nanoparticles over TNT (control sample)

3.5. Electrochemical performance of Pt-TNT/FAB:

To test the electrocatalytic activity of the Pt-TNT/FAB, cyclic voltammetry and linear sweep voltammetry using rotating disc electrode were studied. Cyclic voltammogram in Fig 3.6 A shows typical Pt/C type of profile with hydrogen adsorption and desorption peaks. Charge under hydrogen desorption peak was considered to evaluate electrochemical active surface area (ECSA) of Pt-TNT/FAB using the formula.

$$\text{ECSA} \quad \frac{\text{Charge } [Q_H\ \mu C/cm^2]}{210[\mu C/cm^2] \text{ X Pt loading } [g/cm^2]}$$

Q_H is the charge corresponding to the hydrogen desorption peak,

$Q_M = 210\ \mu C/cm^2$ is the electrical charge associated with the monolayer adsorption of hydrogen

ECSA of the electrocatalyst was found to be as high as 49.8 m^2/gm. The ECSA was higher than Pt-Vulcan XC-72 (13.0 m^2/gm). To understand the ORR kinetics, RDE measurements were carried out. The polarization curve is given in Fig 3.6 B, the onset potential was found to be around 0.79 V vs RHE. It is quite visible that the overpotential for ORR is high compared with the conventional electrocatalysts. This can be ascribed to the presence of semi-conducting TNT that reduces the overall electronic conductivity of catalyst. To determine the kinetic parameters of ORR, RDE measurements were carried out. The polarization curve is given in Fig 3. 6 B, the onset potential and half wave potential was found to be around 0.80 V and 0.63 V, respectively vs RHE. It is quite visible that the overpotential for ORR is high compared with the conventional electrocatalysts. This can be ascribed to the presence of semi-conducting TNT that reduces the overall electronic conductivity of catalyst. To understand the kinetic parameters, rotation dependent polarization curves were studied. By utilizing Koutecky-Levich (K-L) plots, the number of electrons involved in the ORR was analyzed (Fig 3. 6 C). It was found to be ~4 electron transfer at 0.60 V vs RHE. The mass specific activity and specific activity was found to be 519 A/g and 10.4 A/m^2, respectively at 0.60 V vs RHE which is higher than Pt Vulcan XC-72 (mass activity and specific activity was found to be 111 A/g and 8.50 A/m^2, respectively). The obtained mass activity and specific activity values are higher than some of the Pt based composite materials

prepared in literature showing the important relevance of this work. Table 3. 2 gives the comparision of mass activity and specific activity values.

Table 3. 2: Comparision of mass activity and specific activity with litreature

Sample name	Mass activity (A/g) (at 0.9 V)	Specific activity (A/m^2) (at 0.9 V)	reference
1) TiOx-Pt/C	71.0	0.940	[29]
2) Pt-TiO_2 /graphene	-	0.690	[9]
3) Pt-TiO_2@CNT	160	0.0700	[30]
4) Pt-CNT-TiO_2	350	14.8	[16]
5) Pt-TiO_2/MWCNT	13.5	0.00370	[21]
6) Pt/rGO_1-FCB_1	132	0.0311	[32]
7) Pt-TNT/FAB	519 (at 0.6 V)	10.4 (at 0.6 V)	Present work

RDE polarization curve of Pt-TNT/FAB was compared with Pt Vulcan XC-72 as shown in Fig 3. 6 D at 1600 RPM. As we see Pt Vulcan XC-72 showed ORR polarization curve with $E_{1/2}$ of 0.600 V but in case of Pt-TNT/FAB, $E_{1/2}$ was positively shifted to 0.630 V. This positive shift of 30 mV in Pt-TNT/FAB signifies low over potential and higher ORR activity compared to commercial counter part. In order to provide the mechanistic pathway for ORR, Tafel plots constructed from Fig 4 D for Pt-Vulcan XC 72 and Pt-TNT/FAB were presented in Fig 3. 6 E and Fig 3. 6 F, respectively. In each Tafel plot two regions were identified towards low current density region (l.c.d) and high current density region (h.c.d). In each Tafel plot for Pt-Vulcan XC 72, Tafel slope was found to be 168 mV/dec and 227 mV/dec towards l.c.d and h.c.d, respectively. For Pt-TNT FAB, Tafel slope was found to be 225 mV/dec and 455 mV/dec towards l.c.d and h.c.d, respectively. The observed differences in values are attributed to the different ORR intermediates that are formed due to the influence of support between the interaction of Pt and oxygen[31].

Further, to check the catalyst durability, the material was subjected to CV for 2000 cycles of potential scan between 0.6 V to 1.0 V vs RHE at a scan rate of 100 mV/s. Durability of the catalyst was examined by change in mass activity before and after 2000 cycles. It was found that for Pt Vulcan XC-72 the reduction in the mass activity was found to be 30.80 % after 2000 cycles. Whereas for Pt-TNT/FAB the reduction in the mass activity was found to be 20.76 % after

2000 cycles as shown in Fig 3. 6 G. This high retention of activity for Pt-TNT/FAB after 2000 cycles shows high durability than Pt Vulcan XC-72. Similarly CV was performed with only TNTs decorated with Pt nanoparticles (control sample) but did not show any activity due to the poor conducting nature of nanotubes as shown in Fig 3.6 H.

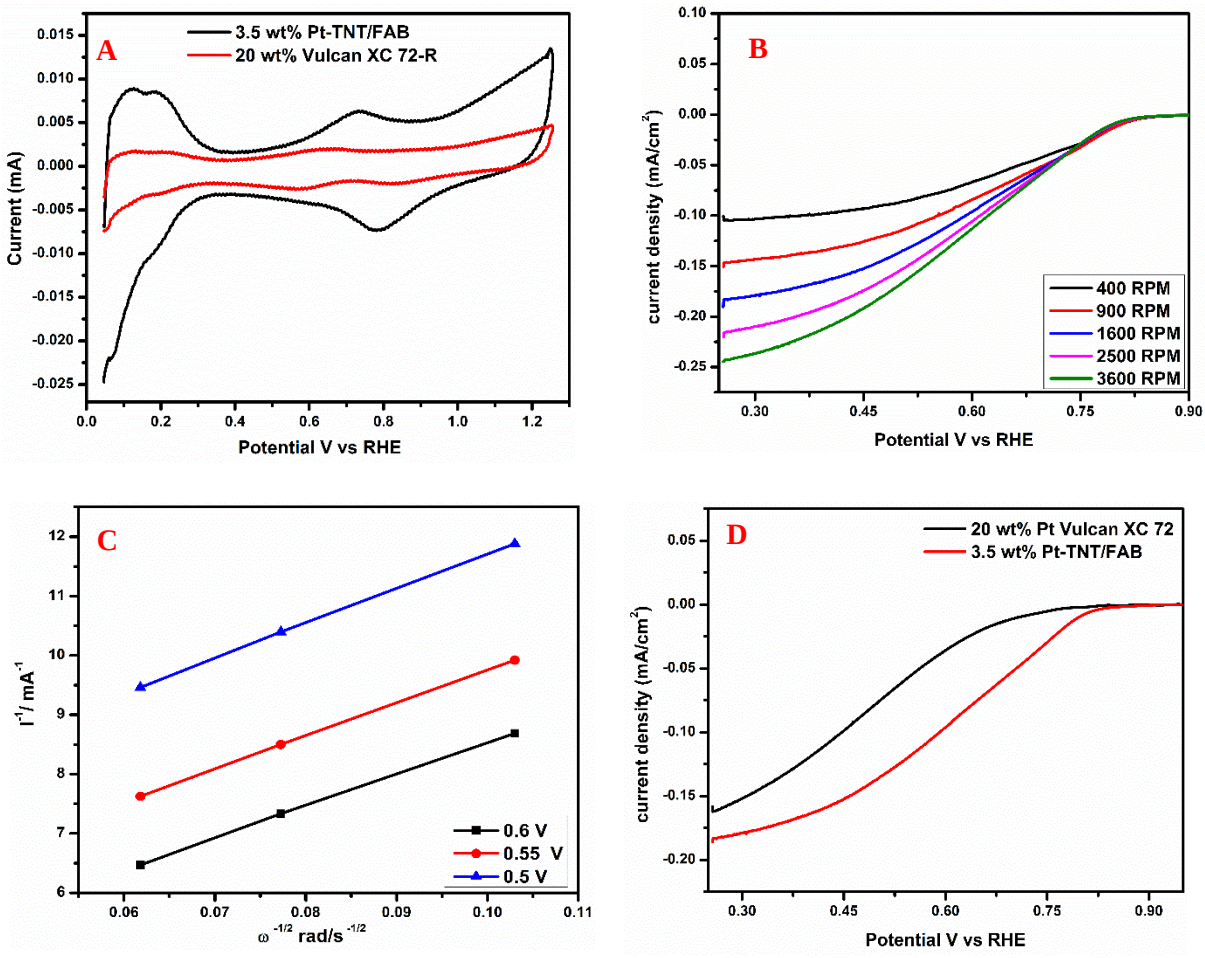

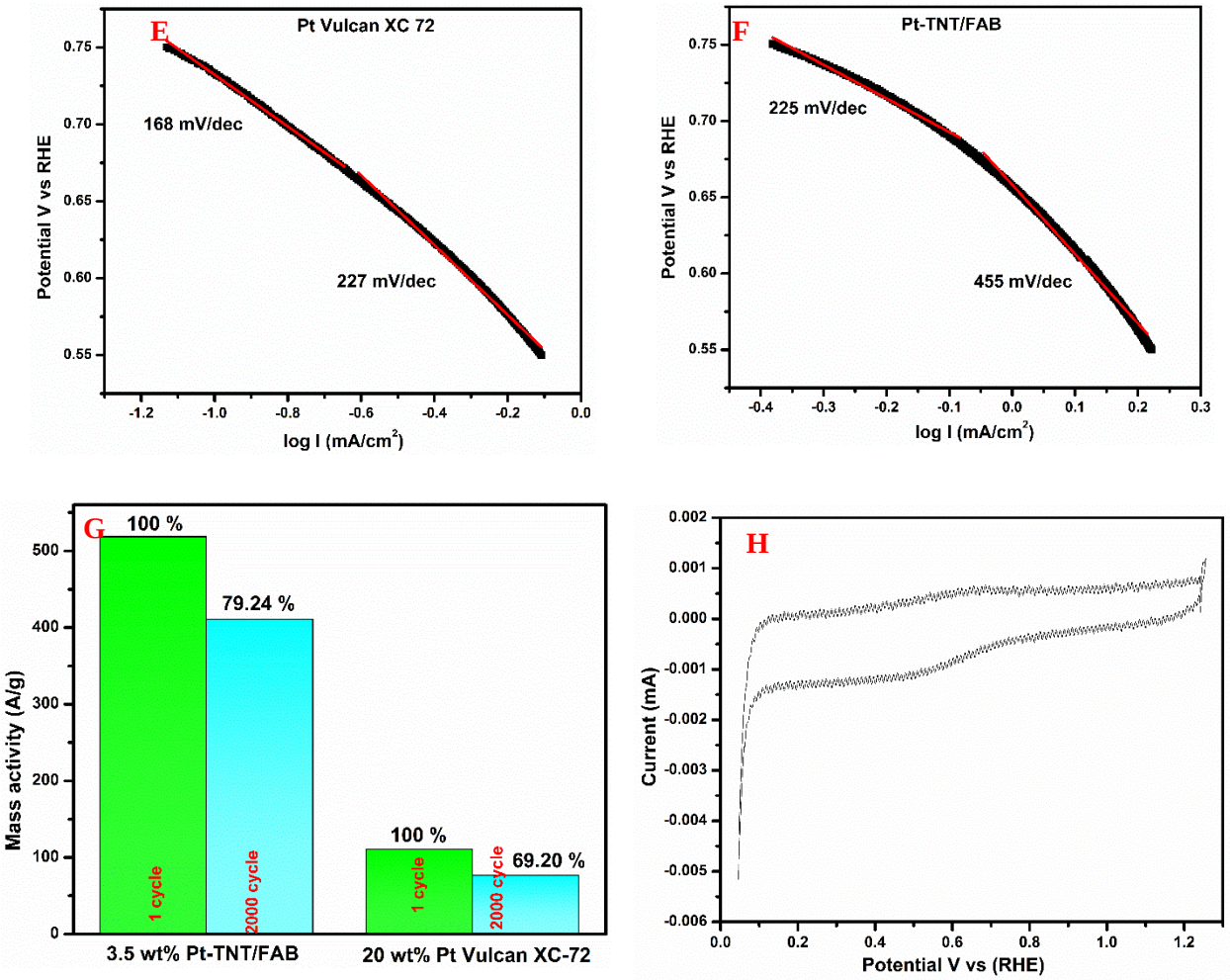

Fig 3.6: A) Cyclic voltammograms of Pt-TNT/FAB and Pt-Vulcan XC 72 in 0.1 M $HClO_4$ (aq) at 30°C in nitrogen at 50 mV/s

B) Linear sweep voltammograms of Pt-TNT/FAB with RDE at a scan rate of 5 mV/s in oxygen atmosphere at different RPM in 0.1 M $HClO_4$ (aq)

C) KL plot for Pt-TNT/FAB at 0.50, 0.55 and 0.60 V

D) Comparision of LSV for Pt-TNT/FAB and Pt-Vulcan XC 72 at 1600 RPM.

E) Tafel plot for Pt-Vulcan XC 72 at l.c.d and h.c.d.

F) Tafel plot for Pt-TNT/FAB at l.c.d and h.c.d.

G) Comparision of mass activity for 1 cycle and 2000 cycle for Pt-TNT/FAB and Pt Vulcan XC 72

H) Cyclic voltammogram of Pt-TNT in 0.1 M $HClO_4$ (aq) at 30°C in nitrogen at 50 mV/s

3.6. Electrochemical ORR studies in nonaqueous medium:

ORR studies were carried with Pt-TNT/FAB in 0.1M LiTFSI in tetraethylene glycol dimethyl ether (TEGDME) electrolyte so that this catalyst can be even applied to Li-air battery (Fig 3.7). Ether based electrolytes have attracted significant attention recently since they have high resistance towards the superoxide radical which is a side product formed during oxygen reduction. Hence in this studies TEGDME was choosen. LiTFSI was choosen as supporting electrolyte since this is most compatible supporting electrolyte with TEGDME.

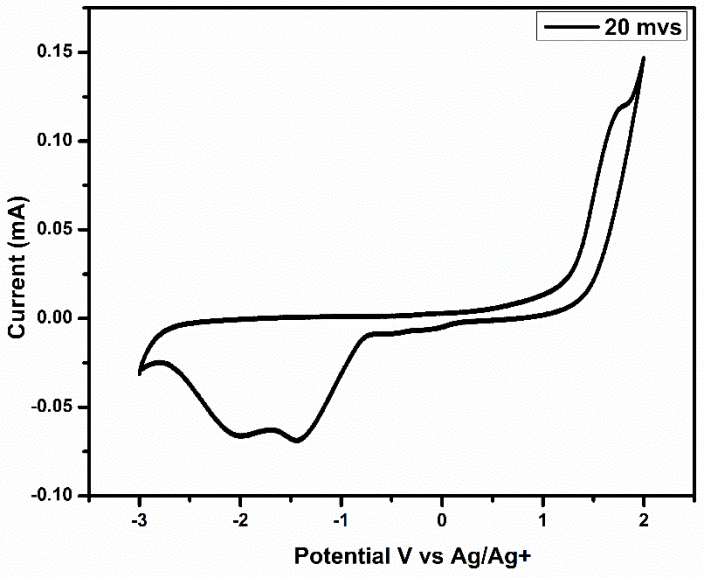

Fig 3.7: Cyclic voltammogram at 20 mV/s in oxygen saturated 0.1 M LiTFSI in TEGDME

Fig 3.7 gives the cyclic voltammogram that was carried out at 20 mV/s in oxygen saturated 0.1 M LiTFSI in TEGDME. There are two reduction peaks corresponding to ORR, one at -1.42 V and other at -1.98 V which are possible due to formation of superoxide which is further undergoing reduction to other products. There is also an anode peak at 1.68 V which is due to oxygen evolution reaction. Effect of scan rate on ORR was studied by varying the scan rate from 10 mV/s to 75 mV/s and it was found that with the increasing scan rate the peak current increased. This shows that this is diffusion controlled process. Fig 3.8 gives the effect of scan rate over ORR.

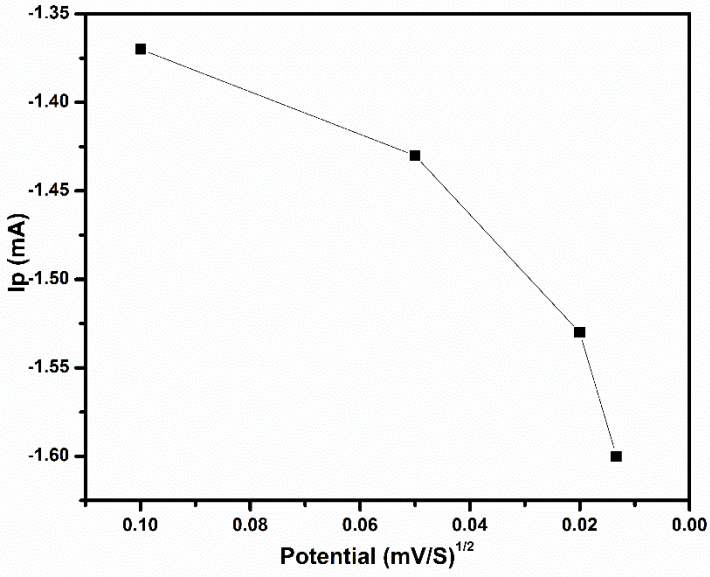

Fig 3. 8: Effect of scan rate over ORR

Further the durability of catalyst towards ORR was investigated by performing CV for 100 cycles at 20 mV/s. As seen in Fig 3.9 there was reduction in ORR for 100th cycle. This reduction of peak is due to accumulation of products on electrode.

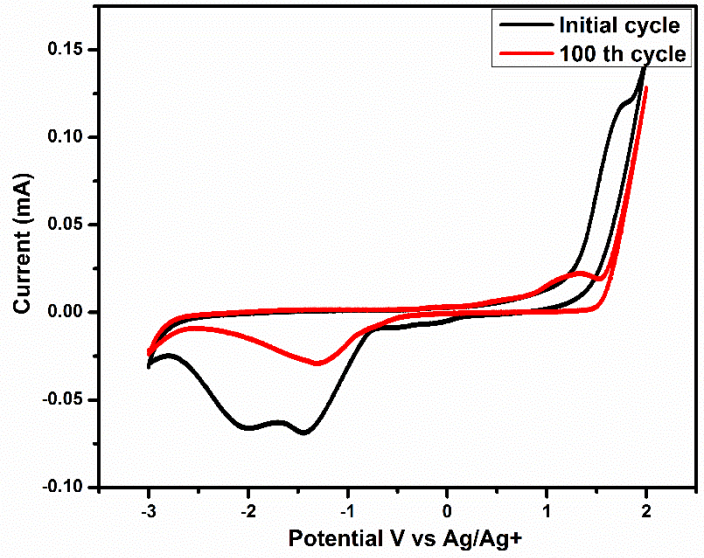

Fig 3.9: Comparision of cyclic voltammogramms at 20 mV/s for 100 cycles in 0.1 M LiTFSI in TEGDME

3.7. Conclusions:

In conclusions, this work presents a plausible idea to decorate ultrasmall metal nanoparticles utilizing composite made of TNT/FAB. Pt nanoparticles were decorated over TNT/FAB by photoreduction utilizing the spill over of photoelectrons from TNT. The systematic characterization revealed the particle size to be ~1.6 nm. The photoreduction process not only enhanced the specific surface area by providing very small nanoparticles but also established a strong anchoring between Pt and substrate. This was clearly understood by XPS characterization. The small size nanoparticles resulted in very high ECSA (49.8 m^2/g) along with high MA and SA than commercially available Pt Vulcan XC 72. With this work I affirm that by photodeposition of Pt and the presence of FAB with high absorptive properties, it is possible to reduce the Pt content to nearly one- tenth with good ORR activity and durability. Further the electrochemical activity towards ORR was also assessed in nonaqueous medium so that this material can be used in Li-air batteries. This material showed peaks corresponding to both ORR and OER siginifying the fact that this can be used as catalyst in Li-air batteries

References:

1 T. Gunji, K. Saaki, A. J. Jeevagan, T.Tanabe, S. Kaneko and F. Matsumoto, *ECS Trans*., 2015, **66**, 1–8.

2 F. Ando, T. Tanabe, T. Gunji, T. Tsuda, S. Kaneko, T. Takeda, T. Ohsaka and F. Matsumoto, *Electrochim. Acta*, 2017, **232**, 404–413.

3 K. Sopian and W. R. Wan Daud, *Renew. Energy*, 2006, **31**, 719–727.

4 J. Lu, L. Li, J. B. Park, Y. K. Sun, F. Wu and K. Amine, *Chem. Rev.*, 2014, **114**, 5611–5640.

5 K. Jukk, N. Kongi, K. Tammeveski, R. M. Arán-Ais, J. Solla-Gullón and J. M. Feliu, *Electrochim. Acta*, 2017, **251**, 155–166.

6 D. Wang, H. L. Xin, R. Hovden, H. Wang, Y. Yu, D. A. Muller, F. J. Disalvo and H. D. Abruña, *Nat. Mater.*, 2013, **12**, 81–87.

7 Y. Nie, L. Li and Z. Wei, *Chem. Soc. Rev.*, 2015, **44**, 2168–2201.

8 B. Ruiz Camacho, C. Morais, M. A. Valenzuela and N. Alonso-Vante, *Catal. Today*, 2013, **202**, 36–43.

9 K. Tiido, N. Alexeyeva, M. Couillard, C. Bock, B. R. MacDougall and K. Tammeveski, *Electrochim. Acta*, 2013, **107**, 509–517.

10 J. Greeley, I. E. L. Stephens, A. S. Bondarenko, T. P. Johansson, H. A. Hansen, T. F. Jaramillo, J. Rossmeisl, I. Chorkendorff and J. K. Nørskov, *Nat. Chem.*, 2009, **1**, 552–556.

11 S. Kobayashi, M. Wakisaka, D. A. Tryk, A. Iiyama and H. Uchida, *J. Phys. Chem. C*, 2017, **121**, 11234–11240.

12 V. R. Stamenkovic, B. S. Mun, K. J. J. Mayrhofer, P. N. Ross and N. M. Markovic, *J. Am. Chem. Soc.*, 2006, **128**, 8813–8819.

13 R. Wang, D. C. Higgins, S. Prabhudev, D. U. Lee, J.-Y. Choi, M. A. Hoque, G. A. Botton and Z. Chen, *J. Mater. Chem. A*, 2015, **3**, 12663–12671.

14 L. Dai, Y. Xue, L. Qu, H.-J. Choi and J.-B. Baek, *Chem. Rev.*, 2015, **115**, 4823–4892.

15 R. Sibul, E. Kibena-Põldsepp, S. Ratso, M. Kook, M. Käärik, M. Merisalu, P. Paiste, J. Leis, V. Sammelselg and K. Tammeveski, *Electrochem. commun.*, 2018, **93**, 39–43.

16 R. Badam, R. Vedarajan, K. Okaya, K. Matsutani and N. Matsumi, *Sci. Rep.*, 2016, **6**, 1–7.

17 M. Manikandan, R. Vedarajan, R. Kodiyath, H. Abe, S. Ueda, A. Dakshnamoorthy, N. Rajalakshmi, K. S. Dhathathreyan and G. V Ramesh, , DOI:10.1166/jnn.2016.11772.

18 R. Badam, R. Vedarajan and N. Matsumi, *Chem. Commun.*, 2015, **51**, 9841–9844.

19 N. T. Cuong, D. H. Chi, Y.-T. Kim and T. Mitani, *Phys. Status Solidi*, 2006, **243**, 3472–3475.

20 C. J. Pan, M. C. Tsai, W. N. Su, J. Rick, N. G. Akalework, A. K. Agegnehu, S. Y. Cheng and B. J. Hwang, *J. Taiwan Inst. Chem. Eng.*, 2017, **74**, 154–186.

21 K. Jukk, N. Kongi, A. Tarre, A. Rosental, A. B. Treshchalov, J. Kozlova, P. Ritslaid and L. Matisen, *J. Electroanal. Chem.*, 2014, **735**, 68–76.

22 S. Hussain, H. Erikson, N. Kongi, A. Tarre, P. Ritslaid, M. Rähn, L. Matisen, M. Merisalu, V. Sammelselg and K. Tammeveski, *Int. J. Hydrogen Energy*, 2018, **43**, 4967–4977.

23 R. Vedarajan, S. Ikeda and N. Matsumi, *Nanoscale Res. Lett.*, 2014, **9**, 573.

24 J. Safari and S. Gandomi-Ravandi, *J. Mol. Struct.*, 2014, **1065**–**1066**, 241–247.

25 B. K. Vijayan, N. M. Dimitrijevic, D. Finkelstein-Shapiro, J. Wu and K. A. Gray, *ACS Catal.*, 2012, **2**, 223–229.

26 F. A. De Bruijn, G. B. Marin, J. W. Niemantsverdriet, W. H. M. Visscher and J. A. R. Van Veen, *Surf. Interface Anal.*, 1992, **19**, 537–542.

27 A. Lewera, L. Timperman, A. Roguska and N. Alonso-Vante, *J. Phys. Chem. C*, 2011, **115**, 20153–20159.

28 C. Jackson, G. T. Smith, D. W. Inwood, A. S. Leach, P. S. Whalley, M. Callisti, T. Polcar, A. E. Russell, P. Levecque and D. Kramer, *Nat. Commun.*, 2017, **8**, 1–11.

29 N. R. Elezovic, B. M. Babic, V. R. Radmilovic, L. M. Vracar and N. V. Krstajic,

Electrochim. Acta, 2009, **54**, 2404–2409.

30 M. Eckardt, C. Gebauer, Z. Jusys, M. Wassner, N. Hüsing and R. J. Behm, *J. Power Sources*, 2018, **400**, 580–591.

31 J. Masa, A. Bordoloi, M. Muhler, W. Schuhmann and W. Xia, *ChemSusChem*, 2012, **5**, 523–525.

32. T. Xuejun , Z. Yachao, C. Longsheng, Y. Limeng, W. Zhiqiang, F. Dahui, G. Yanyan, S. Zhigang, Y. J. Baolian, *Mater. Chem. A*, 2018, **6**, 15074-15082.

Chapter 4

General conclusions

4.1. General conclusions:

The continuous usage of petroleum based energy reserves led to severe emission of carbon dioxide, nitrogen oxides and sulfur oxides. Particularly evolution of carbon dioxide resulted in raise of earth's temperature which is called as "Global Warming". This global warming caused severe damage to environment. Hence there is a need to reduce the usage of these fossil fuels with alternative sustainable energy based systems. This thought made the scientific community to develop an outlook for the development of fuel cells and Li air batteries. This fuel cells was first developed by William Groove in the year 1839. These are highly efficient energy suppliers with low emissions. Their efficiencies can reach as high as 80% in electrical energy conversion and has the capacity to reduce >90% major environmental pollutants. Li air batteries were developed by Littauer and Tsai in the year 1976. This would play one of the key roles in making the transportation sector emission free and its theoretical energy density is 10 times that of Li ion secondary battery.

To spread the wide application of these fuel cells, there are major issues that need to be resolved. An electrocatalyst is required to catalyze the major reactions. In the cathode side oxygen reduction reaction occurs. This reaction is highly sluggish with slow kinetics. Pt/C is the common catalyst employed to catalyze this reaction. It has some disadvantages such as cost corrosion and durability. This thesis is focused on to synthesize an alternate catalyst with new methodologies.

Chapter 1 focusses on general introduction to fuel cells and Li air batteries and their principles. It gives about the drawbacks of fuels cells and gives an overview about ORR and its mechanism. A brief discussions are made about the reaction mechanism and limitations of this reaction. A special emphasis on ORR with different carbon materials were made and also about the improvement in ORR activity by doping different heteroatoms were discussed. Of the various metals that are available so far, Pt plays a key role in catalyzing this reaction. Fig 4.1 gives the mechanism of ORR with Pt. It catalyzes the oxygen reduction to generate water through 4 electron transfer process.

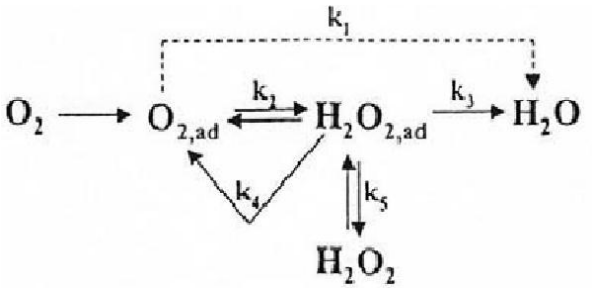

Fig 4. 1: Mechanism of ORR on Pt

Chapter 1 discusses about the role of different shape and size of Pt nanoparticles. The problem of high cost due to Pt can be reduced by utilizing Pt in the form of core shell nanoparticles. These core shell nanoparticles can be prepared with other metals such as Ni, Co. Fe and Au etc. There are various methods for synthesis of these core shell nanoparticles and below Fig 4.2 gives the schematic illustration of synthetic methods.

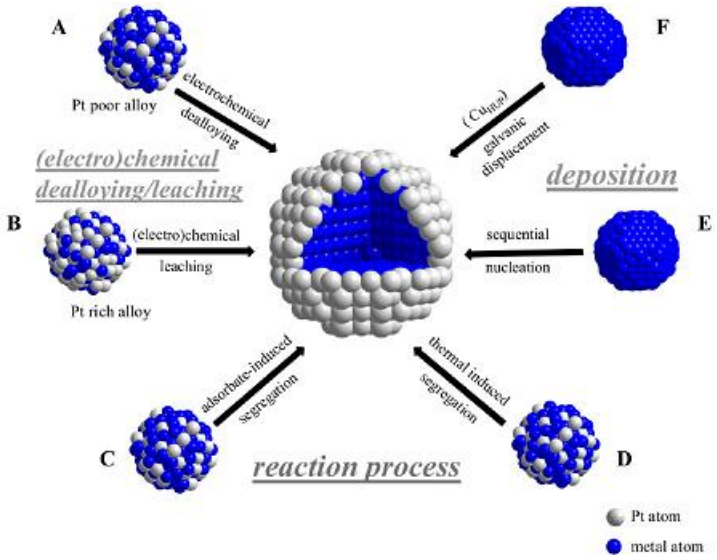

Fig 4.2: Various synthesis methods for core shell nanoparticles

(Figure adapted from J. Phys. Chem. Lett., 2013, 4, 3273–3291)

In order to solve the problem of carbon corrosion, alternative support materials such as TiO_2, WOx, SnO_2 etc. can be used. But of all the materials TiO_2 is superior and can be used as support for Pt nanoparticles because of its high resistance to corrosion. So this chapter also focusses on introduction to titania nanotubes, preparation of titania nanotubes with various

methods with special emphasis on anodization method with mechanism. A brief introduction to various electrochemical process along with rotating disc electrode (RDE) was mentioned.

In polymer electrolyte membrane fuel cells, Pt/C is the most widely used catalyst but it has inherent disadvantages such as cost (as high catalyst loading is required to catalyze highly sluggish oxygen reduction reaction), corrosion and durability problem. Recent research showed that these problems can be solved by utilizing the Pt as shell along with relatively abundant metal (gold) and by replacing the carbon with semiconducting metal oxide such as TiO_2 in nanotubes form. There are many protocals for the synthesis of core shell nanoparticles but all of them are tedious, time consuming, involves using of surfactants and are thermally driven. Therefore there is a great demand to deposit core shell metal nanoparticles in easy, non toxic and sustainable method. Chapter 2 presents a simple and clean method for decoration of three different types of core shell nanoparticles of Pt and Au without using any extreanous reagents by ultrafast electrochemical deposition as shown in Fig 4.3.

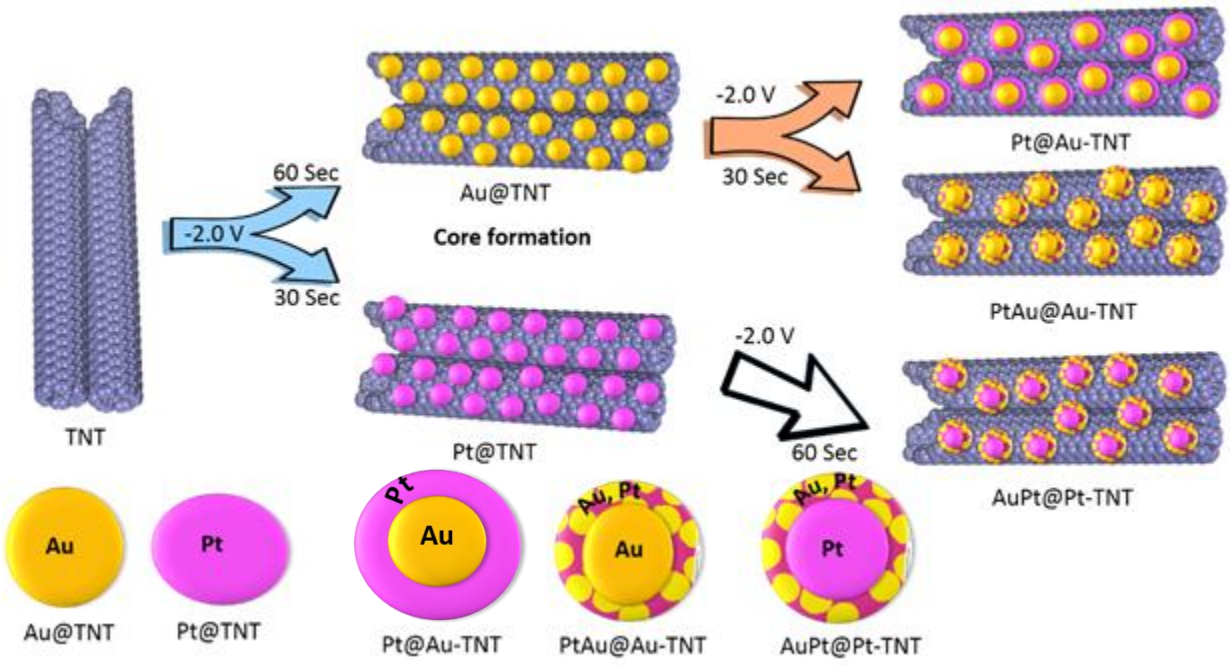

Fig 4.3: Schematic illustration of core shell nanoparticles formation on TNTs by applying potential.

In this study highly ordered TNTs synthesized by electrochemical anodization were employed. Electrochemically deposited metal nanoparticles of high purity, were formed rapidly, and have good adhesion to the TNT. The presence of metal nanoparticles on TNTs have been confirmed by TEM and XPS and core shell formation by EDS mapping. Fig 4.4 shows the EDS mapping images for core shell nanoparticles.

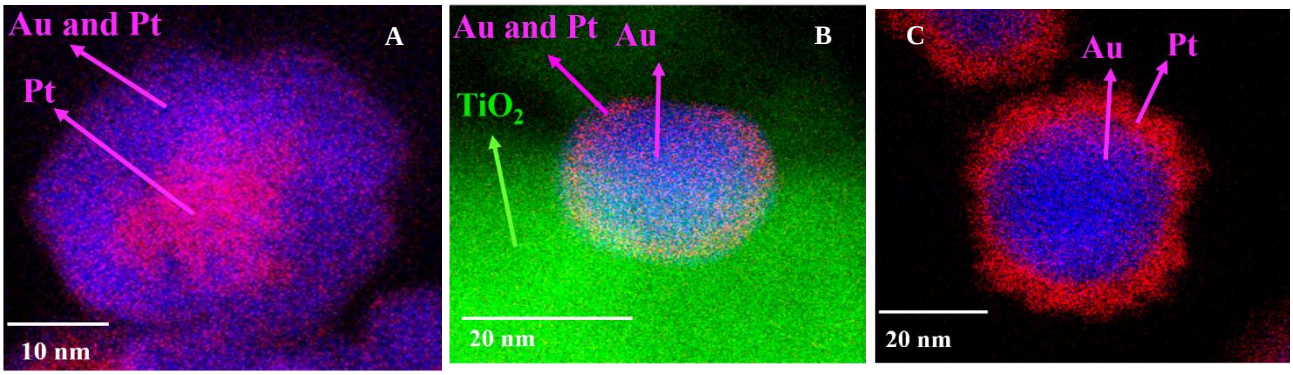

Fig 4.4: EDS elemental mapping images of A) AuPt@Pt-TNT B) PtAu@Au-TNT C) Pt@Au-TNT

The resultant core shell nanoparticles were tested for ORR activity in aqueous (0.1 M KOH) and non aqueous (0.1 M LiTFSI in TEGDME) medium and the corresponding peak currents were measured. My findings suggest that all core shell nanoparticles are active towards ORR. Pt@Au-TNT was found to show relatively high activity as the shell is predominantly covered with Pt.

Chapter 3 focusses on preparation of composites as support materials for Pt nanoparticles decoration to solve the problem of carbon corrosion. Many composites of titania nanotubes with carbon materials such as CNTs, graphene have been prepared to overcome these limitations. But all these carbon materials require arduous preparation methods. Recent report by our group on functionalised acetylene black which showed higher activity than commercially available catalyst is highly advantageous. FAB has many oxygen functionalities which help in nanoparticles decoration and also in absorbing electrolyte thereby reducing interfacial resistance. Herein I aimed at designing a composite material consisting of FAB and TiO_2 nanotubes decorated with Pt

nanoparticles to investigate electrocatalytic activity for oxygen reduction reaction. The research would involve designing of a composite material made of TNTs and FAB. This was followed by decoration of Pt nanoparticles on hybrid material by photoreduction method. Below Fig 4.5 presents the preparation of composite and decoration of Pt nanoparticles over composite thereafter.

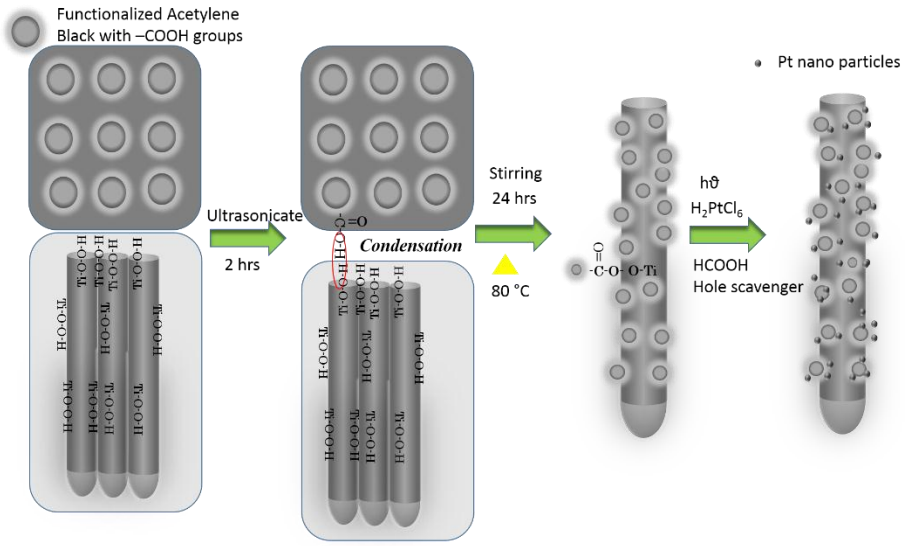

Fig 4.5: Graphical abstract for preparation of composite material and decoration of Pt

The sucessfull formation of composite and Pt decoration thereafter was characterized by XPS, SEM-EDS and XPS. From SEM-EDS, 3.5 wt% Pt was found to be decorated and particle size was found to be 1.6 nm. This extremely small size of Pt nanoparticles was due the availability of photo electrons on titania. This photoelectrons provide many nucleating sites through which size of particles reduces. The as prepared material was tested towards electrochemical ORR activity in 0.1 M $HClO_4$ (aq) and was found to show extremely high ECSA of 49.8 m^2/gm. The ECSA of Pt-TNT/FAB with 3.5 wt% of Pt was higher than conventionally prepared and commercially available Pt Vulcan XC 72. Further the durability of this material was assessed by subjecting to CV for 200 cycles and almost 80% of the activity was retained in terms mass activity. This high retention of activity after 2000 cycles is due to the strong metal substrate interaction.

Further the electrochemical activity towards ORR was also assessed in nonaqueous medium so that this material can be used in Li-air batteries. This material showed peaks corresponding to both ORR and oxygen evolution reaction (OER) signifying the fact that this can be used as catalyst in Li-air batteries.

4.2. Future scope of the work:

Based on the present work, the possible outgrowths of the present work can be as follows:

1) Synthesis of core shell nanoparticles by using metal nanoparticles such as Ni, Co, Pd and Fe etc as core by using this electrodeposition technique over titania nanotubes and to utilize them as electrocatalyst materials for catalyzing ORR.
2) Loading of the core shell nanoparticles that are synthesized in this work in membrane electrode assemblies and to monitor their performance in PEMFCs.
3) Decoration of Pt nanoparticles over TNT/FAB with electrodeposition technique and comparision of size and distribution of nanoparticles with photochemical method.
4) Titania nanotubes can be utilized as support materials by decorating with other heteroatoms so that it will lead to metal free electrocatalyst.

List of Publications and other acheivements:

Bukka Santhosh

A) Publications:

1. **Santhosh Bukka**, Yuhei Umehara, Koichi Higashimine, Raman Vedarajan and Noriyoshi Matsumi "*Ultrafast Electrochemical Deposition of Core Shell Metal Nanoparticles on TiO_2 Nanotubes for Electrocatalytic Applications*", Accepted manuscript, *Mater. Res. Express*
2. **Santhosh Bukka,** Rajashekar Badam, Raman Vedarajan, Noriyoshi Matsumi "Photogeneration of ultrasmall Pt nanoparticles on carbon: A novel strategy for efficient ORR activity with low Pt content", Manuscript under review in *Int. J. of Hydrog. Energy.*

International conference presentations:

2016

1) **Oral presentation:** **Santhosh Bukka**, Yuhei Umehara, Koichi Higashimine, Raman Vedarajan and Noriyoshi Matsumi, "*Electrochemical Decoration of Core Shell Nano Particles over TiO_2 Nano Tubes for Oxygen Reduction Reaction*". 230th Meeting of ECS (The Electrochemical Society) PRIME, Hawaii Convention Center, Hawaii, Honolulu, USA. (Oct 2016)

2017

2) **Poster presentation: Bukka Santhosh**, Raman Vedarajan, Noriyoshi Matsumi, "*Ultra Fast Electrochemical Decoration of Core Shell Nano Particles on TiO_2 Nano Tubes for ORR in Alkaline Medium*". JAIST Japan-India Symposium on Materials Science 2017, Japan Advanced Institute of Science and Technology, Ishikawa, Japan. (Mar 2017)

2018

1) **Oral presentation: Santhosh Bukka**, Raman Vedarajan and Noriyoshi Matsumi, "*TiO_2 nano tubes/functionalised acetylene black composites decorated with Pt nanoparticles as electrocatalyst for oxygen reduction reaction (ORR)*". 255th Meeting of ACS (American

Chemical Society) national meeting and exposition, new Orleans convention center, USA. (March 2018)

2) **Poster presentation:** **Santhosh Bukka**, Rajashekar Badam, Raman Vedarajan and Noriyoshi Matsumi, "*TiO_2 Nanotubes/Functionalized Acetylene Black Composite Decorated with Pt Nanoparticles as Electrocatalyst for ORR*" The 16th International Symposium on Polymer Electrolytes (ISPE-16), Yokohama symposia, Yokohama, Japan (June 2018)

Domestic conferences:

2016

1) **Poster presentation:** **Santhosh Bukka**, Yuhei Umehara, Koichi Higashimine, Raman VEDARAJAN, Noriyoshi Matsumi, *"Electrochemical Decoration of Metal Nano Particles Over TiO_2 Nanotubes for Catalytic Application"* SPSJ (Society of Polymer Science, Japan) Annual Meeting in Kobe Convention Center, Kobe, Japan. (May 2016).

2) **Poster presentation:** **Santhosh Bukka**, Yuhei Umehara, Koichi Higashimine Raman Vedarajan, Noriyoshi Matsumi, "*Ultra Fast Electrochemical Deposition of Core Shell Metal Nano Particles on TiO_2 Nano Tubes for oxygen reduction reaction* ". 65th SPSJ (Society of Polymer Science, Japan), Fall Meeting, in Kanagawa University, Yokohama, Japan. (Sep 2016)

3) **Oral presentation:** **Santhosh Bukka,** Yuhei Umehara, Koichi Higashimine, Raman Vedarajan and Noriyoshi Matsumi, "*Electrochemical Decoration of Core Shell Metal Nano Particles Over TiO_2 Nano Tubes for Oxygen Reduction Reaction*". SPSJ (Society of Polymer Science, Japan) Hokuriku Regional Meeting in Fukui university, Fukui, Japan. (Nov 2016).

2017

1) **Poster presentation:** **Bukka Santhosh,** Raman Vedarajan, Noriyoshi Matsumi "*TiO_2 nano tubes/functionalised acetylene black composites decorated with Pt*

nanoparticles as electrocatalyst for ORR". SPSJ (Society of Polymer Science, Japan), spring meeting in Ehime university, Matsuyama, Japan (2017).

2) **Oral presentation**: **Santhosh Bukka**, Raman Vedarajan, Noriyoshi Matsumi "*Bimetallic Core Shell Nano Particles on TiO_2 Nano Tubes for ORR in Alkaline Medium*". Inorganic polymer conference. Tokyo university of science, Tokyo, Japan (2017).

3) **Poster presentation: Bukka Santhosh,** Raman Vedarajan, Noriyoshi Matsumi "*Ultra Fast Electrochemical Decoration of Core Shell Nano Particles over Titania Nano Tubes for Electrocatalytic Applications".* Chemical Society of Japan, JAIST, Japan (2017).